2018

Biophysical Studies of Guanine Nucleotide-Binding Alpha Subunits

Brian Leverson

LOYOLA UNIVERSITY CHICAGO

BIOPHYSICAL STUDIES OF GUANINE NUCLEOTIDE-BINDING ALPHA SUBUNITS

A DISSERTATION SUBMITTED

TO THE FACULTY OF THE GRADUATE SCHOOL

IN CANDIDACY FOR THE DEGREE OF

DOCTOR OF PHILOSOPHY

PROGRAM IN CHEMISTRY

BY

BRIAN D. LEVERSON

CHICAGO, IL

DECEMBER 2018

ACKNOWLEDGEMENTS

I would like to acknowledge all the people who made the completion of this dissertation possible. I would like to thank my graduate advisor, Dr. Duarte Mota de Freitas, for teaching me how to think critically, patience, and the art of writing logically and scientifically. You are a terrific mentor and an even better friend.

I would also like to thank my dissertation committee, Dr. Miguel Ballicora, Dr. Alanah Fitch, and Dr. Ken Olsen for their guidance and their valuable into my project.

Graduate student colleagues who have brightened my graduate tenure include Tahirah Heath, Jackie Arroyo, and Jonathan Hill. I would like to thank the undergraduate researchers who have contributed to the overall goal of the projects: Saad Kothawala, Andrea Wakim, and Michelle Callegari. I also would like to acknowledge my lab mate Jesse Goosens and former lab mate Dr. Matt Najor for teaching me many of the techniques utilized in this research.

Finally, I would like to thank my family and friends who have help me succeed, believed, and supported me when I was at my weakest. You were understanding and guide me in way I could not imagine. I could not have accomplished this without you. For this I will always be in your debt.

TABLE OF CONTENTS

LIST OF TABLES

LIST OF FIGURES

LIST OF ABBREVIATIONS

2YT	2 x yeast extract tryptone
AC	Adenylyl cyclase
ADP	Adenosine 5’ –diphosphate
$AlCl_3$	Aluminum chloride
AlF_4^-	Tetrafluoroaluminate (III)
AMF	Aluminum magnesium fluoride
cAMP	3’,5’ -cyclic adenosine monophosphate
CD	Circular dichroism
ε	Extinction coefficient
EDTA	Ethylenediaminetetraacetic acid
EGTA	Ethylene glycol – bis (β – aminoethylether) – N,N,N’,N’ – tetraacetic acid
G-protein	Guanine nucleotide binding protein
GDP	Guanosine 5’-diphosphate
GDP•AlF_4^-	Guanosine 5’-diphosphate tetrafluoroaluminate complex
G_i	Inhibitory G protein of AC
$G_{i\alpha}$	α subunit of the inhibitory G protein of AC
G_s	Stimulatory G protein of AC

$G_{s\alpha}$	α subunit of the stimulatory G protein of AC
GTP	Guanosine 5’-triphosphate
GTPγS	Guanosine 5’-[γ-thio]triphosphate
FPLC	Fast protein liquid chromatography
HCl	Hydrochloric acid
HEPES	4-(2-hydroxyethyl)-1-piperazineethanesulfonic acid
His_6 - $G_{s\alpha}$	N – terminus hexahistidine tagged $G_{s\alpha}$ protein
Mg^{2+}	Magnesium ion
$MgCl_2$	Magnesium chloride
M_gSO_4	Magnesium sulfate
NaCl	Sodium chloride
NaF	Sodium fluoride
NaH_2PO_4	Sodium dihydrogenphosphate
NaOH	Sodium hydroxide
PDB	Protein data bank
SDS	Sodium dodecyl sulfate
SDS – PAGE	Sodium dodecyl sulfate polyacrylamide gel electrophoresis
Tris – Cl	Tris(hydroxymethyl)amino methane
UV – Vis	Ultraviolet visible spectrophotometry

CHAPTER ONE

INTRODUCTION

Signal Transduction Pathways

Proteins are linchpin macromolecules in biology, having a wide range of physiological functions, including communication, i.e., signal transduction. Many of the proteins used in signal transduction pathways rely on structural movements, creating two distinct conformations ("on" and "off") [1]. Thus, a change in conformation allows for the protein to act as a gatekeeper, regulating molecules and information passing through the cell membrane. This strategy allows for the cell to react to its environment and vary the intensities and durations of the transmitted signal.

Guanine nucleotide-binding proteins (G-proteins) are among the most common and well-studied protein involved in signal transduction. First described by Alfred Gilman and Martin Rodbell, the G-protein mechanism has been found to play a role in almost all cell types in the human body and utilize a wide variety of ligands to propagate the signal across the cell membrane [2, 3, 4]. Although sharing common features such as GTP binding and hydrolysis, the over 100 different kinds of G-proteins have been classified into two groups; either monomeric small GTPases, such as the Ras superfamily, or larger heterotrimeric membrane-bound proteins, which is the focus of our research (1).

Overview of the G-Protein Mechanism

G-proteins that are heterotrimeric, are composed of an α subunit (Gα), which regulates the activity of effector proteins, and a βγ subunit complex. Inactive $G_{\alpha\beta\gamma}$ are attached to G-protein coupled receptors (GPCR), which are seven-transmembrane domain receptors that are activated by specific hormones. Once activated, GPCRs act as guanine nucleotide exchange factors (GEF), inducing a conformational change in the Gα subunit, which prompt guanosine 5'-triphosphate (GTP) to exchange for guanosine 5'-diphosphate (GDP) and the βγ dimer to dissociate [5, 6, 7]. The released α subunits, as well as the βγ subunits, then bind to the appropriate enzymes thereby stimulating or inhibiting secondary messenger formation [5]. This process is self-regulating with intrinsic low GTPase activity: the bound GTP is hydrolyzed into GDP, effectively deactivating the G_α subunit [5, 8]. Once the G_α subunit signal is terminated, it re-forms the heterotrimer, deactivating the $G_{\beta\gamma}$ subunit and binds to a GPRC, resetting the G-protein cycle [5] (Figure 1).

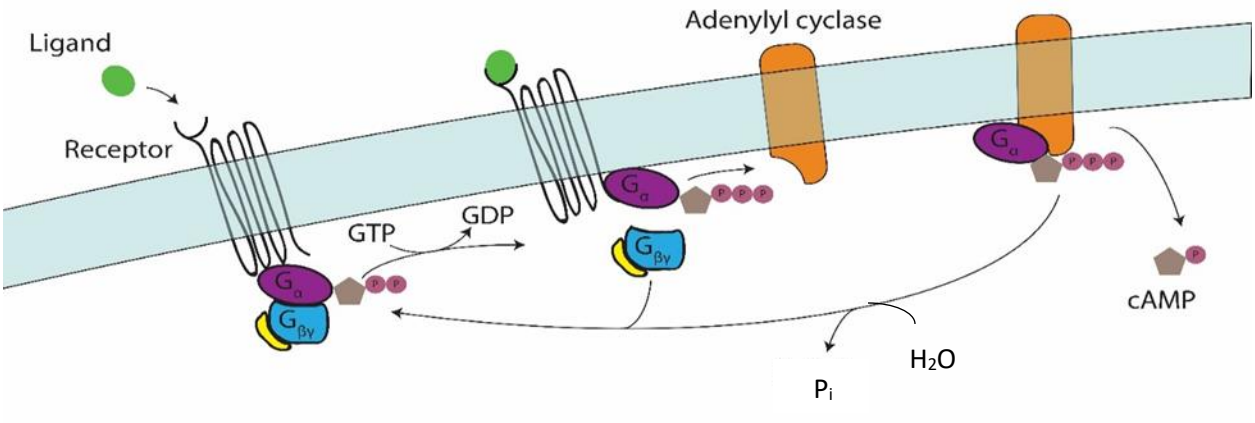

Figure 1. Mechanism of adenylyl cyclase regulation via a G-protein

While some cell functions only utilize the standard mechanism of G-protein signal transduction pathways, others require further regulation of signal strength. Most regulators of G-Protein signaling (RSG) are post- and co-translational covalent modifications at or near the N-terminus and lead to additional signal regulation [9, 10]. One common effect of RSG is the phosphorylation by protein kinase C. The phosphorylation of the G_α subunit interferes with the reformation of the heterotrimeric G-protein, increasing the length of the activation signal via weak interactions [9, 11].

Regulation of G-proteins and their Effectors

GPCR: Regulation of G-proteins

GPCRs are responsible for the first step of the G-protein signal transduction cycle. Activation of GPCRs can be precipitated by chemicals, such as the binding of hormones or neurotransmitters. The β_2 adrenergic receptor (β_2AR), which stimulates the activation of G_s proteins, has, for over the past 40 years, provided a model for the role it plays in G-protein mechanisms[12]. A crystal structure of β_2AR complexed to a nucleotide free G_s heterotrimer shows that the β_2AR binds to the GTPase domain of the G_α subunit [13]. There seems to be no interaction with the $G_{\beta\gamma}$ subunit, however, it is unknown if this occurs in nature because nanobodies, antibodies which facilitate crystallization, bind at the β_2AR-$G_{\beta\gamma}$ interface. Other techniques, such as Ala-scanning mutagenesis, suggest the C-terminus of the G_β subunit bind to the third loop of β_2AR [14, 15, 16] . The GTPase domain and the α-helical domains of the G_α subunit are splayed, opening the nucleotide binding pocket to the cytosol [13].

Once activated, the ternary complex that forms between the GPCR and $G_{s\alpha}$•GDP heterotrimer is cooperative, inducing a 100-fold increase in the G-protein affinity for GTP [12]. It is not completely understood how this occurs; the primary difference between the inactive and activated β_2AR is a 14 Å outward movement of the TM6 alpha helix when measured from the α-carbon of Glu268 and an extension of the TM5 helix into the cytoplasm [13]. These movements form the basis for the theory that Phe139, located on the TM5 helix, moves into a hydrophobic pocket formed by $G_{s\alpha}$ His41 at the beginning of the β1-strand, Val213 at the beginning of the β3-strand, and Phe376, Arg380, and Ile383 in the α5-helix [13]. When the TM5 helix enters the hydrophobic pocket it either perturbs the β1-α1 and β6-α5 loops involved in $G_{s\alpha}$ nucleotide binding or physically pushes GDP out of the nucleotide binding pocket, allowing for GTP binding [13, 17, 18, 19].

G_α Subunits: Structural and Functional Characteristics

Several crystal structures of individual G-protein subunits have been solved. The G_α subunit has a partial structural resemblance to the Ras protein, which is a monomeric protein with intrinsic GTPase activity [20]. The G_α subunit consists of two domains (Figure 2): an α-helical domain, which is composed of six α-helices and is a regulator of its effector [21]. The GTPase domain is a highly conserved Ras-like structure, composed of six β-sheets surrounded by five α-helices [5]. The GTPase domain contains the guanine nucleotide binding pocket, responsible for binding and hydrolyzing GTP, as well as the binding sites for the $G_{\beta\gamma}$ dimer, membrane receptors and downstream effectors [13, 22]. There are five conserved sequences in the GTPase domain, the diphosphate binding loop (P – loop) (GXGESGKS) that holds the α and β phosphates of GTP in

place, the Mg^{2+}-binding loops (RXXTXGI and DXXG), and the guanine ring-binding motifs (NKXD and TCAT). This domain may also play a significant role in coupling specific G-proteins to specific effectors [22]. Both the amino (N) and the carboxyl (C) termini of the G_α subunit are key determinants of receptor-binding specificity and play a critical role in G-protein activation, but their structures are not clear because they are disordered in the crystals [23]. The N-terminus forms an α-helix that is ordered by its interaction with G_β subunit in the heterotrimeric structure of G-proteins [6]. The process of binding GTP and subsequent activation of the proteins relies on a structural shift in flexible segments, switches I, II, and III, located near the γ-phosphate of GTP [24, 25].

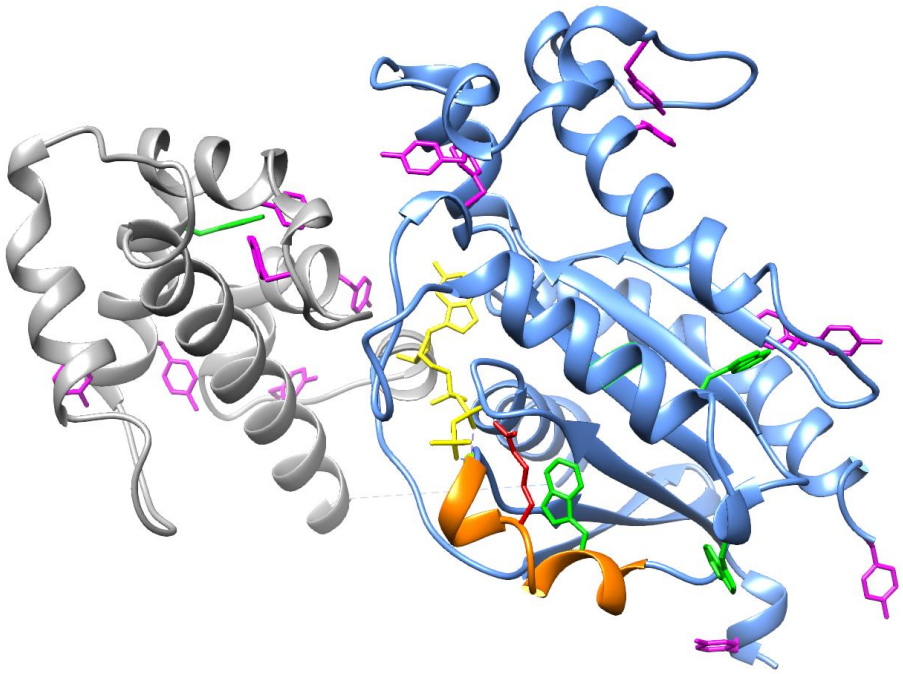

Figure 2. Crystal structure of WT Gsα•GTPγS displaying its four tryptophan residues (green), fourteen tyrosine residues (purple), the GTPγS bound nucleotide (yellow), Mg^{2+} (green sphere), and R234 (red) that is involved in a π-cation interaction with W234 (PDB ID: 1AZT) [22].

$G_{\beta\gamma}$ Dimer: Activation and Regulation

Initially, the $G_{\beta\gamma}$ dimer was thought to only regulate the G_{α} subunit by acting as a stopgap measure to prevent spontaneous activation in the absence of a receptor [26]. This view has evolved significantly, after $G_{\beta\gamma}$ dimer was shown to activate K^+ ion channels, regulate multiple isoforms of adenylyl cyclase (AC), as well as stimulate PI_3 kinase [27, 28, 29, 30]. As the understanding of the $G_{\beta\gamma}$ dimer versatility evolved, research has begun to focus on its composition and mechanisms of interactions with their effectors.

Currently, there are five known G_{β} isoforms, each consisting of seven β-sheets and an α-helix at the N-terminus [10]. In the case of the G_{γ} subunits, there are 12 isoforms, which are composed of two α-helices connected by a loop [31, 32]. While the G_{β} and G_{γ} subunits can be expressed individually in vitro, instances of separated subunits has not been observed in nature [10]. There are two points of contact between the G_{β} and G_{γ} subunits: the β5/β6 sheets and the N-terminal helices of the G_{β} subunit interacts with the C-terminal α-helix of the G_{γ} subunit [33, 34]. When in the G-protein heterotrimer form, the G_{β} subunit only interacts with the GPRC and the G_{α} subunit.

Unlike the G_{α} subunit, the G_{β} and G_{γ} subunits do not significantly change during G protein activation [35]. Once the $G_{\beta\gamma}$ dimer dissociates from the GPCR and the G_{α} subunit, it interacts with the appropriate effector based on the combination of the G_{β} and G_{γ} subunits [32]. Although each effector has unique contact points for the correct docking of the $G_{\beta\gamma}$ dimer, several combinations have similar regulatory effects on the signal intensity [36, 37, 38]. It is not understood how the $G_{\beta\gamma}$ dimer activates the correct effector once separated from the G-protein

heterotrimer [39]. Some theories point to compartmentalization, which would limit the interactions between $G_{\beta\gamma}$ and effectors [10].

G_α Subunits GTPase Mechanism

The exchange of GDP for GTP nucleotides occurs once a GEF, most commonly a GPRC, weakens affinity of the G-protein for the nucleotide [5, 40]. Normally, a G-protein has a high affinity for nucleotide, decreasing the dissociation and limiting the chances for unintentional activation of the protein [7]. GEF act on the P-loop and switch regions I and II, and interferes with their interactions with the phosphates of the bound nucleotide and the Mg^{2+} ion [5]. When the bonds are disrupted, the GDP dissociates, and the empty nucleotide binding pocket is free to bind GTP, due to its higher cellular concentration. Once activated, these highly conserved flexible segments fold, thus reorganizing the protein into a more compact arrangement [23, 41, 42] that is vital for its function [43].

The switch regions of an activated G_α protein position the GTP nucleotide in a Mg^{2+} charged stabilized environment, allowing for a nucleophilic attack of the γ – phosphate of GTP by an activated water molecule [44, 45, 46]. The exact mechanism of the GTP hydrolysis transition state is debated, but one theory states that glutamine 208 and the carbonyl of glycine 209 in $G_{s\alpha}$, are positioned to facilitate a base, arginine 201, to abstract a proton from the water molecule, thus increasing the strength of its nucleophilic attack ability [44]. While this is not the only theory discussion GTP hydrolysis, it is one that addresses the biochemical and computational data regarding this topic [47].

$G_{s\alpha}$ Subunits Signal Amplification of Adenylyl Cyclase

G_{α} proteins are categorized into four major subgroups [8]: $G_{\alpha i}$, $G_{\alpha q}$, $G_{\alpha(12/13)}$, and $G_{s\alpha}$ - the focus of this investigation. $G_{s\alpha}$ is responsible for the stimulation of AC, which produces adenosine-3', 5' - cyclic monophosphate (cAMP) from adenosine 5' – triphosphate [22]. Currently 9 isoforms of AC have been identified in several cell types, which are categorized into 4 groups based on their regulatory properties and are stimulated by the $G_{s\alpha}$ subunit [48]. AC isoforms are composed of a single peptide chain, consisting of an N-terminal cytosolic domain, two membrane-spanning domains, each with six transmembrane α-helices, and two cytosolic domains C_1 and C_2 that are 40% identical. The C_1 and C_2 are further divided according to the regulatory properties, the catalytic (C1a, C2a) and the regulatory (C1b, C2b) subdomains [49, 50]. Variation in isoforms of AC mainly occur at the N-terminus, between residues 1080 and 1353 [50]. Detailed structural information on the complete AC protein is lacking, due to the difficultly in expressing, purifying, and crystalizing the complete AC protein. Due to this, the two cytoplasmic domains (C_1 and C_2) are expressed independently [48]. Although an individual domain is not active, when combined the two domains form the catalytic moiety at their interface and the activity is fully restored [50]. This has led to a lack of information on the membrane bound domain of AC. Although several crystal structures exist, the most widely used system has become the system with the C_1 domain from AC5 and the C_2 domain from AC2, denoted as AC5:C2 [49, 51].

Once AC is bound to an activated $G_{s\alpha}$ subunit, the crystal structure shows that the $G_{s\alpha}$ subunit, when bound to AC5:C2, does not undergo a conformational change until hydrolysis is

completed [22]. The interaction between the $G_{s\alpha}$ subunit and catalytic AC2 domain is maintained by 11 contact points, which create a distinct binding site allowing for simultaneous interaction with other AC effectors, such as the inhibitory $G_{i\alpha1}$ protein [52]. The contact points consist mainly of charged residues Arg231, Arg232, Gln236, Asn239, Lys272, Asn279, Arg280, Lys282, Arg283, Thr284 as well as an aromatic Trp281 [22]. These contact residues are clustered in the switch II region of $G_{s\alpha}$ and interact with the α2' and α3'-β4' loops of the AC C_2 domain [51].

The formation of the $G_{s\alpha}$•GTP•AC complex induces a change in the relative orientation of the C_1 and C_2 domains of AC. This in turn causes changes in the AC active site that improves the catalytic efficiency. While it is not known how this results in an increase cAMP formation, it has been hypothesized that the conformational changes induced by the movement of Asp440 in AC places it in an effective position for the nucleophilic attack on the 3'-hydroxyl group of ATP [51]. Once formed, cAMP acts as a secondary messenger that has three main intercellular effectors: Protein Kinase A, the guanine nucleotide-exchange factor, and cyclic-nucleotide-gated ion channels [53, 54, 55].

$G_{s\alpha}$: Protein Expression

$G_{s\alpha}$ is expressed in several tissues and is encoded by 13 exons in the GNAS gene located on chromosome 20 in humans [56]. Due to alternative pre-mRNA splicing, the $G_{s\alpha}$ transcript has several variants [56, 57]. We focused on the short-$G_{s\alpha}$ variant, which differs from the long variant by the exclusion of 45 nucleotides derived from exon 3 [56]. While some investigations have shown differences between the long and short variant, the long form releases GDP 2-fold faster

and with a different activation response to GTPγS (non-hydrolyzable form of GTP), but it is not yet understood if this results in a biological effect[56].

G-Proteins Participation in Disease States

Disruptions, caused by mutations, to the $G_{s\alpha}$ pathway can result in a up regulation in cAMP [48, 58, 59]. GNAS mutations are linked to adenomas and/or carcinomas of the thyroid and large intestine, disruptions in the endocrine system (the pituitary and adrenal glands), the central nervous system, and the biliary tract among others [60, 61, 62]. Each mutation affects the $G_{s\alpha}$ subunit in unique ways.

Effect of $G_{s\alpha}$ Mutation on the Endocrine System

The mutation $G_{s\alpha}$ R231H, a residue located in the switch II regain, has been associated with pseudohypoparathyroidism (PHP) [63, 64]. PHP is an illness of the endocrine system that is characterized by the resistance to the thyroid-stimulating hormone at the thyroid level, secretion of gonadotropin hormones by the pituitary gland, and release of parathyroid hormone in the kidneys [65]. Decreased hormone sensitivity causes low calcium and high phosphate levels; resulting in cataracts, dental problems, seizures, calcification of the basal ganglia, numbness, and tetany (muscle twitches and hand and foot spasms) [66, 67, 68].

There are 5 variants of PHP, and the R231H mutation contributes to at least 4 of the 5 forms of the disease [69]. Of these, type 1A is the most common, accounting for 70% of all PHP sufferers [67]. Type 1A associated with a group of symptoms referred to as Albright's hereditary osteodystrophy, which includes the additional characteristics of a short stature, a round face,

obesity, and short hand bones [70]. PHP symptoms are generally first seen in childhood and can normally be treated with calcium and vitamin D supplementation [67].

$G_{s\alpha}$ Involvement in Cancer

GNAS has also been established as an oncogene, detected in 4.26% of all known cancers [60]. Of these cancers 88.12%, contain the mutation R201C and 0.24% has the R231H mutation [60, 71]. The mutation R201C is linked to adenomas and carcinomas in the thyroid and large intestine, the pituitary and adrenal glands, the central nervous system, the biliary tract, and in the pancreas among others and R231H are associated with primitive neuroectodermal tumors in the central nervous system [60, 72, 73].

G_{α} subunits resemble the structure of monomeric G-proteins of the Ras superfamily [74], which, when permanently activated, are known to be the most prevalent oncogenes in human cancer [75, 76]. Similar to oncogenic mutations in the Ras protein, the comparable R201C mutation causes constitutive activation of the protein [77]. The resulting increase in cAMP levels causes an up regulation, which, when occurring in the intestines, can cause phosphodiesterases in the intestinal epithelium in mice when paired with an inhibited adenomatous polyposis coli gene [78]. While less research has been conducted into the R231H mutation, it has been observed that the mutation causes down regulation of cAMP formation [79].

Protein Folding

While both R201C and R231H mutations have been identified as oncogenic mutations, alone they are not enough to result in cancer [78]. Yet a single point mutation results in a cascade of structural disruptions that leads to functional irregularities. Many of these disruptions can be

traced back to incorrect folding of the protein secondary and/or tertiary structures. Improper folding of the molten globules can be devastating and is the cause of many diseases [80]. In many of these disease states, such as Parkinson' and Alzheimer's, misfolded protein is associated with a conversion of α-helices into extended β-sheets resulting in the formation of aggregates [81, 82, 83].

Protein folding is a complicated yet surprisingly efficient event, critical for protein viability. A one-dimensional structure composed of a polypeptide chain of undefined length folds onto itself, creating an extremely complex three-dimensional structure. The formation of the three-dimensional structure of a protein occurs over a time scale of 10^{-1} to 10^{3} seconds with over 95% accuracy, suggesting that the formation is not random and that not all conformations are possible [84]. While exactly how nature accomplish this is unknown, we do understand some of the important aspects of the protein that are important and have used this knowledge to create several theories and models to reproduce this act of nature.

The forces that are a factor for proper protein folding are non-covalent interactions (hydrogen bonding, van der Waals interactions, and electrostatic interactions), hydrophobic interactions, and backbone angle preferences as well as thermodynamic effects [85]. Taking these factors into account, the most current accepted theories, model protein folding proceeding through an energy landscape [86, 87]. The theory visualizes protein folding as a funnel-shaped energy landscape (Figure 3). Within the funnel are with many high-energy unfolded structures and only a few low-energy, folded structures [87, 88]. During the folding process, local minima are formed that account for the existence of proteins that are in a partially folded or intermediated

folded stated [89]. As folding occurs, the high energy unfolded structure moves into a more favorable low-energy structure. This occurs via alternative microscopic trajectories from its unfolded state to its native conformation driven primarily by non-covalent interactions [85, 86]. The free energy of the native state is lower than that of the unfolded protein and is in equilibrium with molten globule structures that have native-like structures. When a protein denatures, it does not go directly to a random coil, but rather to one of these molten globule states, which resemble the native state and may continue to bind a ligand and have some activity [86]. Denaturation studies can also be used to understand the formation of aggregates and oligomers, as well as provide insight on how proteins containing high concentrations of β-sheets form amyloid fibrils in diseases such as Alzheimer's [90].

Biophysical Spectroscopic Techniques

Much of what we know in biochemistry has been revealed utilizing a suite of biophysical techniques based on molecular spectroscopy. Using light, at a variety of wavelengths, it has been possible to probe kinetic and thermodynamic properties of biological samples. While there is no single biophysical method that can give the full story regarding a protein structure, combining several can give a broad overview of what components are important for the folding that result in the intended function of the protein.

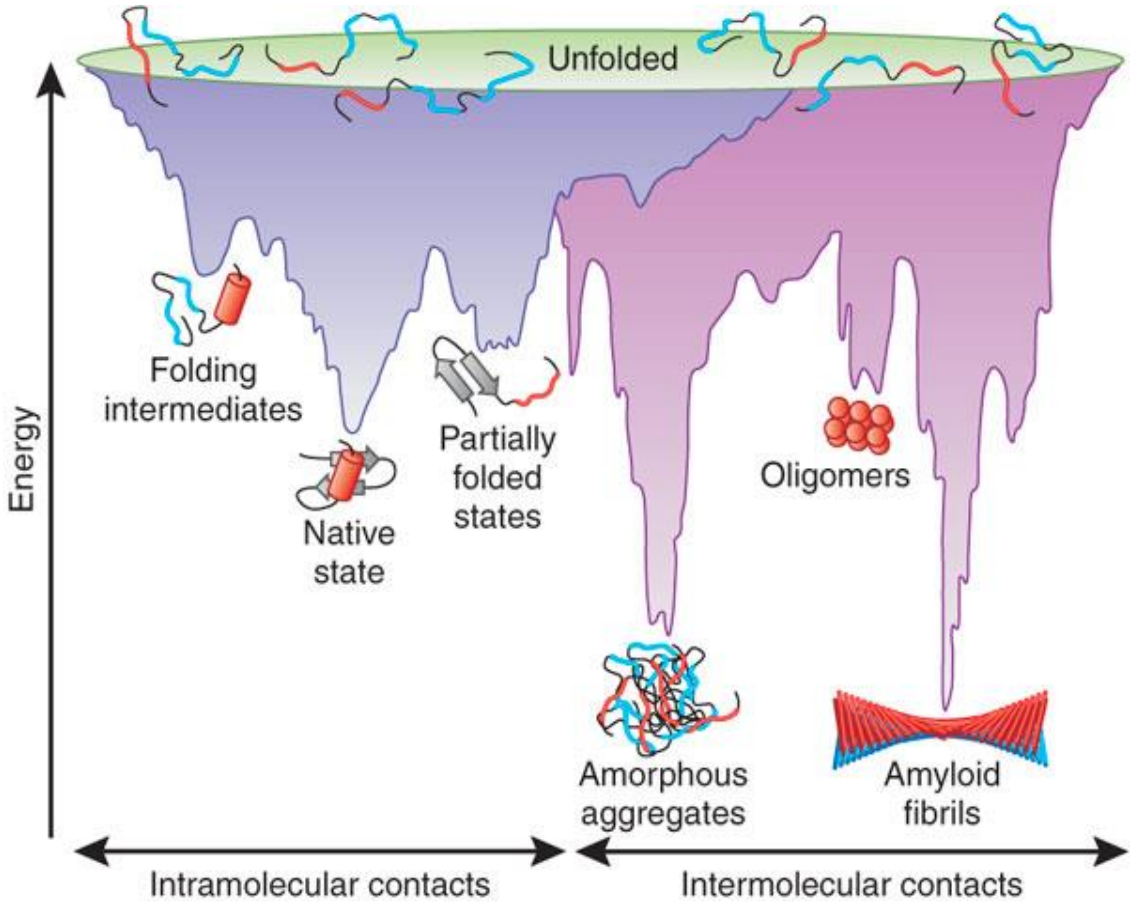

Figure 3. Protein folding and aggregation in an energy landscape scheme. The purple area depicts possible single protein conformations. Local minima are represented by folding intermediates and partially folded states. Unfolded structures are funneled to the native state via intramolecular contacts. The pink area shows multiple protein interactions. Instead of forming a native state, amorphous aggregates or amyloid fibrils form via intermolecular contacts.

UV/Vis Spectroscopy

One of the most basic, yet useful techniques is ultra-violet/visible light (UV/Vis) spectroscopy, which uses light energy to promote electrons from the ground state to various excited states (Figure 4). The non-bonding electrons (n-electrons) can absorb energy in the form of ultraviolet or visible light excite these electrons to higher anti-bonding molecular orbitals [84, 91]. The Laporte's rule explains that molecules containing π-electrons or to excited

transitions (π-π*, n-π*, σ-σ*, and n-σ*) of the electrons (i.e. the lower energy gaps between the HOMO and the LUMO), the longer the wavelength of light it can absorb. Although d → d transitions violate this rule, they are observed in low vibrionic bands due to coupling of electronic and vibrational excitation [92]. The absorption can be quantified by the Beer-Lambert law (A=ε*c*l), where A is the absorbance, l is the pathlength, c is the molar concentration, and ε is the molar extinction coefficient. Since the absorbance is directly dependent on the molar concentration, it can be used to calculate a sample concentration.

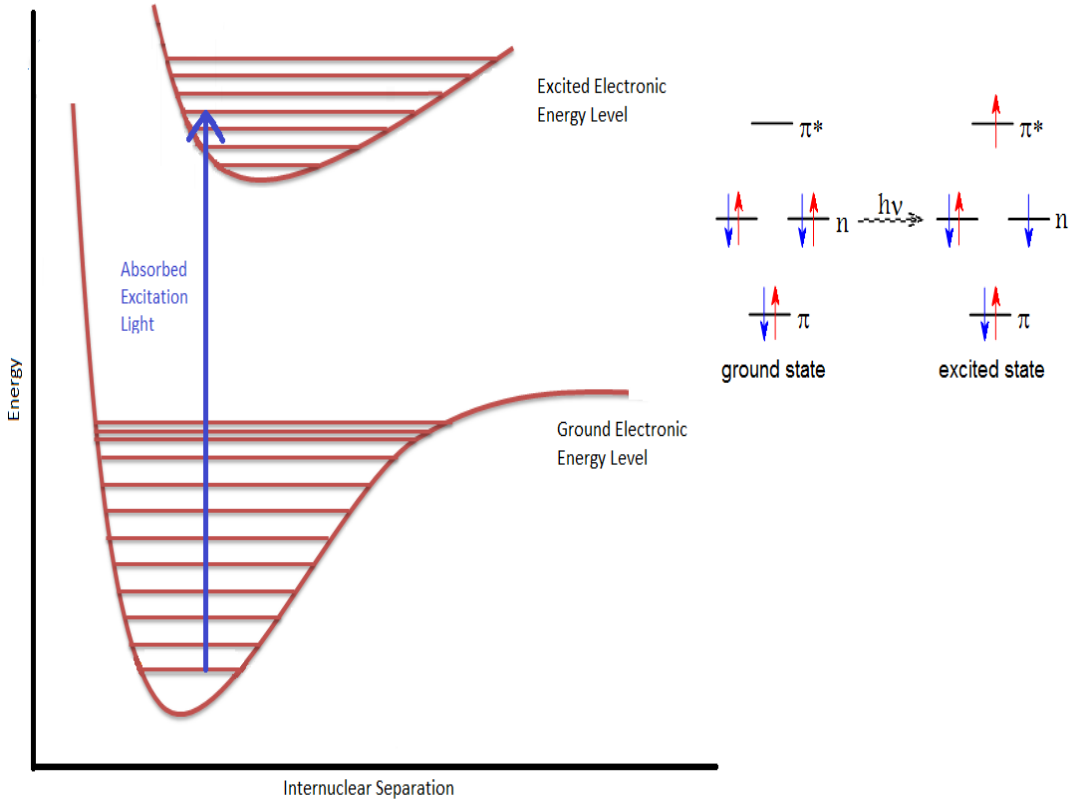

Figure 4. Physical basic of absorbance. An electron in the ground state is promoted to a higher energy level in the excited state by absorbing energy from a photonic source. The electron returns to the ground state as energy, in the form of heat, is lost in vibrational transition during collision with solvent and other molecules.

Each chemical structure absorbs light at slightly different wavelengths, allowing for precise measurements of electronic environments. One particularly useful wavelength in protein biochemistry is 280 nm, which is the wavelength where most aromatic amino acids, including tyrosine, absorb [84]. Although tyrosine is not the only amino acid responsible for absorption, when the protein is properly folded tyrosine is predominantly found at the surface.

Other aromatic amino acids, such as tryptophan, tend to be in the interior of the protein shielded away from the light. This general property of proteins can be utilized monitor folding. As the protein unfolds, tyrosine and to a lesser extent tryptophan are exposed causing an increase in ε and subsequently an increase in absorbance [84].

Fluorescence Spectroscopy

Typically, most excited electrons monitored via absorption spectroscopy return to the ground state by nonradiative transitions because the vibrational energy levels of the ground and excited states overlap [93]. Although this is the most common situation, in some compounds electrons in the excited state have other pathways to return to the ground state. One useful method is to excite using a specific wavelength that will result in the electron to return to the ground state via fluorescence [94]. This occurs when the ground and excited states do not overlap, and the electron is not able to lose all its energy via heat and collisions [92]. Once the excited electron reaches the lowest vibrational energy level of the excited state via a radionationless pathway, the electron will emit a photon at a longer wavelength (Figure 5) [95]. The 0 → 0 transition between the lowest vibrational level will result in a “mirror-image” of the emission and excitation spectra [93].

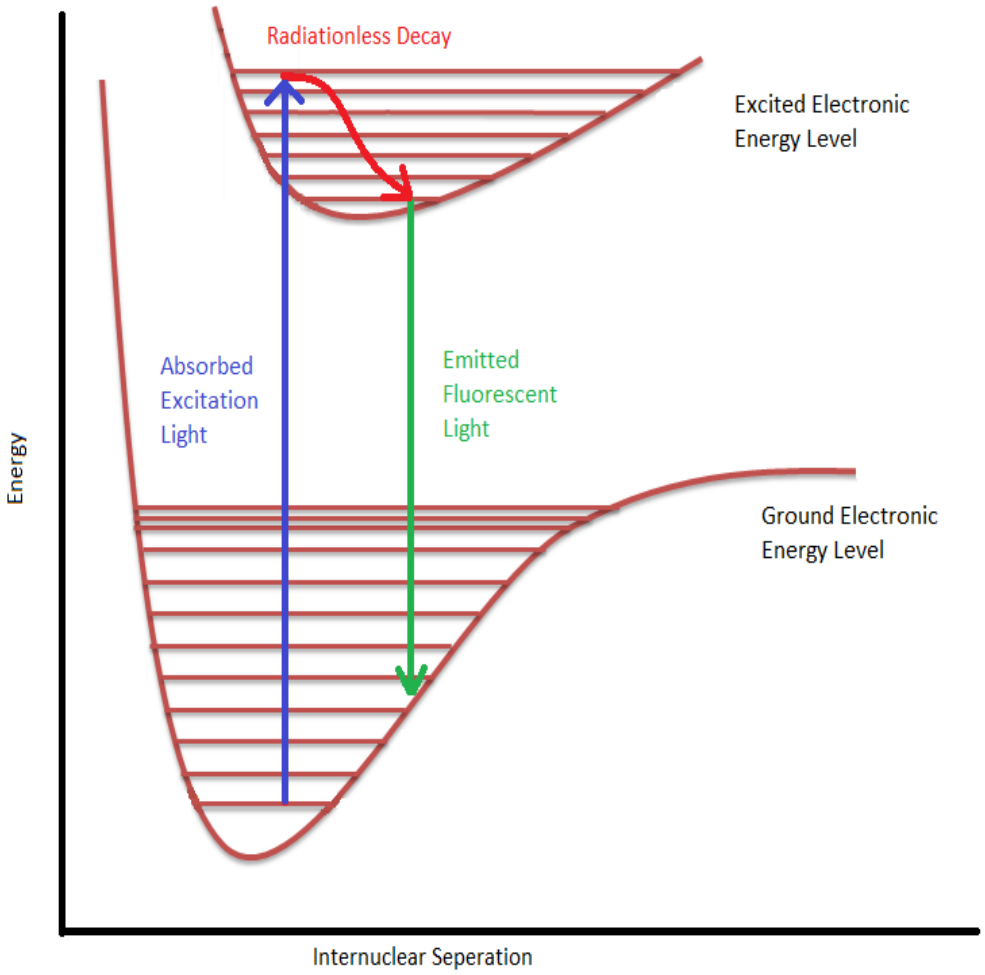

Figure 5. Fluorescence energy diagram. An electron in the ground state is promoted to a higher energy level in the excited state by absorbing energy from a photonic source. In the excited state, the electron loses energy in the form of heat, moving into lower vibrational energy levels. Once it reaches to the lowest vibrational energy level of the excited state, the electron returns to the ground state by releasing a photon, normally at a longer wavelength than absorbed.

Fluorescence spectroscopy holds several advantages over UV/Vis mainly due to its sensitivity. Only a small portion of the light energy originally absorbed is emitted via fluorescence [93]. This results in low background interference, improving the signal to noise ratio.

Fluorescence and Environmental Influences: Shifts in Wavelength

Weber and Laurence worked with numerous polycyclic aromatic compounds and found that, when in water, they were non-fluorescent. However, upon binding to serum albumin, they were highly fluorescent [96]. One of the aromatic compounds studied was 8-Anilinonaphthalene-1-sulfonic acid (ANS), a known extrinsic fluorophore used today to probe the environment of biological molecules through changes in hydrophobic regions [96]. Fluorophores, either natural or synthetic, are molecules that exhibit fluorescence. They are generally organic compounds that contain conjugated π-bonds [93]. Florescence spectroscopy is more sensitive to environmental effects than absorption because the addition of the radiationless depopulation is heavily influenced by solvent polarity [97, 98].

In general, an excited state is more polar than the ground state, therefore when ANS is in the presence of a polar solvent, the energy of the excited state is decreased, resulting in the emission spectra shifting towards longer wavelengths (Figure 6). Decreasing the polarity of results in a shift of the λ_{max} to lower wavelengths (blue shift) and an increase in fluorescence intensity in the emission spectrum [92, 98]. The blue shifts are best explained through the Planck relation: $E = h\nu$, which displays a direct relationship between energy (E) and frequency (ν). Since the speed of light (c), ν and wavelength (λ) are related by λν=c, the equation can also be expressed as $E = \frac{hc}{\lambda}$. Excited states have an electron density that is more distorted than in ground states. Thus, excited molecules are more inclined to interact with a polar environment so as to align the solvent dipoles and cause the emission spectrum to shift toward a higher λ_{max} (red shift) [92, 98]. The fluorescence intensity increases

as the polarity of the environment decreases because the rate of intersystem crossing is reduced in nonpolar solutions. The effects observed with ANS also occur with intrinsic chromophores such as Trp [99].

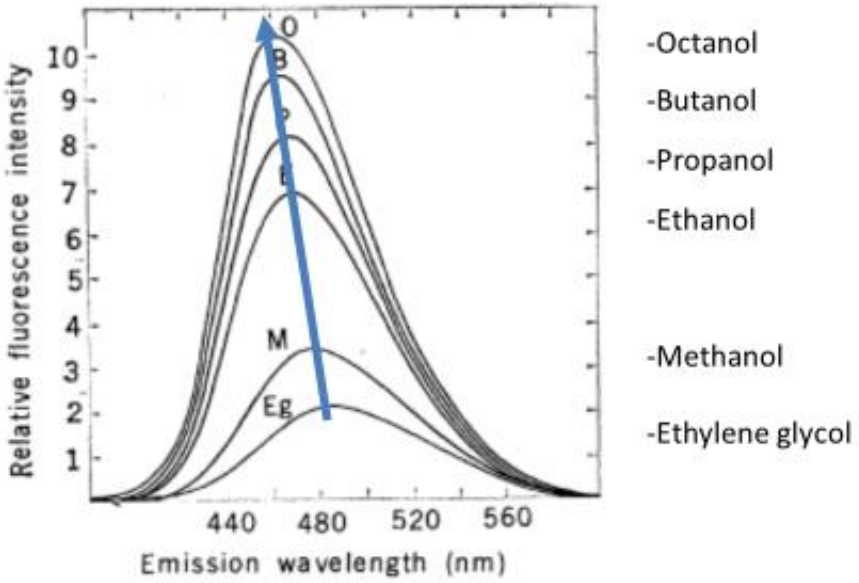

Stryer, L. Fluorescence Spectroscopy of Proteins. *Science* 1968: 526-533

Figure 6. Effect of an increase in the solvent polarity on the fluorescence intensity from the ANS fluorophore at λ_{max} and the blue shift.

Monitoring G_α Subunit Conformational Change

Utilizing these properties of fluorescence spectroscopy, Gilman and co – workers [100] established this technique as an indirect method to investigate G–protein activity. Unique to G-proteins is the fact that they contain a relatively large amount of Trp residues, e.g., $G_{s\alpha}$ contains four Trp residues located throughout the internal structure of the protein. The presence of Trp residues in most proteins is scarce and they typically provide a role of stability [101]. G_α subunits are unique in that the conformational changes that occur upon activation can be monitored through the change in the environment of the Trp residues. Trp154 in $G_{s\alpha}$ is located in the α –

helical domain, and Trp234, Trp277, and Trp281 are contained in the switch II region within the GTPase domain [22] (Figure 2). The addition of an activator, such as AlF_4^- (transition state analog) or GTPγS to G_α•GDP, results in a conformational change, which causes the burial of Trp residues [102, 103, 104]. The change in the Trp environment, from solvent exposed to one that is hydrophobic, causes an increase in the intrinsic tryptophan fluorescence of the protein [103, 104].

Chabre worked with the α – subunit of G_t and was able to determine that the increase in fluorescence observed upon activation came primarily from Trp207, which is the equivalent of Trp234 in $G_{s\alpha}$ [22, 105, 106]. $G_{t\alpha}$ contains two tryptophan residues, therefore, investigation of the mutant Trp207Phe led to the conclusion that Trp207 was the major contributor to the observed fluorescence. This work was built upon by Najor and co-workers by examining the $G_{i\alpha1}$ subunit. They found that Trp211, the counterpart to $G_{t\alpha}$ Trp207, was primarily responsible for the observed increase in fluorescence [107]. Because $G_{s\alpha}$ has four Trp residues, more than any G-protein previously studied, the contribution of each individual Trp towards the overall intrinsic fluorescence is much more complex.

Red-Shift and π-Cation Interaction

In addition to the increased fluorescence observed in $G_{t\alpha}$ conformational changes, Chabre was able to detect a shift of the λ_{max} to higher wavelengths (red-shift) in the emission spectra, contrary to what one would expect in a movement into a non-polar environment [105]. Hamm and co – workers [108] explained that the red-shift, also observed in $G_{i\alpha1}$, was a result of a change in the distances between R204 and W207 from 7.24 Å in the inactive conformation to 4.63 Å in the active.

The electrostatic interaction formed between the positively charged guanidinium group of Arg204 and with the π-electron system of Trp207, lowers the overall energy gap between the ground and exited states. The electronic distribution at the sp^2 hybridized carbon atom in the ring structure creates a partial positive charge around the outer edges and a partial negative charge at the center [101]. The interaction energy ranges from 1 – 5 kcal*mol^{-1} [109], and has been shown to be crucial for protein stability [110].

Circular Dichroism

Although powerful biophysical techniques, UV/Vis can probe the outer protein surface and fluorescence spectroscopy can give insight into localized environments, they both lack the ability to examine the secondary structure. Circular dichroism (CD) bridges this gap, enabling direct measurement of the secondary structure without disrupting non-covalent interactions [111]. Similar to the previous techniques, CD utilizes light absorbed by biomolecules, but unique to CD, the light is polarized [112]. Light can be described as an electric field vector that oscillates with a characteristic frequency [113]. When polarized, the frequency oscillates in a single plane [92, 114]. In the case of the CD two planes of rotating polarized light are used, one rotating right (R) and the other to the left (L) (Figure 7A) [84]. Molecules that are chiral interact differently with each plane of polarized light, changing the velocities of propagation of a light wave. This effect lowers the total R polarized light absorbed. When the planes are recombined, there is a difference reflected in the absorption of the L and R polarized light.

Biomolecules, such as proteins, which are composed of chiral L-amino acids (except for glycine) are extremely susceptible to this detection method. The optical activity of a protein is

the sum of the individual contributions from monomeric units interacting with each other, forming a polymeric arrangement [92, 114]. These arrangements, while complex, are composed of three basic structures (α helix, β-pleated sheets, and random coil) (Figure 7B and 7C), each producing unique spectra in the 190 nm to 240 nm wavelengths. While CD spectra shows a combination of all three spectra, with a comprehensive database, deconvolution of the spectra is possible, leading to the estimation of the percent secondary structure composition[92, 114].

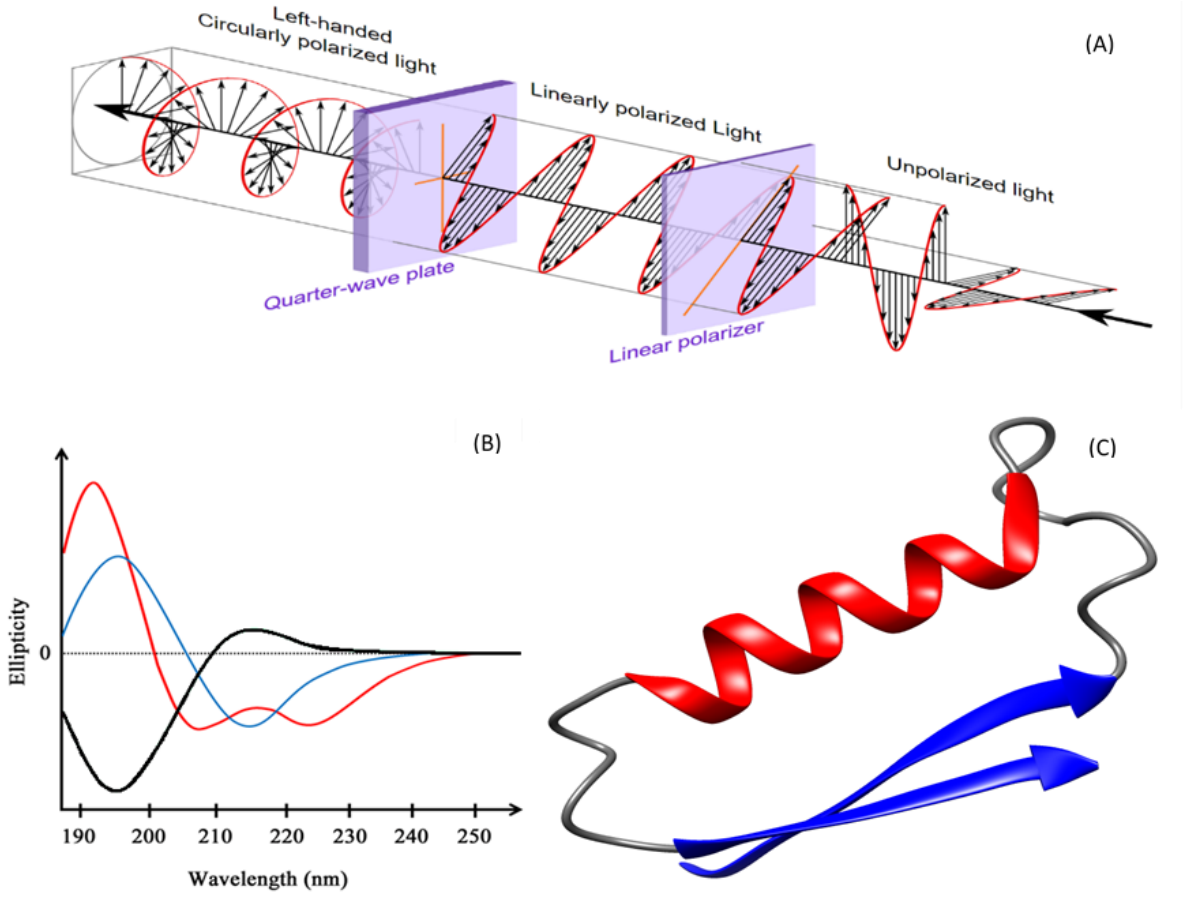

Figure 7. Circular polarized light generated from unpolarized light A) Circular polarized light generated from unpolarized light B) CD spectra representing three distinct secondary structures. The α helix (red) shows a distinct double hump, β-pleated sheets (blue) have a single valley, and the random coil (black) has a single hump. C.) Representation of three distinct structures described in 7B using the same color scheme.

Project Aims

G-proteins have been intensely studied over the years due to their role as signal transduction proteins. It is well understood that G-protein mutants are associated with several disease states, making them obvious targets for medical treatments and drug discovery. For improved drug design to occur, we need to expand our basic understanding of the system and differences that occur in the disease states. One particular question that needs to be addressed is the change of stability when the G-protein is in a diseased state.

The overarching goal of this dissertation is to further develop our understanding of the role that abnormalities in the structure of Gα subunits play in cancer. The structure of a protein is essential to its biological function. Occurrences of mutations in DNA manifest in changes in the amino acid sequence that can lead to a plethora of problems, such as misfolding, interference with effector sites, unwanted translational modifications, etc. Utilizing the combinations of temperature denaturation and molecular dynamics, we plan to study the consequences of these mutations. The specific aims of the work in this conducted in this dissertation are as follows: 1) probe the accessibility of buried Trp, solvent-exposed Tyr residues, as well as determine the secondary structure content of wild-type and Trp/Arg mutants under denaturation conditions; 2) investigate the π-cation interactions between Trp and Arg residues in G_{α} proteins as unfolding occurs; 3) ascertain how the oncogenic $G_{s\alpha}$ R231H mutation results in a decrease in signal transduction efficiency compared to wild-type.

The work discussed in this dissertation will investigate if the denaturation properties are unique of $G_{s\alpha}$ and how the oncogenic mutation $G_{s\alpha}$ R231H affects folding. This research will develop a stronger foundational understanding of the wild-type $G_{s\alpha}$ system as well as measure the structural destabilizing effects of the R231H mutation. Applying these ideas, we plan to study the effect of the R231H mutation on GTP hydrolysis by utilizing time-based intrinsic fluorescence spectroscopy and P_i formation. A comparison of the structural and functional properties of WT $G_{s\alpha}$ and R231H to those of WT $G_{i\alpha1}$ and R208Q was also conducted.

CHAPTER TWO

FOLDING OF G_α SUBUNITS: IMPLICATIONS FOR DISEASE STATES

Introduction

Guanine nucleotide binding proteins (G-proteins) represent a family of proteins involved in intricate networks of intercellular signaling. Heterotrimeric G-proteins are comprised of α, β, and γ subunits that interact with transmembrane G-protein coupled receptors (GPCR). Upon activation of a receptor by an extracellular stimulus, the α-subunit undergoes a conformational change that allows exchange of GDP for GTP with concurrent dissociation from the βγ-dimer and GPCR, and a further relay of a signal via an interaction with an intracellular effector. The signal terminates following hydrolysis of the bound GTP, thereby returning the α-subunit back to its inactive state and its re-association with the βγ heterodimer and the GPCR [10, 44, 115]. While there are four families of G_α proteins, we limited this study to $G_{i\alpha1}$ and $G_{s\alpha}$, which stimulate or inhibit the production of cAMP by regulating the activity of adenylyl cyclase (AC).

The crystal structures from $G_{i\alpha1}$ in the inactive GDP-bound conformation [116], as well as from the active states of both $G_{i\alpha1}$ [117] and $G_{s\alpha}$ [51] using GTPγS, a non-hydrolyzable GTP analogue, have been solved. The crystal structure of $G_{s\alpha}$ complexed with the target AC is also known [51]. G_α is composed of two domains: the α-helical domain and the GTPase domain. The α-helical domain consists of six α-helices that form a lid over the guanine nucleotide-binding site of the GTPase domain. The GTPase domain is composed of six-stranded β-sheets surrounded by five

α-helices, and, in addition to the nucleotide binding site, the GTPase domain also contains binding sites for the $G_{\beta\gamma}$ dimer and the GPCR. Also, in the GTPase domain are the switch regions known as switch I, switch II, and switch III that are located near the nucleotide-binding site. The switch regions undergo a drastic structural change when going from the inactive GDP-bound conformation to the active GTP-bound conformation [118]. In GDP-bound $G_{i\alpha1}$, switch II and switch III are disordered in the X-ray structure [42, 116], but, upon activation, they become ordered around the γ-phosphate of GTP [117].

Protein folding is a complicated and yet a surprisingly efficient event that is critical for protein viability. Protein folding is driven primarily by non-covalent interactions and proceeds through an energy landscape from its unfolded state to its native conformation [85, 119, 120, 121]. The free energy of the native state is lower than that of the unfolded protein, which is in equilibrium with molten globules that have a native-like structure. When a protein denatures, it does not go directly to a random coil, but rather to one of these molten globule states, which resemble the native state and may be able to bind a ligand and retain some activity [122, 123, 124]. Improper folding of the molten globules can have devastating consequences and is the cause of many diseases [80].

Hydrophobic interactions contribute the most toward protein stability, but other interactions such as hydrogen bonding and electrostatic interactions are important as well [51]. Tryptophan (W) residues are uncommon and play a key role in protein stability via hydrophobic interactions at the core of the protein. $G_{i\alpha1}$ contains three Trp residues while $G_{s\alpha}$ has four. The Trp residues in $G_{i\alpha1}$ are W131, W211, and W258 (depicted in cyan in Figure 8), which

respectively correspond to W154, W234, and W277 in $G_{s\alpha}$. There is an additional Trp residue in $G_{s\alpha}$, W281, that has no corresponding equivalent in $G_{i\alpha1}$. Gilman and co-workers [103, 104] reported that intrinsic Trp fluorescence could be used to investigate conformational changes in G_α proteins that occur during activation, because the fluorescence intensity increases when individual Trp residues move toward a more hydrophobic environment. Najor et al. [107] built upon this property to quantify the contribution of each Trp residue towards the overall fluorescence by using phenylalanine (F) mutants of $G_{i\alpha1}$. We explored this feature to determine the stability at the core of the protein by determining melting temperatures (T_m) from wild-type (WT) and Trp mutants of $G_{i\alpha1}$ and $G_{s\alpha}$. In addition, a π- cation interaction between W211 and R208 (W234 and R231 in $G_{s\alpha}$) is present in the active conformations of WT G_α proteins [108], which can be detected by red shifts in their fluorescence emission spectra. Disrupting the π-cation interaction may also have consequences for stability.

Both $G_{i\alpha1}$ and $G_{s\alpha}$ have an abundance of tyrosine (Y) residues (13 for $G_{i\alpha1}$ and 14 in $G_{s\alpha}$) (Figure 8) from which we can take advantage of the UV absorbance to determine the T_m values at the surface of the protein for WT and Trp mutants. Although Tyr as well as Trp residues absorb light at 280 nm, in both G_α proteins Tyr residues far outnumber Trp amino acids resulting in absorbance changes that are primarily dependent on Tyr residues. To obtain a more detailed picture of protein unfolding, we also used circular dichroism (CD) to monitor the secondary structure of the proteins.

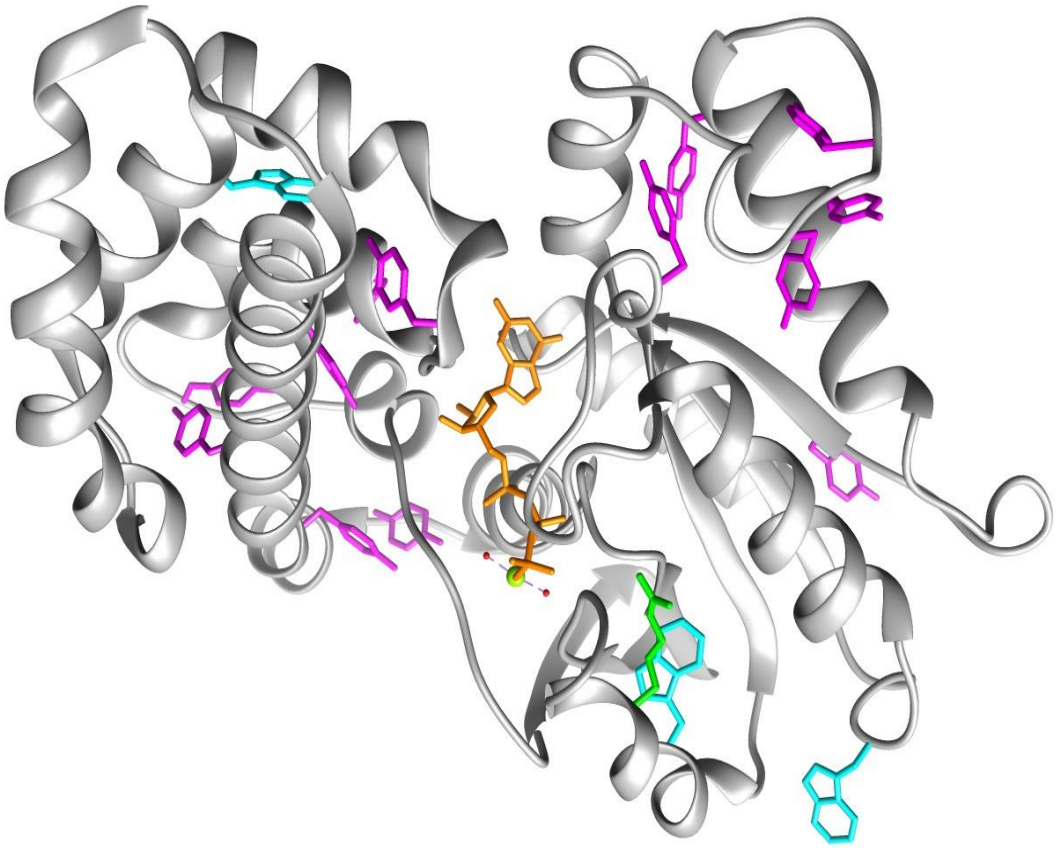

Figure 8. WT $G_{i\alpha1}$•GTPγS displaying its three tryptophan residues (cyan), thirteen tyrosine residues (purple), Arg208 (green), GTPγS bound nucleotide (orange), and Mg^{2+} (green sphere).

Protein stability is an important characteristic of protein function. G-protein signaling must be tightly regulated to ensure appropriate responses to extracellular stimuli. Improperly functioning G_α proteins have been implicated in many disease states, including McCune-Albright syndrome [125], bipolar disorder [126], and cancer [60, 127]. The focus of this study was to compare the stability of WT $G_{i\alpha1}$ and WT $G_{s\alpha}$ from different vantage points: from the inside core of the protein to its surface of the protein, and from an overview of the overall secondary structure. Secondly, we investigated the contribution of each Trp residue individually and

probed the interaction between one of them and the nearby arginine (R) and its effect on protein stability. To elucidate putative folding mechanisms in disease states, we utilized several biophysical techniques to probe the contributions of non-covalent interactions toward the stability of G_α proteins. Computational methods were also used to model the interactions.

Methods

Expression and Protein Purification

$G_{\alpha i1}$ and $G_{s\alpha}$ were obtained and purified as previously described [128]. Single-point Trp mutants of $G_{\alpha i1}$ and $G_{s\alpha}$ were prepared by site directed mutagenesis using a kit provided by Stratagene (La Jolla, CA). After purification on a Ni^{2+} affinity column followed by a Superdex 200-pg size exclusion column, the purity of GDP-bound G_α proteins was found to be greater than 95% as estimated by SDS – PAGE. Protein was stored at -80 °C in 20 mM Tris, pH 8.0 buffer containing 10% (v/v) glycerol, and 1 mM DTT.

Fluorescence Measurements of Protein Activation

Experiments were performed with a PTI Quanta Master fluorimeter (Photon Technologies, Inc., Mirmingham, NJ). Indirect activity assays were conducted with excitation and emission wavelengths set at 280 nm and 340 nm, respectively. Assays were initiated after 60 sec by addition of 20 µM of GTPγS to pre-incubated 400 nM G_α• GDP protein samples in buffer containing 50 mM HEPES, pH 7.5, 2 mM $MgSO_4$, and 1 mM DTT, and was monitored for 3 hrs at 25 °C. The GDP- and GTPγS- bound proteins that were characterized by the activity assays were used in the following denaturation studies.

Fluorescence-Measured Protein Denaturation

Emission spectra for both GDP- and GTPγS-bound proteins were recorded over the wavelength range of 300 to 400 nm with the excitation wavelength set at 280 nm. Signal integration time was 0.2 sec with the bandpass for excitation and for emission set at 5 nm. The denaturation experiments started at a temperature of 4 °C followed by 4 °C increments and concluding at the highest temperature before precipitation occurred. There was a 2 min equilibration period at each set temperature. All T_m values were calculated from fluorescence intensities at the spectral λ_{max} positions for the selected temperatures, using methods adapted from those previously described [129].

UV/Vis-Measured Protein Denaturation

The environments of Tyr (and to a lesser extent W) residues in G_α proteins were monitored on a Hewlett Packard UV – Vis spectrophotometer. All samples contained 50 mM Tris, pH 7.5, 1 µM G_α•GDP protein, 1 mM DTT, and 2 mM $MgSO_4$. Prior to initiating the experiments, samples were incubated with their respective nucleotide, 2.5 µM G_α•GDP or 20 µM GTPγS, at room temperature for 1 hr. The temperature was increased from 20 °C to 80°C, at 0.3 °C/min over 180 mins. For each temperature studied, samples were equilibrated for 1 min and the absorbance was monitored in the wavelength range of 220-300 nm. All melting temperatures were calculated from the absorbance values at 280 nm values for the different temperatures, using methods previously described [130].

CD-Measured Protein Denaturation

Experiments were performed using an Olis DSM 20 circular dichroism spectrophotometer. All samples were measured in a cylindrical quartz cuvette with a 1 mm pathlength and contained either 3 µM G_{α}•GDP or 24 µM G_{α}•GTPγS, in 10 mM phosphate, pH 7.5 buffer, 1 mM DTT, and 2 mM $MgSO_4$. Data were collected at 150 V every 1 nm in the wavelength range of 190 nm to 260 nm. The temperature was increased from 20 °C to 100 °C at 4 °C increments with an incubation time of 3 min at each temperature studied. The CONTIN LL algorithm with was used to deconvolute the spectra using reference sets with denatured proteins [131] to calculate the percent of each type of secondary structure and T_m values for each protein studied [132, 133].

Refolding of G_{α} Subunits

To test whether unfolding of G_{α} proteins was reversible, fluorescence emission scans and CD spectrophotometry were used. Once spectra from the final temperature of an unfolding experiment were obtained, G_{α} samples were cooled down in 8 °C increments and incubation times remained the same as indicated above for each respective technique. Final temperatures varied depending on aggregation and ability to refold. All renaturation experiments were stopped at 4 °C for fluorescence measurements and at 20 °C for CD experiments.

Molecular Modeling

The coordinates of GDP (1BOF,[42]) and GTPγS (1GIA, [117]) derivatives of $G_{i\alpha1}$, and GTPγS of $G_{s\alpha}$ (1AZT, [22]) were downloaded from the Protein Data Bank (PDB, [134]). Missing loops in the $G_{i\alpha1}$

structures were modeled using Swiss Model [135] and the corresponding transducin structures (1TAG,[136] , 1TAD, [137] and 1TND,[106]). The simulations were done using procedures previously described [107]. Unrestrained dynamics was run for 14 ns before the data were acquired for an additional 1 ns. The simulations were done at 37 °C (310 K) and 50 °C (328 K). These data were then used in the analyses. The initial Trp point mutation models were generated using VMD [138] and then subjected to the same equilibration procedure as the wild type structures. All molecular graphic diagrams were generated using VMD [138]. Pairwise Van der Waals and electrostatic interaction energies were calculated using NAMD [139]. The solvent accessible surface area (SASA) was measured with the SASA routine in VMD (32). The SASA values, and the van der Waals and electrostatic energy values presented in Table 5 were calculated for the final 1 ns in each simulation and then averaged.

Results

Fluorescence Emission Spectra of G_α Subunits

To calculate melting temperatures in both the active and inactive conformations of the WT proteins, we measured the changes in fluorescence intensity, resulting from increases in the solvent exposure of Trp residues. The amino acid F was chosen as a replacement for Trp because of its similar structure and size characteristics, as well as low quantum yield and distinct λ_{max} values [98, 107].

The fluorescence intensity of WT $G_{i\alpha1}$•GDP at 50 °C decreased by 53% when compared to that observed at 20 °C (Figure 9), and continued declining until 70 °C, at which point there was no change in intensity and the protein was fully unfolded. A transition midpoint (T_m) of

39 °C was calculated for WT $G_{i\alpha1}$•GDP, and the Trp mutants in the same conformation were not significantly different from the WT protein (Table 1). For $G_{s\alpha}$ in the GDP conformation, the T_m values for the WT protein were also not significantly different from all Trp mutants (Table 2).

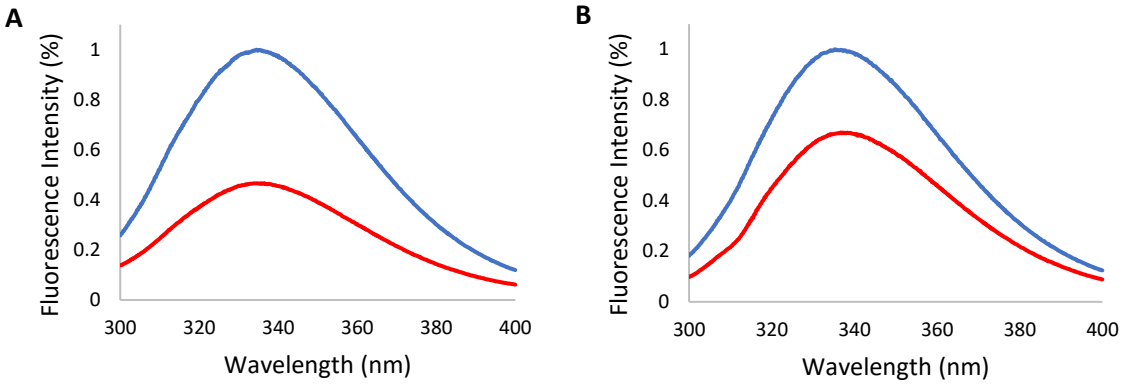

Figure 9. Intrinsic Trp florescence of WT Giα1 proteins. Emission spectra of 0.4 µM of WT $G_{i\alpha1}$•Mg^{2+} at 20 °C (blue) and 50 °C (red) in the A) GDP or B) GTPγS conformations.

Table 1. Estimated melting temperature (°C) for $G_{i\alpha1}$ proteins using three spectroscopic methods

	Fluorescence		UV/Vis		CD	
$G_{i\alpha1}$ variant	GDP	GTPγS	GDP	GTPγS	GDP	GTPγS
WT	39 ± 0.6	49 ± 2.0*	48 ± 0.1	67 ± 0.2*	44 ± 0.5	71 ± 2.2*
W211F	35 ± 1.8	37 ± 2.2†	47 ± 0.2	52 ± 2.8†	54 ± 1.7†	57 ± 0.1†
W131F	38 ± 0.7	52 ± 2.1*	50 ± 1.4	54 ± 3.0†	44 ± 1.1	71 ± 0.8*
W258F	42 ± 0.5	59 ± 1.7*†	46 ± 0.2	63 ± 0.5*†	50 ± 1.7†	68 ± 0.3*

$n \geq 3$; S.E.M. ≤ 3, for all measurements

* = $p \leq 0.05$ vs GDP-bound conformation

† = $p \leq 0.05$ vs WT in the same conformation

Table 2. Estimated melting temperature (°C) for $G_{s\alpha}$ proteins using three spectroscopic methods[1]

	Fluorescence		UV/Vis		CD	
$G_{s\alpha}$ variant	GDP	GTPγS	GDP	GTPγS	GDP	GTPγS
WT	41 ± 1.7	39 ± 1.0	54 ± 2.0	64 ± 1.5*	52 ± 1.4	57 ± 1.1*
W154F	45 ± 2.7	41 ± 2.1	53 ± 0.4	60 ± 0.8*	50 ± 1.1	57 ± 2.4*
W234F	40 ±1.8	33 ± 2.1†*	53 ± 1.0	57 ± 2.0†	51 ± 1.7	53 ± 1.5†
W277F	45 ± 0.6	46 ± 1.7†	51 ± 0.7	60 ± 1.1*	51 ± 1.7†	58 ± 0.8*
W281F	41 ± 1.1	40 ± 0.8	53 ± 1.5	62 ± 1.8*	54 ± 1.9	56 ± 0.9*

[1] $n \geq 3$; S.E.M. ≤ 3, for all measurements

* = $p \leq 0.05$ vs GDP-bound conformation

† = $p \leq 0.05$ vs WT in the same conformation

For the $G_{i\alpha1}$•GTPγS, the fluorescence intensity at 50 °C was 33% of that observed at 20 °C, indicating that the active conformation is more stable than the GDP-bound structure (Figure 9B). Apart from the W211F mutant, the T_m values for the other Trp $G_{i\alpha1}$ mutants in the $G_{i\alpha1}$•GTPγS conformation were also significantly higher than in the GDP conformation (Table 1). Interestingly, the WT $G_{i\alpha1}$•GTPγS showed only a 10 °C increase, while the W131F and W258 mutants in the GTPγS conformation were approximately 14 °C and 17 °C higher than their respective GDP conformations. The behavior of WT $G_{s\alpha}$•GTPγS and its activated mutants was the opposite of $G_{i\alpha1}$ proteins in the GTPγS conformation. Alignment of the protein sequences indicates that W234F in $G_{s\alpha}$ and W211F in $G_{i\alpha1}$ are both located in the switch II region. The W234F mutant was unique, because its T_m value in the GTPγS conformation (33 °C) was significantly lower than in the GDP conformation (40 °C) (Table 2), and the analogous mutation in $G_{i\alpha}$ (W211F) has essentially the same T_m in both the GDP and GTP bound forms (Table 1). The T_m values for WT $G_{s\alpha}$ and its W154F, W277F, and W281F mutants in the $G_{s\alpha}$•GTPγS conformation were not significantly different from their GDP counterparts.

π-Cation Interactions in G_α Subunits

To gain insight into the stability of the switch II region in WT $G_{i\alpha1}$, which coordinates with Mg^{2+} in the nucleotide binding pocket, we monitored the π-cation interaction between R208 and W211 that occurs upon activation from the GDP-bound to the GTPγS conformation. At 20 °C, the λ_{max} position exhibited a red shift of 3.5 nm (Figure 10A), which gradually decreased until 70 °C, at which point the instability of the GDP conformation prevented further measurements (Figure 10B). Similar changes in the value of the λ_{max} position were observed for the WT $G_{s\alpha}$ protein until around 53 °C, where it switched from a red to a blue shift (data not shown).

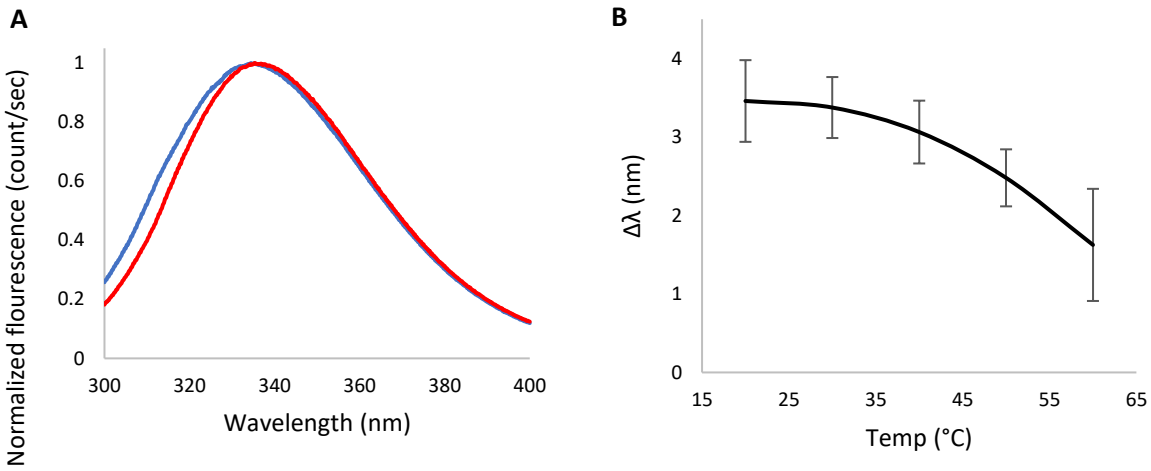

Figure 10. A) Normalized emission spectra of WT $G_{i\alpha1}$•GDP•Mg^{2+}before (blue) and after (red) activation with GTPγS at 20 °C ; B) Temperature variation of the difference between the λ_{max} values of the GTPγS and GDP conformations.

UV/Vis Absorption Spectra of G_α Subunits

A useful property of G_α proteins is that Trp residues move to the hydrophobic core of the protein upon activation [42]. Thus, the spectroscopic and thermal properties of these sites allow for probing the interior of G_α subunits by using fluorescence emission spectroscopy. By

contrast, Tyr residues are predominantly located at the surface of the G_{α} protein and are therefore useful for determining information on structural changes at or near the exterior of the protein [42]. As the protein unfolds, Trp residues begin to contribute toward the absorbance. Because Trp has an absorptivity that is 4 times larger than Tyr at 280 nm, Trp would contribute significantly toward the Δ_{abs} if it were not for the higher number of Tyr vs. Trp residues in $G_{i\alpha1}$ (3 vs. 13) and in $G_{s\alpha}$ (4 vs. 14). In contrast, Phe absorptivity is approximately 30-fold lower than that of Tyr and the λ_{max} is 257 nm, resulting in a negligible contribution toward absorbance at 280 nm.

An increase in absorbance intensity at 280 nm, which was associated with Tyr residues becoming more solvent exposed, was observed at temperatures above 44 °C for WT $G_{i\alpha1}$•GDP. The melting curve for $G_{i\alpha1}$ in the GTPγS form was shifted to the right of the GDP conformation (Figure 11A). A T_m value of 48 °C was calculated for WT $G_{i\alpha1}$•GDP and 54 °C for WT $G_{s\alpha}$•GDP, and, for the Trp mutants, the T_m values were not significantly different from their WT GDP counterparts (Tables 1 and 2). For the GTPγS conformations, the T_m values for WT $G_{i\alpha1}$ and WT $G_{s\alpha}$ were significantly higher than for the GDP counterparts, but were not significantly different for proteins in which the Trp residue involved in a π-cation interaction was mutated to Phe, i.e., W211F for $G_{i\alpha1}$ and W234F for $G_{s\alpha}$ (Tables 1 and 2).

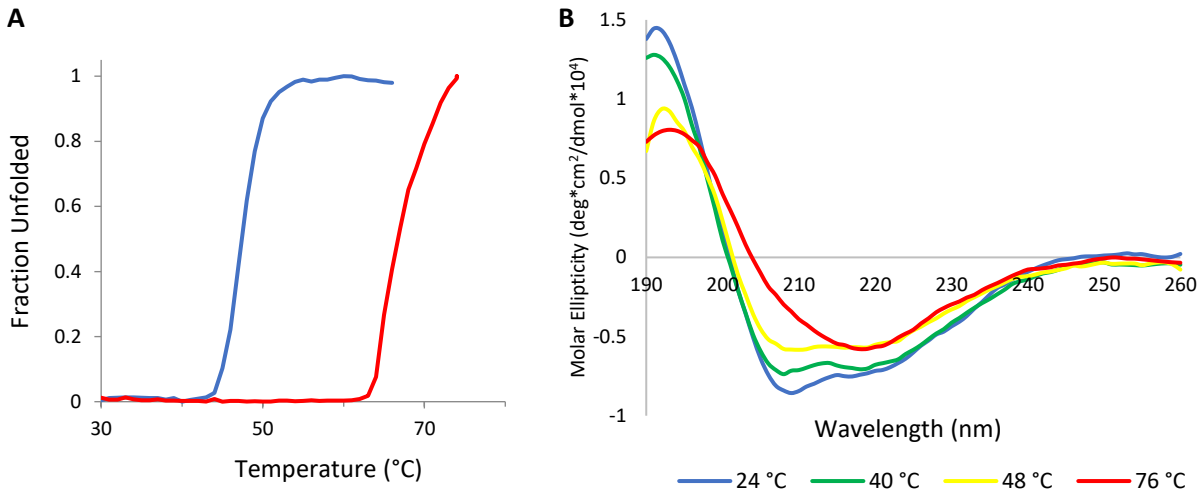

Figure 11. Temperature dependence of the absorption spectra. A) Absorption spectra of 2.5 µM WT $G_{i\alpha1}$•Mg^{2+} in the GDP (blue) and GTPγS (red) conformations, and of the B) CD spectra of 1.0 µM WT $G_{i\alpha1}$•GDP•Mg^{2+}

Temperature-Dependence of the Secondary Structure of G_α Subunits

At 20 °C, the CD spectra of WT $G_{i\alpha1}$•GDP (Table 3) and of WT $G_{s\alpha}$•GDP (Table 4) were indicative of proteins that have secondary structures rich in α– helix (40% and 36%, respectively). The percent of α-helix that we observed for WT $G_{i\alpha1}$•GDP was in agreement with that also reported by others using CD (43%) [140], which is less than in the reported structure deposited in the PDB (47%) [42]. As the temperature increased, the CD absorbance intensity at 190 nm decreased, while the minima at 205 nm and 222 nm, which are signatures of α–helix, converged to a new minimum at 215 nm (Figure 11).

The data in Table 3 indicated that, regardless of the conformation, WT $G_{i\alpha1}$ initially was predominantly α–helical, but, at higher temperatures, it became increasingly dominated by β-strands and to a lesser extent by random coil. By comparison, WT $G_{s\alpha}$ in both conformations

had less α–helical and turn content but more random coil and had a less dramatic α/β temperature-induced conversion (Table 4). A CD-determined T_m value of 44 °C was calculated for WT $G_{i\alpha1}$•GDP, while the W211F mutant afforded the highest T_m value (Table 2). Experiments with WT $G_{i\alpha1}$•GDP at temperatures greater than 64 °C did not exhibit significant changes in the CD spectra, with the protein eventually precipitating out of solution at 84 °C. Apart from the W211F mutant, WT and Trp mutants of $G_{i\alpha1}$ in the GTPγS conformation withstood temperatures near 100 °C without precipitation.

Table 3. Composition of WT $G_{i\alpha1}$ secondary structure at various temperatures[1,2,3]

	GDP				GTPγS			
T (°C)	α	β	RC[4]	T[4]	α	β	RC[4]	T[4]
20	40	19	26	17	44	12	26	18
40	35	24	24	17	42	14	24	20
52	27	25	27	20	42	13	25	20
64	22	29	29	21	39	16	24	21
80	18	32	28	21	23	26	26	24
92	-	-	-	-	22	36	51	21

[1] n ≥ 3; S.E.M ≤ 3
[2] All numbers reported as percentages
[3] Hyphens denote temperatures at which proteins denatured
[4] RC and T stand for random coil and turns

At 80 °C, the secondary structure of WT $G_{i\alpha1}$ protein in the active conformation had at least an additional 5% of α–helix content compared with the GDP conformation (Table 3). Except for the $G_{s\alpha}$ W234F and W211F $G_{i\alpha1}$ mutants, the T_m values for the active conformations of WT $G_{s\alpha}$ and the remaining Trp mutants are significantly higher than for the inactive forms. The CD-determined T_m values for the inactive and active conformations of W234F $G_{s\alpha}$ and

W211F $G_{i\alpha1}$ are not significantly different, and the T_m value for the active conformations are significantly lower when compared to the WT proteins (Table 1).

Table 4. Composition of WT $G_{s\alpha}$ secondary structure at various temperatures[1,2,3]

	GDP				GTPγS			
T (°C)	α	β	RC[4]	T[4]	α	β	RC[4]	T[4]
20	36	18	33	13	37	16	33	13
40	30	22	34	14	33	20	34	13
52	29	24	34	13	31	20	35	14
64	28	25	34	13	26	24	36	14
80	25	27	35	13	20	27	39	14

[1] *n* ≥ 3; S.E.M ≤ 3 for all measurements
[2] All numbers reported as percentages
[3] Hyphens denote temperatures at which proteins denatured
[4] RC and T stand for random coil and turns

Refolding

We have also investigated the ability of G_α subunits to refold after completion of the denaturation process. A decrease in temperature was accompanied by an increase in fluorescence intensity indicating that the Trp residues were refolding into hydrophobic environments, as demonstrated for WT $G_{i\alpha1}$•GTPγS (Figure 12A). Refolding WT $G_{i\alpha1}$•GDP from 96 °C to 4 °C exhibited no significant increase in fluorescence; however, upon renaturation from 48 °C, the observed increase in the fluorescence intensity indicated a refolding recovery of 21% (Figure 12B). When refolding from 32 °C, which is less than the fluorescence-determined T_m value of 39 °C (Table 1), WT $G_{i\alpha1}$•GDP exhibited the largest recovery (72%).

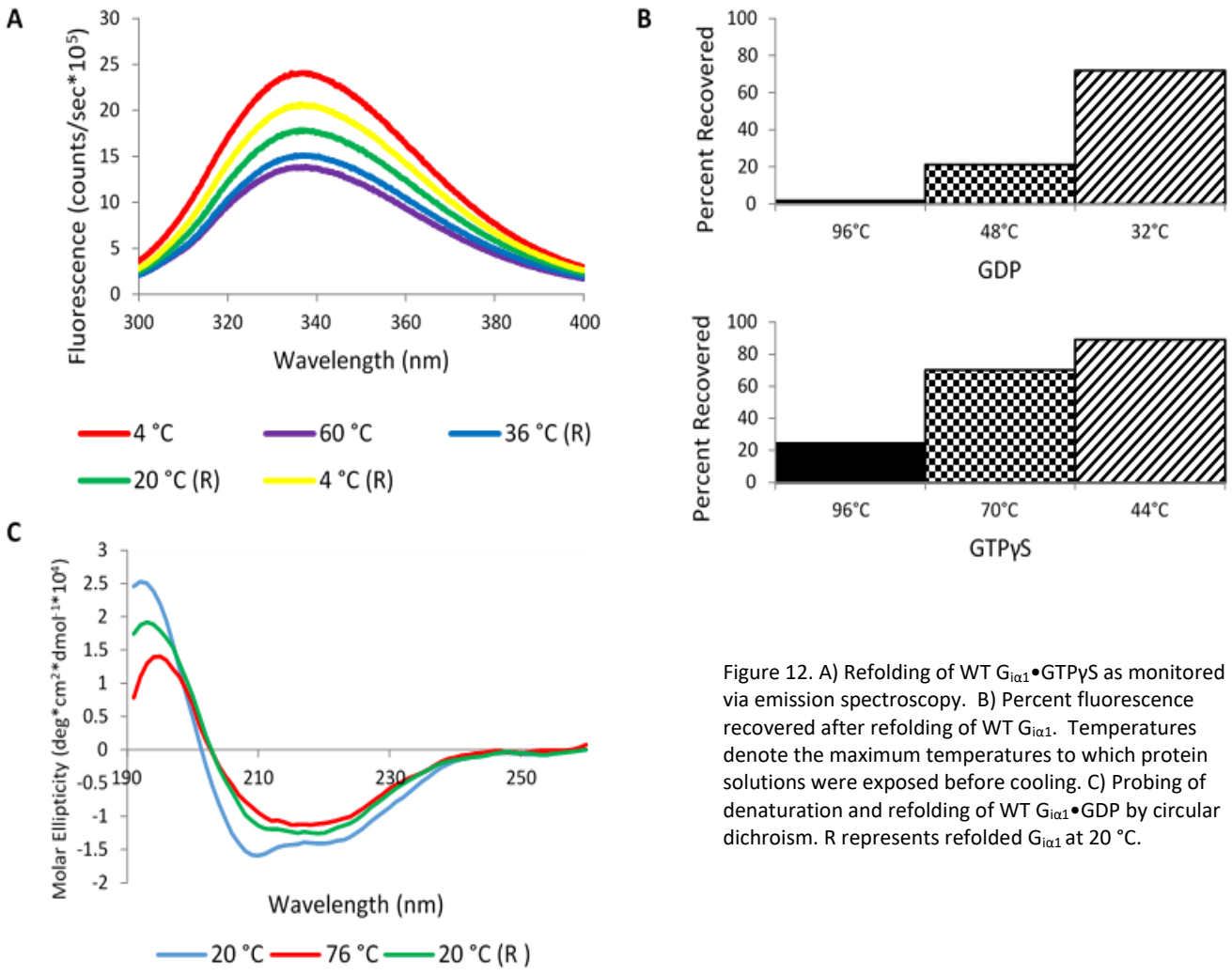

Figure 12. A) Refolding of WT $G_{i\alpha1}$•GTPγS as monitored via emission spectroscopy. B) Percent fluorescence recovered after refolding of WT $G_{i\alpha1}$. Temperatures denote the maximum temperatures to which protein solutions were exposed before cooling. C) Probing of denaturation and refolding of WT $G_{i\alpha1}$•GDP by circular dichroism. R represents refolded $G_{i\alpha1}$ at 20 °C.

Unlike WT $G_{i\alpha1}$●GDP, the GTPγS conformation experienced increases in fluorescence intensity even when refolding was initiated from 96 °C, i.e., at temperatures larger than the T_m (Figure 12 and Table 1). These observations demonstrate that the ability of G_α subunits to refold is nucleotide dependent. Although this is the case for both G_α proteins, WT $G_{i\alpha1}$ was able to recover the most folded structure compared to WT $G_{s\alpha}$ (spectra not shown). Such traits were

drawn out by fluorescence spectra of WT $G_{i\alpha1}$•GTPγS that revealed a 76% recovery after denaturation at temperatures up to 70 °C. By contrast, we found that WT $G_{s\alpha}$•GTPγS only recovered 30% of its folded structure after denaturation at temperatures ≤ 84 °C. In addition, WT $G_{s\alpha}$•GDP precipitated at temperatures less than 80 °C during renaturation.

CD was also used to monitor the reversibility of protein unfolding. As shown in Figure 12, when WT $G_{i\alpha1}$•GDP was cooled from 76 °C to 20 °C, there was a concomitant increase in the spectral intensity at 190 nm and a decrease at 222 nm. Spectral deconvolution showed that, at 80 °C, WT $G_{i\alpha1}$•GDP consisted primarily of 18% α-helices and 32% β–sheets (Table 3), but when the protein refolding occurs as the temperature is lowered to 20 °C, an increased the α-helical content to 31%, while the percentage of β–sheets decreased to 18%. Terminating the denaturation process at 52 °C rather than at 76 °C resulted in recovery of 88% of the original α–helical structure. Similar effects were observed with WT $G_{i\alpha1}$•GTPγS. Although this conformation was more resistant to unfolding as evidenced by an initial 44% α – helical content at 20 °C (Table 3), 93% of which was recovered when refolding from 76 °C to 20 °C.

Discussion

Protein stability is critical for biological function. Our study focused on characterizing the non-covalent interactions that contribute to the stability of G_α proteins and to the reformation of the protein structure after unfolding. Surprisingly, given the importance of G_α proteins, there has been few studies of their stabilities [141, 142].

A comparison of the WT $G_{i\alpha1}$ crystal structures in the GDP and GTPγS conformations [42, 117] reveals that the GDP -bound structure has a larger surface area than the active GTPγS

conformation. One would predict that, compared to the GDP form, a denser folding profile for the GTPγS conformation of WT $G_{i\alpha1}$ would result in a more stable structure, as evidenced by the higher T_m values calculated from fluorescence emission, tyrosine absorption and CD spectra, as well as from the larger interaction energies calculated for the GTP-bound protein (Table 2 and Table 1). This conclusion is also supported by SASA calculations for WT $G_{i\alpha1}$ indicating that protein activation resulted in a 2.6% decrease in overall solvent exposure (19,520 $Å^2$ for GDP-bound protein vs. 19,010 $Å^2$ for the active conformation). Therefore, WT $G_{i\alpha1}$•GTPγS is more stable, thus requiring more energy to unfold.

Utilizing Trp→ Phe single point mutations, we followed the unfolding by measuring the temperature dependence of the fluorescence emission spectra of nine G_α proteins (WT and three Trp mutants of $G_{i\alpha1}$, and WT and four Trp mutants of $G_{s\alpha}$) in the inactive GDP and active GTPγS conformations. Because burial of Trp residues in hydrophobic pockets is known to result in an increase in ΔF_{max} [143], protein unfolding is accompanied by a decrease in fluorescence intensity. In the GDP forms (Table 2), the fluorescence-measured T_m values for WT $G_{i\alpha1}$ were not significantly different ($p < 0.1$) from its Trp mutants. Except for the W211F mutant, the T_m values were however significantly smaller than for the active WT $G_{i\alpha1}$, W131F, and W258F proteins ($p < 0.01$). The GTPγS conformation of the W211F mutant proved to be the least stable of all the active $G_{i\alpha1}$ proteins and displayed a fluorescence-derived T_m value similar to its GDP conformation (Table 2), which is the opposite of the general trend of higher melting temperatures observed for the GTPγS conformations. The difference in the interaction energies for the GDP and GTP found during the molecular dynamics simulations was smaller for

the W211F than for the WT which might contribute to the active conformation of this mutant being less stable.

Unlike WT $G_{i\alpha1}$ for which crystal structures are known for the inactive and active conformations [42, 117], only the structure of WT $G_{s\alpha}$•GTPγS has been published [22], precluding an explanation of protein stability based on compactness or differences in GTP and GDP interaction energies with the protein. The fluorescence-derived data in Table 1 indicate that WT $G_{s\alpha}$ and its mutants do not follow the same folding pattern as for $G_{i\alpha1}$. For T_m values calculated from fluorescence spectra, there is no significant difference between the active and inactive conformations of WT $G_{s\alpha}$ and of its W154F, W277F and W281F mutants suggesting that, with the exception of W234F $G_{s\alpha}$, stability of the protein structure around the Trp residues in $G_{s\alpha}$ is different from $G_{i\alpha1}$ (Figure 13). Time-based emission assay monitoring percent change in intrinsic tryptophan fluorescence of (A) WT $G_{s\alpha}$ and (B) WT $G_{i\alpha1}$ and their respective Trp mutents after the addition of GTPγS shows that, at room temperature, the ΔF_{max} values were significantly lower for WT $G_{s\alpha}$ relative to WT $G_{i\alpha1}$. Since ΔF_{max} is a result of Trp movement, this trend suggests that, after activation, a smaller displacement of the Trp residues occurs in $G_{s\alpha}$ compared to $G_{i\alpha1}$. Therefore, unlike WT $G_{i\alpha1}$, the Trp residues in the GDP conformation of WT $G_{s\alpha}$ are relatively protected in hydrophobic environments, presumably accounting for the insignificant difference between the T_m values from WT $G_{s\alpha}$•GTPγS and WT $G_{s\alpha}$•GDP (Table 1). The insignificant differences between the T_m values from the active and inactive conformations of the W154F, W277F and W281F mutants of $G_{s\alpha}$ are likely to have the same origin.

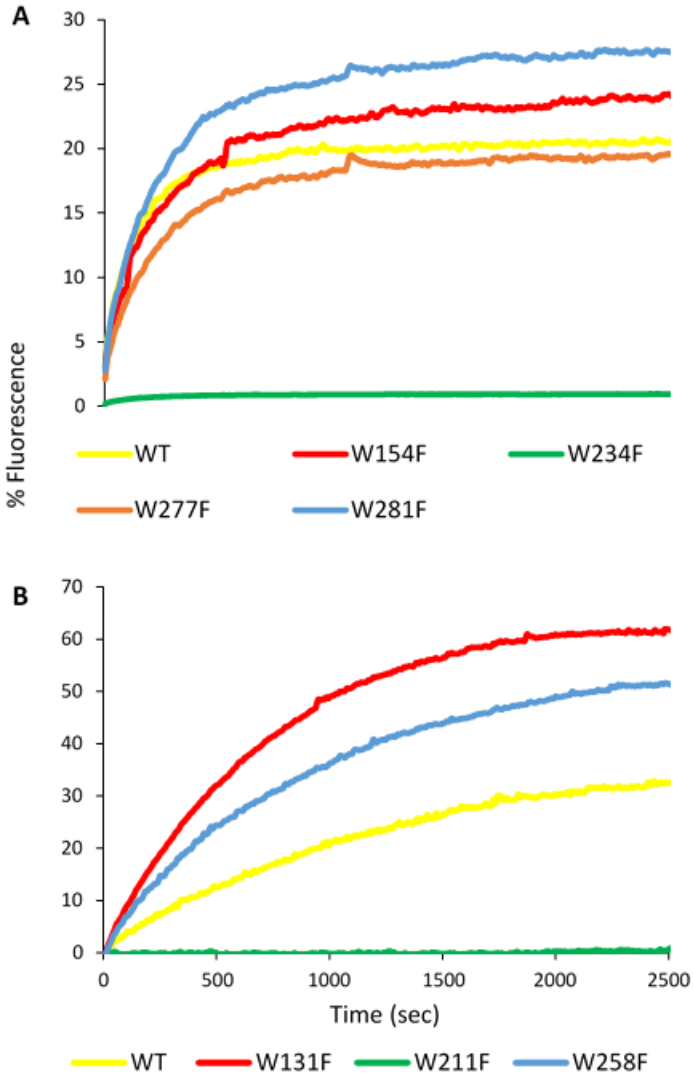

Figure 13. Time-based emission assay monitoring percent change in intrinsic tryptophan fluorescence of (A) WT $G_{s\alpha}$ and (B) WT $G_{i\alpha1}$ and their respective Trp mutents after the addition of GTPγS.

The W211F mutant of $G_{i\alpha1}$ and the W234F mutant of $G_{s\alpha}$ do not show detectable changes in ΔF_{max} (Figure 13, panels A and B). The W211 residue in WT $G_{i\alpha1}$ has been shown to have the largest difference in solvent accessibility between the inactive and active conformations, and therefore contributes the most toward ΔF_{max} [107]. Not surprisingly, for the

W211F mutant of $G_{i\alpha1}$, no ΔF_{max} is observed (Figure 13B). Similarly, the W234 residue in $G_{s\alpha}$ likely undergoes a similar large decrease in solvent accessibility during the course of the conformational change, as evidenced by the negligible ΔF_{max} observed in the W234F mutant (Figure 13A). The fluorescence-derived T_m values for the W211F mutant of $G_{i\alpha1}$ are not statistically different in the two conformations (Table 2), presumably because of the absence of the W211-R208 cation-π interaction. Interestingly, the T_m value for the W234F mutant is significantly lower than for WT $G_{s\alpha}$ (Table 2).

The secondary structure of WT $G_{i\alpha1}$ proved to be the most stable in its GTPγS form relative to the GDP conformation (Table 2). At 20 °C and upon binding of GTPγS, we identified a 4% increase in the α–helical content of WT $G_{i\alpha1}$ (Table 3), but not for WT $G_{s\alpha}$ (Table 4). Activation of WT $G_{i\alpha1}$ creates a hydrophobic pocket via folding of the switch regions [42], resulting in a protein that has an ordered secondary structure with an increased α- helical content [116]. The smaller ΔF_{max} observed for activation of WT $G_{s\alpha}$ relative to WT $G_{i\alpha1}$ (Figure 13) may be related to a smaller change in the secondary structure of WT $G_{s\alpha}$. In either conformation, as the temperature increased, the α-helical content of both WT G_{α} proteins was reduced and the subunits became richer in β–sheet while the random coil and turn structures were not altered significantly from the native form. We have done molecular dynamics simulations of the thermal unfolding of the monomeric G_{α} proteins and have not observed an increase in β-sheet, although the amount of α-helix decreased. These simulations may indicate that the β-sheet increase is due to aggregation.

A shift in secondary structure from primarily α-helices to β-sheets poses an increased risk for protein aggregation that may lead to amyloidogenesis [80]. Amyloid fibril formation occurs when unfolded, native-like proteins aggregate into long filaments of packed β – sheets [87, 144, 145]. Many debilitating neurodegenerative diseases, such as Parkinson's, Creutzfeldt-Jakob's, and Alzheimer's, have been proposed to arise from the accumulation of amyloid fibrils in the brain or in the central nervous system [80]. *In vitro* studies have shown that it is not uncommon for proteins to form amyloid fibrils under denaturing conditions [146, 147]. Furthermore, fibril formation has been shown to inhibit refolding into the native conformation [148].

The -absorbance assays helped visualize the global unfolding of G_{α} subunits from another perspective. The T_m values for WT $G_{i\alpha1}$ that were calculated from the absorbance of Tyr residues, which are dispersed on the protein surface, correlate with the unfolding process (Figure 4A). UV/Vis experiments with $G_{i\alpha1}$ showed that the protein surface in the GTPγS conformation to be significantly more stable than the Trp microenvironments, while the CD-determined values indicated that the surface unfolded before the secondary structure (Table 2). In the case of WT $G_{s\alpha}$•GTPγS, the UV/Vis-calculated T_m value was the highest compared to those derived from the other measurements, indicating that the surface of the WT $G_{s\alpha}$ is the last to unfold (Table 1). In the W211F mutant of $G_{i\alpha1}$ and in the W234F mutant of $G_{s\alpha}$, no significant difference between the T_m values was observed upon activation. One possibility is that π-cation interactions involving W211 in $G_{i\alpha1}$ and W234 in $G_{s\alpha}$ affect unfolding proximal to Tyr residues. π-cation interactions are found in many proteins [149, 150]. They are known to contribute significantly to thermal stability [110, 151]. The average energy for W-cation interactions

is -2.9 ± 1.4 kcal/mol [110, 151]. For the W154F, W277F and W281F mutants of $G_{s\alpha}$, the UV/Vis-determined T_m values were significantly higher for the active conformations. For $G_{i\alpha1}$, however, only the W258F mutant was stabilized, suggesting a distinct folding pattern for the two G_α subunits in each conformation.

We have examined the thermal denaturation of the G_α proteins using three different optical probes: absorbance, fluorescence and CD. These probes primarily measure changes in the environments of Tyr residues or Trp residues or the secondary structure, respectively. Since they give different T_m values for the same protein (Table 1 and Table 2), the denaturation of both Gα proteins appears to be multi-state rather than two-state [152]. The differences in T_m values in G_α that were observed by different methods may be rationalized via an analysis of the hydrophobic interactions, which are fundamental folding determinants for all proteins. Non-covalent interactions underpin the driving forces in protein folding. The observed T_m values suggest that denaturation of the active conformation of $G_{i\alpha1}$ starts near W131 and W258 microenvironments, and then propagates outward through the protein surface where the Tyr residue proximal to W258 is located, and at this point of unfolding leaving the secondary structure intact. Additional heating results in the conversion of α-helixes into β-sheets and random coil, possibly involving aggregation until precipitation occurs. In contrast, denaturation of the active conformation of $G_{s\alpha}$ initiates equally around all Trp residues, continuing to the secondary structure, and is completed near the Tyr residues.

The robustness and resistance of a protein to misfolding minimize the chances for disease. The reversibility of folding observed with WT $G_{i\alpha1}$ via fluorescence emission and CD

(Figure 12A and 12C) can therefore shed important light on the misfolding of G_α subunits. During the course of denaturation, a protein may develop multiple intermediate conformations, or molten globule states, which are reflected by the different T_m values obtained by the three techniques [153]. The fluorescence spectra monitored, to a significant degree, the polarity changes surrounding the Trp sites. Oscillations of the non-polar side chains at these sites would generate molten globules with relatively low thermal energies. These movements would account for the lower T_m values calculated from fluorescence measurements, compared to those obtained with the other two spectroscopic probes. Multiple Tyr residues, which may be involved in hydrogen bonding, are distributed throughout G_α. Once protein unfolding is initiated, molten globule states that are populated will exhibit diminished secondary structure, which is determined by hydrogen bonding. The additional contribution of hydrogen bonding associated with Tyr microenvironments and secondary structure relative to primarily hydrophobic interactions present in the vicinities of Trp residues may explain the higher T_m values measured from Tyr absorption and CD spectra.

Previous work by Najor et al. [107] and Hamm and coworkers [108] showed that W211 forms a π-cation interaction with R208 in WT $G_{i\alpha1}$•GTPγS, as evidenced by a red shift of 2.5 nm in the λ_{max} value (Figure 13A). Molecular dynamic simulations predict that the conformational change from the inactive to the active conformation results in an increase in the electrostatic interaction between W211 and R208 from -0.96 kcal/mol to -2.85 kcal/mol, which is consistent with the higher stability seen in the active conformation (Table 5). Thus, stronger ligand-protein interactions would help stabilize the GTPγS-bound structure. Molecular dynamics studies

showed that the interaction energy between GTP and $G_{i\alpha1}$ at 323K (-621.7 kcal/mol) indicated that it GTP binds more tightly than GDP (-494.4 kcal/mol). This binding energy partially may explain why the GTP-bound structure refolds better.

Table 5. Interaction energies between R208 and W211 for $G_{i\alpha1}$ WT

Temperature	GDP		GTP		Δ (GTP-GDP)	
	Electrostatic	VDW	Electrostatic	VDW	Electrostatic	VDW
37 °C	-0.96	-3.38	-2.85	-4.38	-1.89	-1.00
50 °C	0.33	-2.16	-1.38	-4.61	-1.71	-2.45
Δ (50 °C - 37 °C)	1.29	1.22	1.47	-0.23	0.18	-1.45

S.E.M. ≤ 3.0
*Values are in kcal/mol

An increase in temperature at which the simulation was conducted (37 °C → 50 °C) resulted in weakening of the W211-R208 π-cation interaction, which is supported by the observed decrease in the $\Delta\lambda_{max}$ (Figure 13B). The increased Van der Waals interactions calculated at higher temperatures may be associated with these residues swinging into more hydrophilic environments upon unfolding. This conclusion is supported by a blue (rather than red) shift observed upon the GTPγS activation of $G_{s\alpha}$ at temperatures higher than 53 °C. For the W211F mutant of $G_{i\alpha1}$, there was no significant difference between the T_m values from the active and inactive conformations further suggesting that the π-cation interaction is important for the structural integrity of $G_{i\alpha1}$.

This study underscores the importance of π-cation interactions toward protein stability. The disruption of these non-covalent interactions may lead to significant decreases in the stabilities for the active conformations of G_α subunits and could promote improper folding. Mutations of the arginine residue involved in the π-cation interaction have been identified in

the R208Q $G_{i\alpha1}$ and in the R231H $G_{s\alpha}$ oncogenes [127], and are thought to have similar characteristics as the Trp mutants. The loss of the π-cation interaction could translate in changes in structure-function relationships by disrupting the signaling cascade for cAMP. Future studies will focus on the effect of these mutations on the structure and function of oncogenic G_α subunits.

CHAPTER THREE

FOLDING OF ONCOGENIC ARGININE MUTATIONS IN $G_{\alpha i1}$ AND $G_{\alpha s}$ PROTEINS

Introduction

Guanine nucleotide-binding proteins (G-proteins) are regulatory membrane bound proteins that play an indispensable role in transferring extracellular information across the cell membrane to affect intracellular events. G-proteins are heterotrimeric in that they are composed of an α subunit (G_α), which regulates the activity of the effector protein, and a βγ subunit complex [115]. Inactive G_α subunits are complexed with G-protein coupled receptors, that, once activated by specific ligands, induce conformational changes in the G_α subunits, which prompt the exchange of guanosine 5'-diphosphate (GDP) for guanosine 5'-triphosphate (GTP) and the dissociation of the βγ dimer [5, 6, 7]. An α-subunit regulates the appropriate enzyme through direct contact. This process is self-regulated, with hydrolysis of bound GTP to GDP effectively deactivating G_α and reforming the heterotrimeric G-protein [5].

G-proteins are involved in stimulus-sensitive signal transduction pathways that have been fine tuned to allow the cell to respond to changes in the environment. Disruptions in this balance may lead to disease states. While there are several families of G_α proteins [154], we limited this study to $G_{i\alpha1}$ and $G_{s\alpha}$, which regulate the activity of adenylyl cyclase (AC) (Figure 14) [155]. $G_{s\alpha}$, encoded by the *GNAS* gene, up-regulates the synthesis of the secondary messenger cyclic AMP, and the *GNAI1* gene that encodes for $G_{i\alpha1}$, decreases the concentration of cAMP [48].

GNAS mutations are linked to several cancers, such as adenomas and/or carcinomas in the thyroid and large intestine, the pituitary and adrenal glands, the biliary tract and the pancreas, and in the central nervous system [60, 127]. Mutations in *GNAI1*, on the other hand, are associated with carcinomas in the large intestine, and are found in hematopoietic and lymphoid tissue, and in the upper digestive tract [60]. The mutations in *GNAS* and in *GNAI1* genes, in which several are contact points with AC, have been detected in 4.2% and 0.4% of tumors found in humans respectively [60, 71].

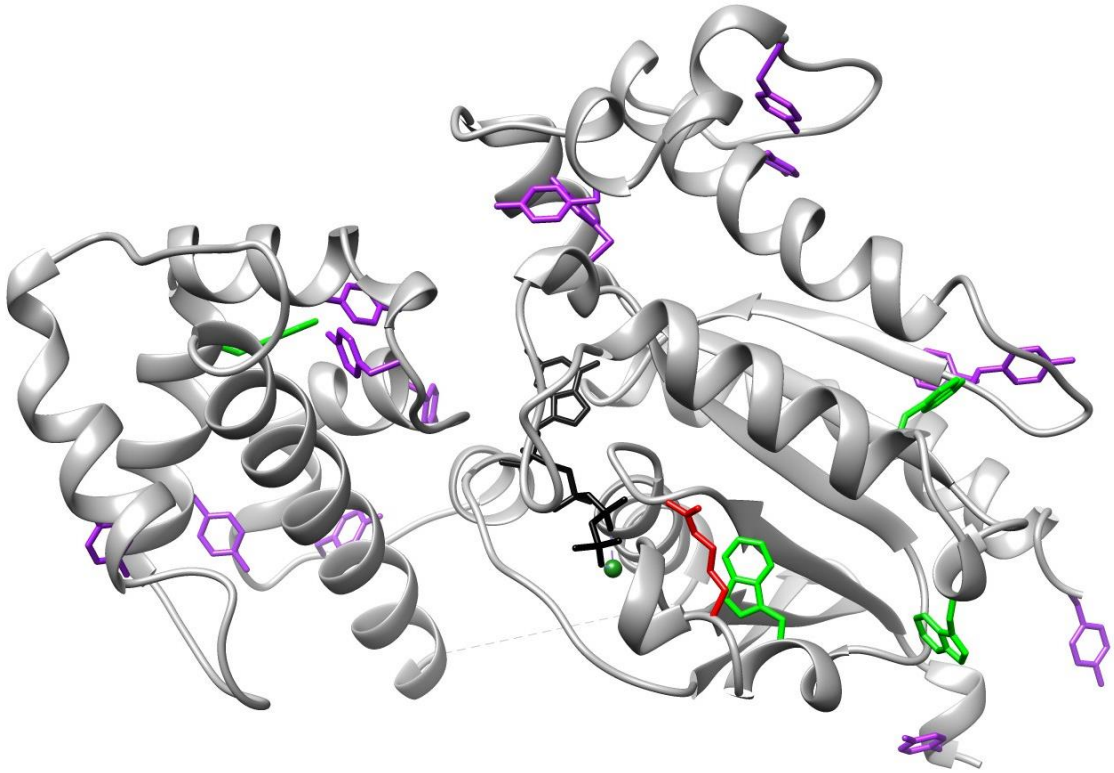

Figure 14. Crystal structure of WT $G_{s\alpha}$•GTPγS displaying its four tryptophan residues (green), fourteen tyrosine residues (purple), GTPγS bound nucleotide (black), Mg^{2+} (green sphere), and R231 (red) that is involved in a π-cation interaction with W234 (PDB ID: 1AZT).

One mutation of interest involves an arginine located close to a tryptophan in the conserved switch II region of G_α subunits [13, 22, 42]. Figure 1 shows that the guanidinium group of R231 in $G_{s\alpha}$ (R208 in $G_{i\alpha1}$) is involved in a π-cation interaction with the indole ring of W234 $G_{s\alpha}$ (W211 in $G_{i\alpha1}$), when the protein is in the active conformation [23, 106, 108, 136]. The oncogenic mutations, R231H in $G_{s\alpha}$ and R208Q in $G_{i\alpha1}$, disrupt this interaction, which has been shown to be crucial for protein stability [110]. Furthermore, it has been reported that the R231H $G_{s\alpha}$ mutation results in a decrease in cAMP production [79], although the mechanism of action is unknown. Loss of the π-cation interaction could cause changes in the secondary structure by altering the points of contact between G_α subunits and AC. Alternatively, these mutations could cause changes in the positions of residues vital to GTPase activity.

The focus of this study is to gain an understanding of the structural differences on the protein stability of the oncogenic R231H in $G_{s\alpha}$ and R208Q in $G_{i\alpha1}$ mutants. Several biophysical spectroscopic techniques was used for monitoring temperature-induced denaturation. Our results indicate that the Arg mutations that resulted in the loss of the π-cation interaction were not evident in the secondary structures at room temperature, but a decrease in protein stability was observed at higher temperatures. Computational methods were used to interpret the structural variations in the WT $G_{s\alpha}$ and $G_{i\alpha1}$ proteins and their corresponding mutants.

Methods

Expression and Protein Purification

$G_{\alpha i1}$ and $G_{s\alpha}$ were obtained and purified as previously described [107, 128]. Single-point Arg mutants of $G_{\alpha i1}$ and $G_{s\alpha}$ were prepared by site directed mutagenesis using a kit provided by Stratagene (La Jolla, CA). After purification on a Ni^{2+} affinity column followed by a Superdex 200-pg size exclusion column, the purity of GDP-bound G_{α} proteins was found to be greater than 95% as estimated by SDS – PAGE. Protein was stored at -80 °C in 20 mM Tris, pH 8.0 buffer containing 10% (v/v) glycerol, and 1 mM DTT.

Fluorescence Monitored GTPγS Exchange

Experiments were performed with a PTI QuantaMaster fluorimeter (Photon Technologies, Inc., Mirmingham, NJ). Indirect activity assays were conducted with excitation and emission wavelengths set at 280 nm and 340 nm, respectively. Assays were initiated after 60 sec by addition of 20 μM of GTPγS to pre-incubated 400 nM G_{α}• GDP protein samples in buffer containing 50 mM HEPES, pH 7.5, 2 mM $MgSO_4$, and 1 mM DTT, and was monitored for 3 hrs at 25 °C. The GDP- and GTPγS- bound proteins that were characterized by the activity assays were used in the following denaturation studies.

Fluorescence-Measured Protein Denaturation

Emission spectra for both GDP- and GTPγS-bound proteins were recorded over the wavelength range of 300 to 400 nm with the excitation wavelength set at 280 nm. Signal integration time was 0.2 sec with the bandpass for excitation and for emission set at 5 nm. The denaturation experiments started at a temperature of 4 °C followed by 4 °C increments and

concluding at the highest temperature before precipitation occurred. There was a 2 min equilibration period at each set temperature. All T_m values were calculated from fluorescence intensities at the spectral λ_{max} positions for the selected temperatures, using methods adapted from those previously described [129].

UV/Vis-Measured Protein Denaturation

The environments of Y (and to a lesser extent W) residues in G_α proteins were monitored on a Hewlett Packard UV – Vis spectrophotometer. All samples contained 50 mM Tris, pH 7.5, 1 µM G_α•GDP protein, 1 mM DTT, and 2 mM $MgSO_4$. Prior to initiating the experiments, samples were incubated with their respective nucleotide, 2.5 µM G_α•GDP or 20 µM GTPγS, at room temperature for 1 hr. The temperature was increased from 20 °C to 80°C, at 0.3 °C/min over 180 mins. For each temperature studied, samples were equilibrated for 1 min and the absorbance was monitored in the wavelength range of 220 – 300 nm. All melting temperatures were calculated from the absorbance values at 280 nm values for the different temperatures, using methods previously described [130].

CD-Measured Protein Denaturation

Experiments were performed using an Olis DSM 20 circular dichroism spectrophotometer. All samples were placed in a cylindrical quartz cuvette with a 1 mm pathlength and contained either 3 µM G_α•GDP or 24 µM G_α•GTPγS, in 10 mM phosphate, pH 7.5 buffer, 1 mM DTT, and 2 mM $MgSO_4$. Data were collected at 150 V every 1 nm in the wavelength range of 190 nm to 260 nm. The temperature was increased from 20 °C to 100 °C at 4 °C increments with an incubation time of 3 min at each temperature studied. The CONTIN LL

algorithm with was used to deconvolute the spectra using reference sets with denatured proteins [131] to calculate the percent of each type of secondary structure and T_m values for each protein studied [132, 133].

Results and Discussion

The π-Cation Interaction in Gα Subunits

It is well known that the Trp located in the switch II region of G_α proteins is responsible for an increase in the fluorescence intensity of 30-45 % [107, 108] because, when activated, the switch II Trp moves into a more hydrophobic microenvironment [104, 107, 156]. Additionally, a red-shift was detected when comparing the differences in wavelengths at maximal emission intensities (λ_{max}) of the WT $G_{s\alpha}$ and its R231H mutant in the GDP and GTPγS conformations (Figure 15A). The red-shift was a result from a π-cation interaction between the positively charged guanidinium group of R231 in $G_{s\alpha}$ (R208 in $G_{i\alpha1}$) with the π-electron system of W234 $G_{s\alpha}$ (W211 in $G_{i\alpha1}$) [107, 108]. Red-shifts of 3.1 ± 0.3 nm and 3.45 ± 1.0 nm were determined at 20 °C for WT $G_{s\alpha}$ and WT $G_{i\alpha1}$, respectively (Figure 15B and Figure 16). The red-shift for WT $G_{s\alpha}$ gradually decreased up to 52 °C, after which it became a blue-shift until precipitation occurred at 68 °C. This observation signifies that the electrostatic interaction between W234 and R231 weakens as the protein unfolds and severs at higher temperatures resulting in a blue-shift. The R231H $G_{s\alpha}$ mutation afforded a $\Delta\lambda_{max}$ value of 1.6 ± 0.2 nm (blue-shift) at 20 °C, revealing a disruption of the π-cation interaction when compared to the WT $G_{s\alpha}$ (Figure 15B). R231H $G_{s\alpha}$ is missing the positive charge of the Arg residue, thus the π-electrons of Trp234 can no longer form electrostatic interactions and instead move into a hydrophobic pocket after activation. With an

increase in temperature, the $\Delta\lambda_{max}$ value of the R231H $G_{s\alpha}$ mutant did not change significantly until R231H $G_{s\alpha}$•GDP precipitated 72 °C, indicating that Trp234 does not form new interactions with other charged residues in the switch II region during thermal denaturation.

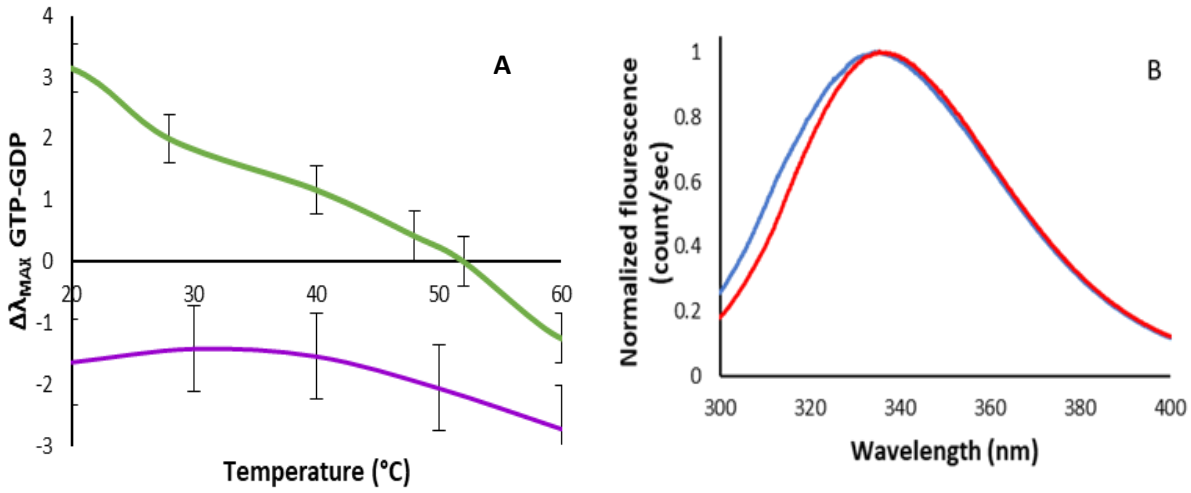

Figure 15. A) Normalized emission spectra of WT $G_{s\alpha}$•GDP•Mg^{2+}before (blue) and after (red) activation with GTPγS at 20 °C (n ≥ 3); B) Temperature variation of the difference between the λ_{max} values of the GTPγS and GDP conformations of carious WT $G_{s\alpha}$ (green) and $G_{s\alpha}$ R231H (purple) (n ≥ 3).

Similar to the WT $G_{s\alpha}$ protein, the red-shift of WT $G_{i\alpha1}$ decreased as the temperature increased, but it did not become blue-shifted (Figure 16). The differences in the two systems could be attributed to the increased stability of the WT $G_{i\alpha1}$•GTPγS protein compared to WT $G_{s\alpha}$•GTPγS (Chapter Two). The greater stability would require higher temperatures to disrupt non-covalent interactions, protecting the π-cation interaction in the active conformation of WT $G_{i\alpha1}$. As for the behavior of the R231H mutant described above, a temperature-dependent decrease in the magnitude of the blue-shift would be expected for the R208Q $G_{i\alpha1}$ mutant. However, a red-shift of 1.7 ± 0.7 nm was observed at 20 °C. The red-shift gradually declined to a

negligible $\Delta\lambda_{max}$ value of 0.3 ± 0.8 nm until denaturation occurred at 60 °C (Figure 16). The measured red-shift at 20 °C was unexpected, indicating the presence of another interaction mechanism for stabilization of π-electrons that was absent in the WT $G_{i\alpha1}$, R208Q $G_{i\alpha1}$, and $G_{s\alpha}$ systems.

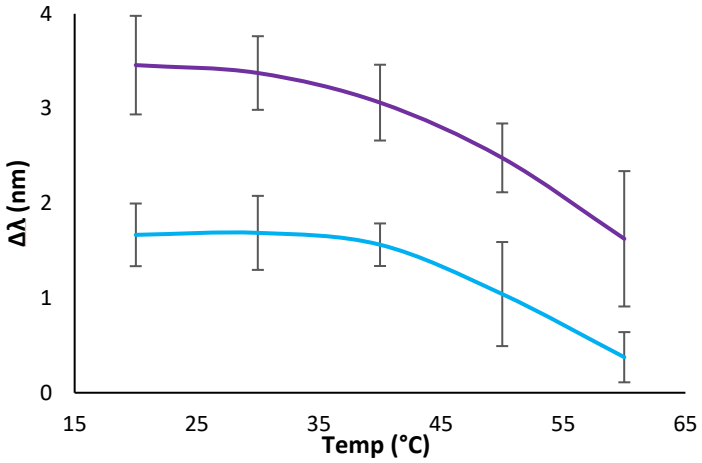

Figure 16. Temperature variation of the difference between the λ_{max} values of the GTPγS and GDP conformations for WT $G_{i\alpha1}$ (purple) and $G_{i\alpha1}$ Arg208Gln (blue) (n ≥ 3).

To investigate this possibility, we simulated the structures of WT and R208Q $G_{i\alpha1}$ in both conformations and compared the relative positions of the corresponding residues. Utilizing these models, we calculated the differences in the GTP and GDP conformations electrostatic interaction energy between the W211 and the R208 residues to be -3.98 kcal/mol for WT $G_{i\alpha1}$ (Table 1). For the R208Q mutation, the electrostatic interaction energy decreased to -0.84 kcal/mol (Table 6) indicating that, because there is a weaker interaction with W211, the red-shift is unlikely due to an interaction between these residues [157]. Further examination revealed that, for the mutant, Q208 mutation has a weaker electrostatic interaction with E245 (-1.22

kcal/mol) at the end of the α3 helix, than R208 in WT $G_{i\alpha1}$•GTPγS (-79.75 kcal/mol), thus perturbing both the α3 helix and the switch II region [158]. These disruptions propagate outwards towards F215 and orient it into a position that can interact with F199. A small T-oriented π-π stacking with Van der Waals interaction energy of -1.59 kcal/mol is formed in the active conformation, which is not found in the WT $G_{s\alpha}$, R231H $G_{s\alpha}$, and WT $G_{i\alpha1}$ systems (Figure 17).

Table 6. Calculated interaction energies (kcal/mol) within residues from the WT $G_{i\alpha1}$ and Arg mutants

	Electrostatic		VdW		Total		Distances	
	WT	R208Q	WT	R208Q	WT	R208Q	WT	R208Q
W211-R208(Q)	-3.98	-0.84	-6.24	0.99	-10.22	0.15	4.42	6.13
R208(Q)-E245	-79.75	-1.22	2.28	0.04	-77.47	-1.18	2.61	5.07
F215-F199	0.04	-0.01	-0.16	-1.59	-0.12	-1.60	8.93	4.83
W258-F259	1.90	-1.05	-0.16	-0.27	1.73	-1.31	6.05	5.20

Calculated interaction are in kcal/mol

Distances measured in Å

In addition to calculating interactions energies (Table 6), surface area solvent accessibility (SASA) values (Table 7) were also determined to gain insight into the interactions in these proteins. The SASA value for W211 in WT $G_{i\alpha1}$ was -121 $Å^2$ compared to -57 $Å^2$ in R208Q, but for W258, it decreased to -98 $Å^2$ in the R208Q protein from -37 $Å^2$ in the WT $G_{i\alpha1}$ (Table 7). Therefore, as an interaction between F199 and F215 is formed during activation, a gap opens up between the switch II region and α3 helix, allowing water to enter, thereby reducing the contribution of W211 the fluorescence intensity as measured by an increase in SASA. The changes in SASA values indicate that W258 becomes the primary contributor towards fluorescence intensity at 350 nm as well as explains the lower intensity observed in the R208Q mutant (Figure 18). Only in the R208Q protein, the W258 residue interacts with F259 in a π-π

interaction. In WT and R208Q $G_{i\alpha1}$ proteins, the calculated total interaction energies are 1.74 and -1.32 kcal/mol, respectively (Table 5). Therefore, when W258 in the R208Q moves into a hydrophobic environment, a red-shift is predicted as observed at 20 °C (Figure 16).

Table 7. Change in SASA (Å^2) exposure of W residues in WT $G_{i\alpha1}$ and R208Q mutant

	WT	R208Q
W211	-121	-57
W258	-37	-98

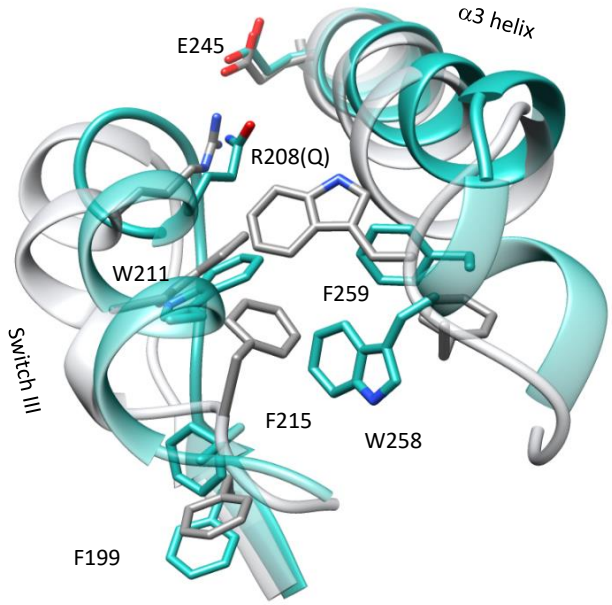

Figure 17. Movement of residue interactions in WT $G_{i\alpha1}$ (gray) and R208Q (green) as a result of the disruption of π-cation interaction.

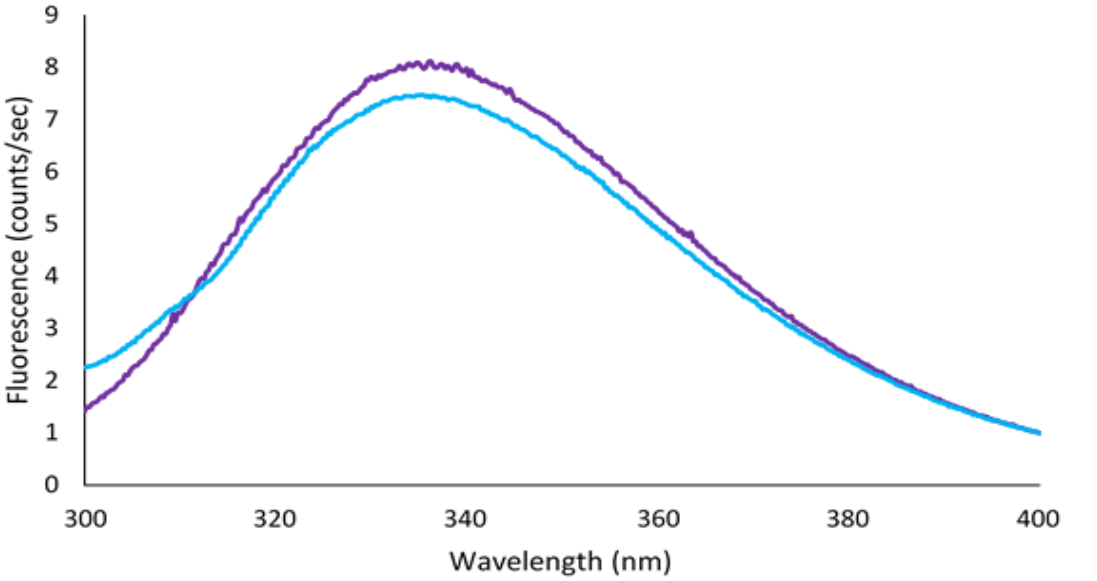

Figure 18. Emission spectra of WT (purple) and R208Q (blue) $G_{i\alpha1}$ proteins in the GTPγS conformation

Temperature Denaturation of Gα Proteins

π-cation interactions are well known to contribute to protein stability and previous experiments suggest that disruptions in mutants can propagate through networks of non-covalent interactions [110, 150, 159, 160]. To gain a complete picture of the impact of disrupting π-cation interactions, thermal denaturation experiments were used to test the structural stability of the WT and mutant proteins. The melting temperatures (T_m) values were estimated for the active and inactive conformations of the Arg mutants and compared to the respective WT proteins. Denaturation was measured *via* the changes in fluorescence intensity and UV absorbance resulting from changes in the solvent exposure of Trp and from Tyr residues, and from the change in the percent secondary structure.

Solvent exposure of Trp residues

The fluorescence emission spectra profile of the oncogenic mutants was measured between 20 - 80 °C. The decrease in fluorescence intensity due to the exposure of Trp to increasingly hydrophilic environments during unfolding was used to estimate melting temperatures for WT $G_{i\alpha1}$, WT $G_{s\alpha}$, R231H $G_{s\alpha}$, and R208Q $G_{i\alpha1}$ proteins (Figure 19A, Table 8).

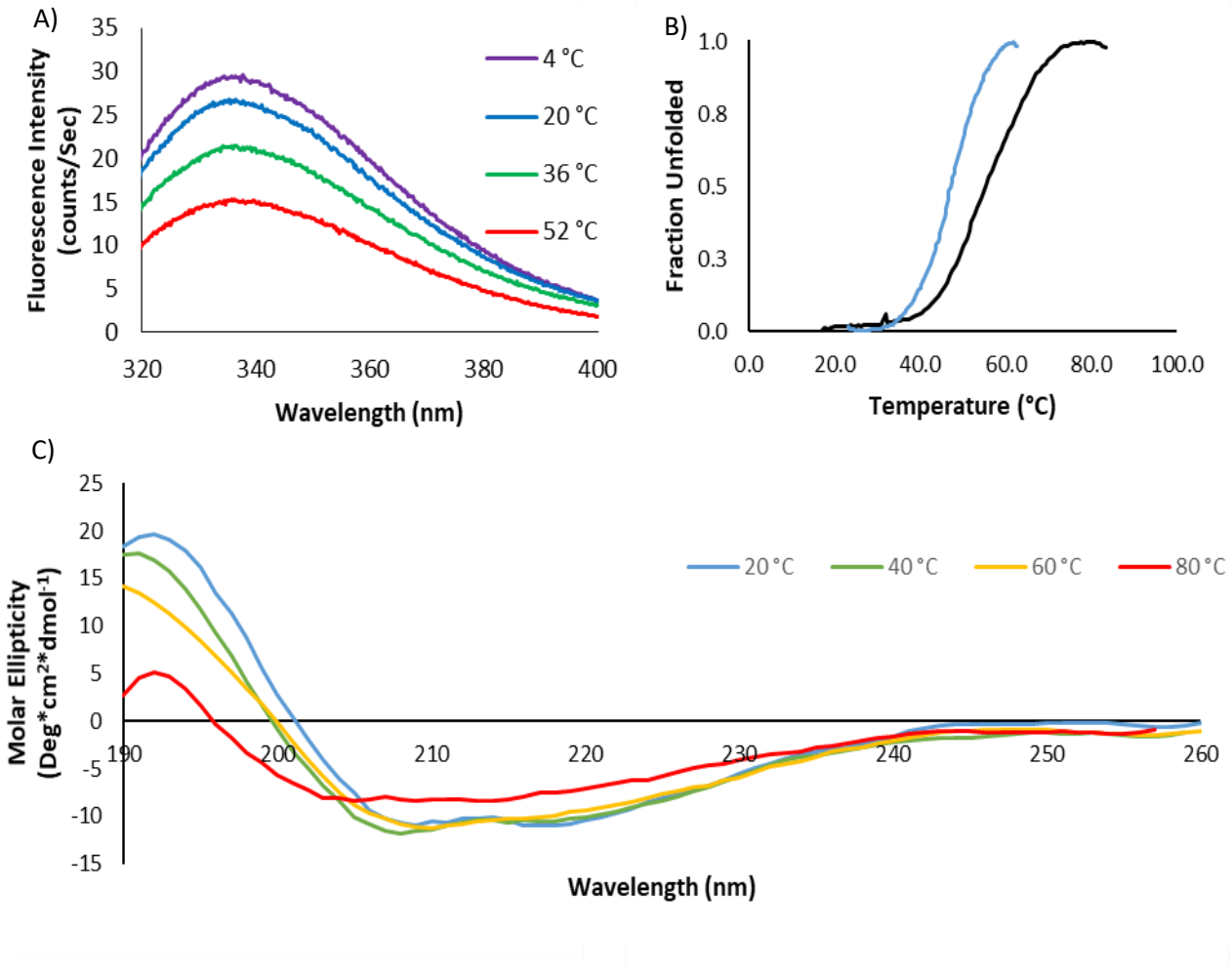

Figure 19. Temperature dependence of the A) Fluorescence emission spectra of R231H $G_{s\alpha}$ •GTPγS as a fuction of temperature (20 -100 °C) B) Absorption spectra of 2.5 µM WT $G_{i\alpha1}$•Mg^{2+} in the GDP (blue) and GTPγS (red) conformations, and of the C) CD spectra of 1.0 µM WT $G_{i\alpha1}$•GDP•Mg^{2+}.

The fluorescence intensity of WT $G_{1\alpha1}$•GDP at 50 °C decreased by 53% when compared to that observed at 20 °C (Figure 20A), and continued declining until 70 °C, at which point there was no change in intensity and the protein was fully unfolded. A T_m value of 41.1 ± 3.0 °C was previously determined for WT $G_{s\alpha}$•GDP and the 39.0 ± 1.1 °C for WT $G_{i\alpha1}$•GDP (Table 2) (Chapter Two). The observed fluorescence T_m values for the R231H $G_{s\alpha}$•GDP and R208Q $G_{i\alpha1}$•GDP mutants were not significantly different (0.2 to 0.9 °C lower) when compared to their WT counterparts (Table 8), which is reflected in 52% decreases in fluorescence intensity (Figure 20A and 20C). The π-cation interaction only forms in the active conformation and the Arg residue is not involved in structurally significant interactions in the GDP conformation. Therefore, the loss of the stabilizing effect from the π-cation interaction would not be evident in non-covalent interactions in the inactive conformation (Chapter Two). Although the T_m measurements are technique-dependent, there were no significant differences between the mutant and their respective WT protein in the GDP conformation (Figure 20A and 20C, Table 8) (Chapter Two).

Table 8. Estimated melting temperature (°C) for G_α WT and mutant proteins using three spectroscopic methods

	Fluorescence		Circular Dichroism		UV/Vis Spectroscopy	
Protein variant	GDP	GTPγS	GDP	GTPγS	GDP	GTPγS
$G_{s\alpha}$ WT	41.1 ± 1.7	38.7 ± 1.0	51.9 ± 2.0	57.4 ± 1.5*	53.5 ± 1.4	63.7 ± 1.1
$G_{s\alpha}$ R231H	38.8 ± 0.5†	34.8 ± 0.8*†	50.9 ± 2.7	56.4 ± 2.4*	50.5 ± 1.8†	54.9 ± 0.9*
$G_{i\alpha1}$ WT	39.0 ± 0.6	48.7 ± 2.0*	44.2 ± 0.5	70.9 ± 2.0*	47.6 ± 0.1	66.5 ± 0.2*
$G_{i\alpha1}$ R208Q	35.1 ± 2.5†	36.9 ± 0.3*†	44.1 ± 2.1	56.8 ± 1.8*†	46.6 ± 0.1	59.5 ± 0.2*†

Temperatures given in °C

* = Stastically different than GDP-bound conformation of same variant

† = Stastically different than WT with comparable conformation

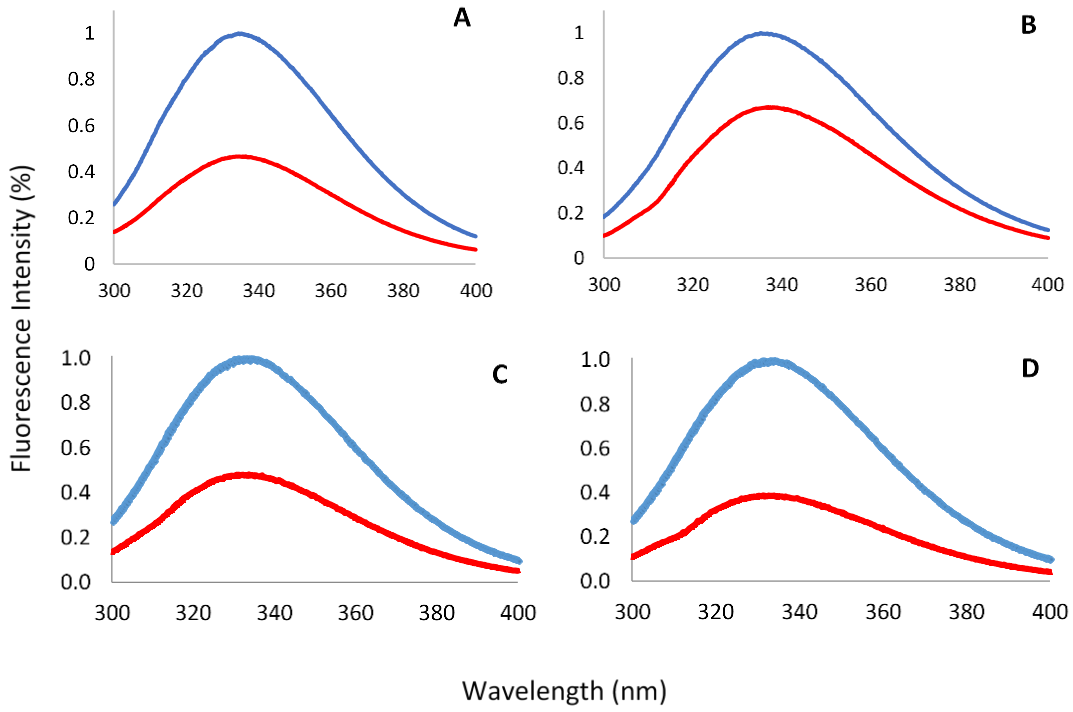

Figure 20. Intrinsic Trp florescence of WT and R208Q $G_{i\alpha1}$ proteins. Emission spectra of 0.4 µM of $G_{i\alpha1}$•Mg^{2+} at 20 °C (blue) and 50 °C (red) in the WT A) GDP or B) GTPγS conformations and the R208Q C) GDP or D) GTPγS conformations.

In the case of the active conformation, however the melting temperature profiles for WT and mutant proteins are different. The T_m value for Trp microenvironments of the R231H $G_{s\alpha}$•GTPγS mutant is significantly lower than that of the WT in the active and inactive conformations. The T_m values for the R208Q $G_{i\alpha1}$ mutant was 11.8 °C lower compared to the WT. The larger ΔT_m observed for the $G_{i\alpha1}$ protein is consistent with the propagation of the destabilizing effect of the R208Q $G_{i\alpha1}$ mutation as evidenced by the continued presence of a red-shift, corroborating the changes to the non-covalent interactions. A comparison of the fluorescence intensities at 20 °C and 50 °C for R208Q $G_{i\alpha1}$•GTPγS and WT $G_{i\alpha1}$•GTPγS illustrates the drastic difference in Trp microenvironments at higher temperatures. A 62% decrease in

fluorescence intensity (Figure 20D) was observed for R208Q $G_{i\alpha1}$•GTPγS compared to 33% decrease for WT $G_{i\alpha1}$•GTPγS (Figure 20B).

Solvent exposure of Tyr residues and temperature dependence of secondary structure

Analogous to the fluorescence experiments, the estimated T_m values from UV/Vis spectrophotometry and from the secondary structures for the mutants were significantly lower than the respective WT proteins in the GTPγS conformation (Table 8). The ΔT_m occurred only for the active conformation, whereas the R231H $G_{s\alpha}$ mutant was 8.8 °C lower (Figure 19B) and the R208Q $G_{i\alpha1}$ was 7.0 °C lower for UV/Vis, and, for circular dichroism (CD), R231H $G_{s\alpha}$ mutant was 4.0 °C lower (Figure 19C) and the R208Q $G_{i\alpha1}$ was 14.2 °C lower for CD than their WT counterparts (Table 8). These calculations support the hypothesis that the π-cation interaction is integral to the stability of G_α subunits in the active conformation and that, at higher temperatures, its disruption propagates outward, thereby altering the non-covalent interactions in the overall protein structure.

Interestingly, the loss of the π-cation interaction results in a change in the unfolding progression. For the active conformation of WT $G_{s\alpha}$, the calculated T_m values indicate that the denaturation initiates at the hydrophobic Trp microenvironments and then radiates toward the secondary structure, followed by the Tyr residues at the surface. In contrast, for the WT $G_{i\alpha1}$, the disruption begins in the Trp environments, though the unfolding around Tyr residues precedes the loss of the secondary structure. However, both Arg mutants deviate from these paths. Starting from the local Trp environments, the secondary structure and the outer surface

unfold simultaneously, indicating that the lack of the π-cation interaction changes the propagation of the non-covalent network within the mutant proteins [161, 162].

Secondary structure content

Circular dichroism was also used to probe the secondary structure content of the inactive and active conformations at various temperatures. The measured R231H $G_{s\alpha}$•GDP α-helical content at 20 °C was 32.7 ± 1.2 % vs. 34.8 ± 1.6 % in WT $G_{s\alpha}$•GDP, showing an insignificant difference in the secondary structure compared to literature values (WT W denaturation paper) [22, 42, 136]. Like the inactive conformations, GTPγS-bound proteins exhibited a α-helical content of 33.0 ± 1.7 % for R231H $G_{s\alpha}$•GTPγS vs. 36.0 ± 2.7 % for WT $G_{s\alpha}$•GTPγS at 20 °C. The R208Q $G_{i\alpha1}$ mutation resulted in similarly insignificant differences in α-helical content for the active and inactive conformations of the WT and mutant $G_{s\alpha}$ proteins. These results were unexpected given that there was a significant decrease in the stability of the arginine mutants. This suggest that, although there is a change in protein stability, the arginine mutation may not change the interaction with the AC effector. The change in the cAMP production caused by the arginine mutation is more likely due to a change in the rate of hydrolysis of the GTP nucleotide.

When the temperature was increased from 36 °C to 64 °C for the inactive conformations of WT as well as for the $G_{s\alpha}$ and $G_{i\alpha1}$ mutant proteins, the CD spectra showed a dramatic change in secondary structure, with a 15% – 20 % decrease in α helical percentage. The primarily α – helical proteins became increasingly dominated by β – sheets, increasing from 10 % to 30 %. Temperatures above 64 °C displayed change in the spectra and the protein eventually

precipitated at 84 °C. Neither mutation significantly diverged from their WT counterpart, as was expected from the previously discussed stability study.

In the case of the active GTPγS conformations, the secondary structure of the WT and mutants of $G_{s\alpha}$ and $G_{i\alpha1}$ proteins did not significantly diverge in the temperature range 20 °C to 40 °C, but for temperatures between 32 °C and 64 °C a dramatic deviation from WT $G_{s\alpha}$ was observed in the α – helical content of R231H $G_{s\alpha}$ (data not shown) and R208Q $G_{i\alpha1}$ mutants (Figure 21). The occurrence of unfolding in α-helical structure at different temperatures may be related to the lack of the π-cation interaction in the mutant proteins.

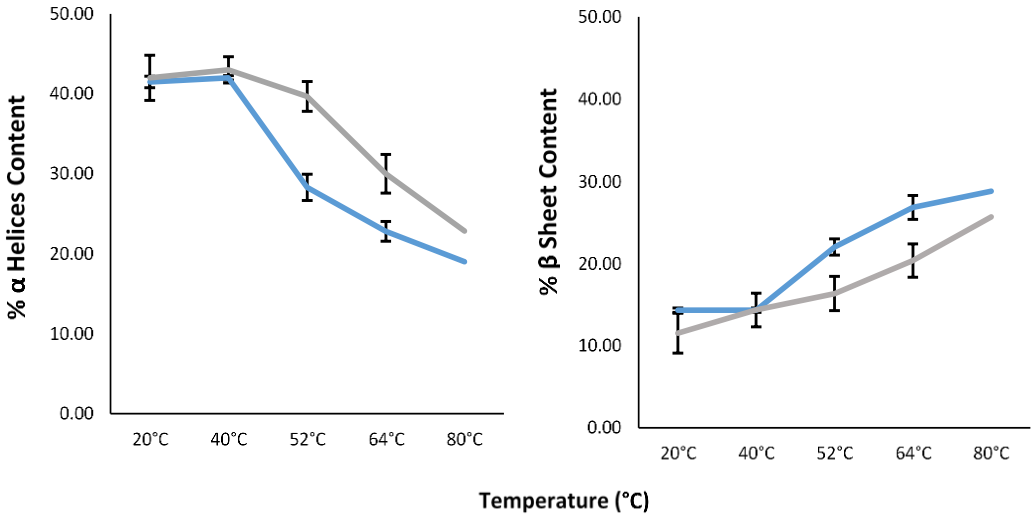

Figure 21. Calculated % A) α - helices and B) β - sheets in the GTPγS conformations of WT $G_{i\alpha1}$ (Gray) and R208Q (blue) as a function of temperature.

Conclusion

This study highlights the importance of the π-cation interaction towards protein stability. Mutations of an essential Arg residue involved in the interaction leads to a destabilization of the switch II region and the complete loss of the red-shift in the case of

R231H $G_{s\alpha}$. The R208Q mutation in $G_{i\alpha1}$ did not abolish the red-shift with an increase in temperature, leading us to conclude that the decreased interaction between residues Q208 and E245 results in the weakening the structural integrity in the immediate vicinity of the residues. The weak Q208-E245 interaction propagated outward, leading to the formation of a F199-F215 π-π interaction in R208Q $G_{i\alpha1}$•GTPγS. As a result, the W258 residue, which is involved in a π-π stacking interaction with F259, moves into a more hydrophobic microenvironment thus accounting for a red-shift. Although the mutations alter the position of several residues, they do not change the secondary or tertiary structures at room temperature as measured by CD. These results suggest that the differences in the production of cAMP between the WT and the mutant proteins are not a consequence of changes in the contact points between AC and G_{sa} [79]. While the structures are not changed at room temperatures, at higher temperatures there are significant decreases in the percent of α – helices. Although the cleavage of the π-cation interaction most likely does not directly modulate the levels of cAMP concentration by altering the secondary structure, the changes in the non-covalent interaction network could translate in functional modifications at the level of GTP hydrolysis.

CHAPTER FOUR

COMPARISON OF THE STRUCTURE FUNCTION RELATIONSHIPS IN WILD-TYPE G_α SUBUNITS AND THEIR ARG MUTANTS

Introduction

Heterotrimeric G-proteins are composed of an α, a β, and a γ subunit that act as binary switches oscillating between "on" and "off" states, amplifying extracellular signals into the cytoplasm in the form of secondary messengers. G-proteins work synergistically with receptors at the surface of the cell. In the inactive conformation, complexes are formed between G-protein coupled receptors (GPCR) and a GDP-bound heterotrimer. When an extracellular ligand binds to a specific receptor, a conformational change ensues, causing the G_α subunit to exchange GDP for GTP, and release the receptor and the $G_{\beta\gamma}$ subunit. The G_α protein further relays the signal through direct interactions with effector proteins until GTP is hydrolyzed, which results in a return to the inactive state [10, 44].

Folding in G_α proteins is highly conserved and consist of two domains: an α helical domain and a GTPase domain [44]. The former is composed of six α helices and is important for effector and regulator selectivity [44]. The GTPase domain is similar in structure and function to those of the Ras superfamily and contains six β sheets at the core surrounded by five α helices [8]. This domain houses the nucleotide binding site, which contains a Mg^{2+} cofactor, and is surrounded by three flexible switch regions designated switch I through III. The switch regions

contain many conserved residues that are oriented around the γ-phosphate of GTP and are crucial for GTP hydrolysis [163].

G_α proteins have a relatively slow turnover rate compared to most enzymes [103, 164]. The ability to remain active for a longer period is important to allow for appropriate signal propagation through interactions with an effector. The extent to which the cell responds to stimuli is dependent on the time the G_α subunit is in the active conformation, which in turn is dictated by the rate of GTP hydrolysis. Homeostasis relies on a delicate equilibrium that can be deleterious. Therefore, cellular signaling must be highly regulated.

Mutations in genes that encode G_α proteins have been shown to be involved in a myriad of serious diseases, among which is cancer [60, 127, 165]. Admittedly, cancer is not the result of any single mutated gene and there are a plethora of tissue-specific permutations that can give rise to cancer [166]. Although cancer can arise from improper regulation of pathways involving many G_α proteins, this study focuses on the cyclic AMP pathway (cAMP), which is stimulated by $G_{\alpha s}$ and inhibited by $G_{\alpha i1}$ through interactions with adenylyl cyclase (AC) [44]. Cyclic nucleotides are secondary messengers commonly associated with tumorigenesis and have been found to be either upregulated or downregulated, depending on the type of [167].

The R231H $G_{\alpha s}$ and the corresponding R208Q $G_{\alpha i1}$ mutation have been found in tumors of the central nervous system and large intestine, respectively [60, 71, 168]. This highly conserved arginine is located in the switch II region, which contains residues critical for GTP hydrolysis. To investigate the effects of these mutations on the function of each G_α protein, GTP hydrolysis studies were conducted. $G_{\alpha i1}$ and $G_{\alpha s}$ contain Trp residues, which upon activation, move into

more hydrophobic environments. As a result, the increase in fluorescence intensity can be used as an indirect measurement of protein activity [104]. Exchange of GDP for GTP is accompanied by an increase in fluorescence which returns to the original intensity at a rate proportional to GTP hydrolysis [103]. The steady-state rate of GTP hydrolysis is determined by the rate of GDP release. For obtaining the time the protein is in active conformation, which is more biologically relevant when studying effects downstream in the signaling pathway [169], fluorescent measurements were used to calculate single turnover rates under conditions of pre-steady-state. Malachite green was also used for measuring the increase in the concentration of inorganic phosphate (P_i) that was released during the course of a single turnover of the enzyme [170, 171].

We investigated how the functional differences observed by fluorescence and malachite green assays for WT G_α proteins and their corresponding mutants could be rationalized in terms of structure. To determine any differences between WT $G_{\alpha i1}$ and its oncogenic mutant in the active conformation, we solved the X-ray structure R208Q $G_{\alpha i1}$ protein bound to GTPγS (a non-hydrolyzable GTP analog) and compared it with that of the published WT $G_{\alpha i1}$•GTPγS [117]. Furthermore, to probe the microenvironments in the vicinity of the mutations that are located in the flexible switch II region, molecular dynamics (MD) simulations were conducted on both R208Q and R231H mutants, as well as on WT $G_{\alpha i1}$ and WT$G_{\alpha s}$ proteins.

We found that a network of molecular interactions was disrupted as a result of the mutations in the switch II region, which propagated to other local motifs within the protein. In the case of $G_{\alpha i1}$, catalytic residues involved in Mg^{2+} binding and in the orientation of a nucleophilic water moved away from the nucleotide binding site while the opposite was seen in

the simulated $G_{\alpha s}$ mutant. Interestingly, the residues involved in binding to AC were left mostly unchanged for both WT $G_{\alpha i1}$ and $G_{\alpha s}$ and their respective mutants. Using a combination of spectroscopic and *in silico* techniques, we were able to elucidate the functional consequences of oncogenic mutations in the switch II regions of $G_{\alpha s}$ and $G_{\alpha i1}$. We propose that both mutants result in lower cellular concentrations of cAMP as a result of altered GTP hydrolysis.

Materials and Methods

Cloning and Mutagenesis

Wild-type $G_{\alpha i1}$-C-His6x from rat and wild-type bovine $G_{\alpha s}$-C-His6x have previously been cloned into the pQE-60 vector (Qiagen) *via DpnI* restriction sites and co-transformed into BL21 *E. Coli* with the pREP4 repressor plasmid. Site-directed mutagenesis was performed to create the R208Q $G_{\alpha i1}$ point mutation using the QuikChange II kit (Agilent) and the forward, 5'- GCC CAG AGA TCA GAG CAG AAG TGG ATT CAC -3', and the reverse, 5'- GTG AAT CAA CTT CTG CTC TGA TCT CTG GCC -3', primers. The R231H $G_{\alpha s}$ mutant was purchased from Bio Basic.

Crystallization Conditions, Data Collection and Structure Determination

Purified R208Q $G_{\alpha i1}$•GTPγS was crystallized by using the hanging drop vapor diffusion method under slightly modified conditions [172]. The total drop size of 6.00 µL was composed of 4.80 µL protein solution (7.0 $mg*mL^{-1}$ $G_{\alpha i1}$•GTPγS, 80.0 mM HEPES pH 7.4, 120.0 mM succinic acid, 8.0 mM DTT, 1.0 mM GTPγS, and 25.0 mM $MgSO_4$) and 1.20 µL reservoir solution (2.0 M $(NH_4)_2SO_3$ pH 8.0). Aliquots of 1.0 mL reservoir solution were placed in each well of a 24 – well plate (VDX). Crystals formed after six days at 20 °C. The R208Q $G_{\alpha i1}$•GTPγS crystals with the best

morphology were transferred into a cryo-protectant (well solution supplemented with 25% (v/v) glycerol) before being flash cooled in liquid nitrogen.

Monochromatic data sets were collected at the LS-CAT, Advanced Photon Source (APS) at Argonne National Laboratory (ANL). Diffraction data were collected at a wavelength of 0.98 at 100K using a Dectris Eigen 9M detector. All data sets were indexed and integrated using HKL2000, with the best data set being processed to a resolution of 2.07 Å.

The structure of R208Q $G_{\alpha i1}$•GTPγS was solved by molecular replacement using PHASER in the Phenix software suit [173]. The initial search model was based on a previously published structure of WT $G_{\alpha i1}$•GTPγS (PDB code: 1GIA). Model building was performed using Coot and refined using Phenix, and the structure was analyzed using Coot and UCSF Chimera [174]. Final refinement statistics are presented in Table X. Structural figures were created using UCSF Chimera [174].

Expression, Purification, and Preparation of G_{α} Proteins

Recombinant proteins were expressed and purified as described [128] to a purity of ≥ 95% and stored at -80 °C. All purified proteins were subject to a time - based fluorescent emission assay to ensure proper function prior to any further functional assays. Mg^{2+}-free G_{α}•GTPγS proteins were prepared by dialysis for six hours in 50.0 mM TrisCl pH 8.0, 0.005 % n,octyl-β-D-glucopyranoside, 1.0 mM EDTA, and 10.0 mM DTT, and again in 50.0 mM TrisCl pH 8.0, 0.01 mM GTPγS, and 10.0 mM DTT for an additional six hours.

Fluorescence Assays for Nucleotide Binding and Hydrolysis

Experiments were performed with a PTI QuantaMaster fluorimeter (Photon Technologies, Inc., Mirmingham, NJ). Time-based assays were conducted with excitation and emission wavelengths set at 280 nm and 340 nm, respectively. Apo G_{α}•GDP was incubated with 20.0 µM GTP for 3 hours at 20.0 °C to exchange GDP for GTP.

Malachite Green Assay

Malachite Green (Abcam) assays were performed on a Biotek ELx808 microplate reader OD. An aliquot of 10.0 µM Apo G_{α}•GDP was incubated with 5.0 µM GTP for three hours at 4°C (50.0 mM HEPES pH 7.4, 2.0 mM EDTA, 100.0 µM GTP, 1.0mM DTT, and 0.2 mg*mL^{-1} BSA). Following GTP exchange, 1.0 mM $MgSO_4$, and 40.0 µM GTPγS were added to the reaction mixture. After 10 minutes, the reaction was quenched with 30.0 µL Malachite green and protected from light for 30 min. P_i was then determined by addition of 230.0 µL to a 96 – well plate using phosphate standards.

Molecular Dynamics Simulations

The coordinates of $G_{\alpha i1}$•GDP (PDB ID: 1BOF,[42]) and $G_{\alpha i1}$•GTPγS (PDB ID: 1GIA, [117]) were downloaded from the Protein Data Bank (PDB, [134]). Missing loops in the $G_{\alpha i1}$ structures were modeled using Swiss-Model [135] and the corresponding transducin structures (PDB ID: 1TAG,[136], 1TAD, [137] and 1TND,[106]). The simulations were done using procedures previously described [107]. Unrestrained dynamics were run for 14 ns before the data were acquired for an additional 1 ns. The simulations were done at 37 °C (310 K) and 50 °C (328 K). These data were then used in the analyses. The R231H point mutation models were generated using VMD [138] and subjected to

the same equilibration procedure as the wild-type structures. All molecular graphics diagrams were obtained using UCSF Chimera [174]. Pairwise Van der Waals and electrostatic interaction energies were calculated using nanoscale molecular dynamics (NAMD) [139]. The solvent accessible surface area (SASA) was measured with the SASA routine in VMD. The values presented Figures 26 and 27 were calculated for the final 1 ns in each simulation and then averaged. The simulation was equilibrated for 15 ns, and the interaction energy (E_i) between networking residues were calculated using NAMD with $p \leq 0.001$.

Results and Discussion

Fluorescence Changes Resulting from Nucleotide Exchange

To examine if the oncogenic mutations hinder GTP binding, we measured the rates for the exchange of GDP with GTPγS (a non-hydrolyzable GTP analog). Time-based intrinsic tryptophan fluorescence is a well-established technique for gauging the activity of G_α proteins [104]. Activation with nucleotide triphosphate results in an increase in fluorescence intensity emanating from a change in the environment surrounding tryptophan residues to one that is more hydrophobic. Upon addition of GTPγS, both WT $G_{\alpha i1}$ and WT $G_{\alpha s}$ showed an increase in fluorescence intensity of approximately 35-40 % over a 100 min timespan (Figure 22), which is within the expected range of 30-35 % for GTPγS activation reported in the literature [104]. The mutants showed smaller increases in fluorescence intensity as the WT proteins: the R208Q $G_{\alpha i1}$ mutant exhibited an approximate increase of 20 % (Figure 22A), while the R231H $G_{\alpha s}$ mutant showed a 25 % increase (Figure 22B). W211 in $G_{\alpha i1}$ and W234 in $G_{\alpha s}$ are the major contributors toward the intrinsic fluorescence of these proteins. The differences in the maximal fluorescence

intensities between the WT proteins and their respective mutants can be attributed to these specific Trp residues moving into environments with different hydrophobicity. The pseudo first-order rate of GTPγS exchange is limited by the rate of dissociation of GDP (k_{app}) [175]. Using a similar analysis for the rate of change in fluorescence that was previously described in [176, 177], the calculated k_{app} values for WT $G_{\alpha i1}$ was 0.03 min^{-1} and 0.02 min^{-1} for the R208Q mutant (Table 9).

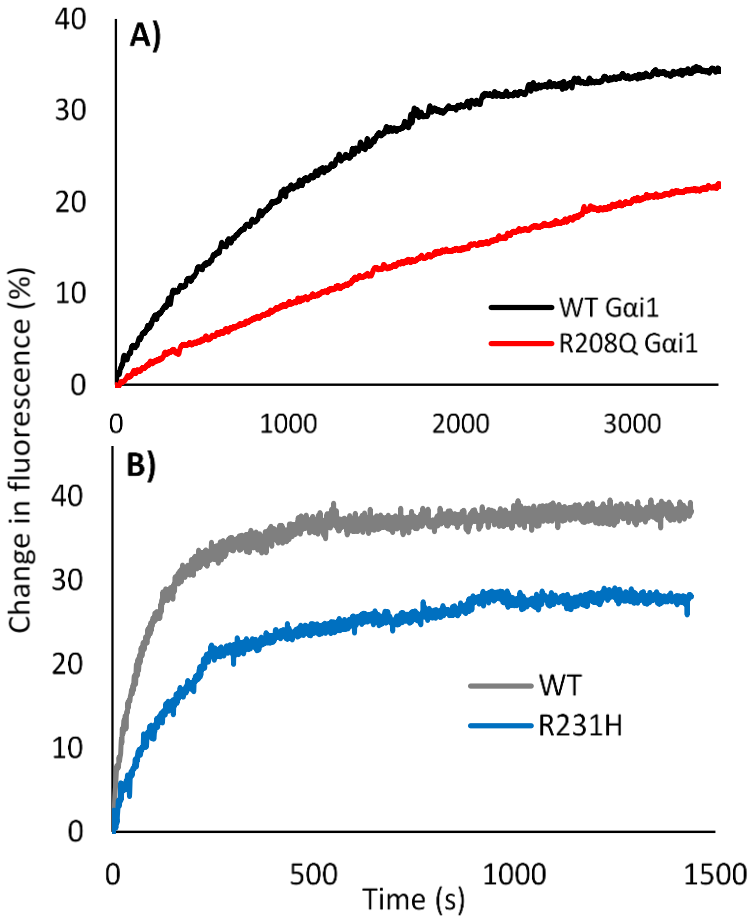

Figure 22. Changes in time-based fluorescence emission resulting from exchange of GDP for GTPγS bound to G_{α} proteins. Fluorescence intensities were normalized to zero upon nucleotide addition. (A) WT $G_{\alpha i1}$ (black) vs R208Q $G_{\alpha i1}$ (red). (B) WT $G_{\alpha s}$ (gray) vs the R231H mutant (blue).

Table 9. Pseudo first-order rate constants for GTPγS exchange and GTP hydrolysis

Protein	GTP exchange	GTP hydrolysis	P_i formation
$WTG_{i\alpha1}$	0.03 ± 0.01	2.9 ± 0.2	3.0 ± 0.1
R208Q $G_{i\alpha1}$	0.02 ± 0.01	1.5 ± 0.3	1.9 ± 0.3
$WTG_{s\alpha}$	0.52 ± 0.03	3.4 ± 0.5	3.6 ± 0.2
R231H $G_{s\alpha}$	0.27 ± 0.02	4.8 ± 0.2	4.4 ± 0.9

Rate constants given in units of min^{-1}
Errors reported as standard deviations, n≥3

Under the same conditions, the WT $G_{\alpha s}$ showed a GTPγS exchange rate of 0.52 min^{-1} whereas for the R231H mutant, k_{app} was 0.27 min^{-1} (Table 9). Although the k_{app} values previously reported for $G_{\alpha s}$ are approximately two-fold higher (0.28 min^{-1} and 0.13 min^{-1}, respectively [79]), their ratio is similar to that in our study, which might be due to different methodology used and experimental conditions. In conclusion, both G_α mutants showed a decreased nucleotide exchange rate, but they were still able to bind GTP and attain the active conformation.

Fluorescence Changes Resulting from GTP Hydrolysis

G-proteins function as molecular switches that turn on or off cellular responses. Therefore, the rate of GTP hydrolysis is what dictates the magnitude of the cellular response. Because the rate for nucleotide exchange is much slower than for hydrolysis, the steady-state turnover rate is largely determined by the release of GDP [103]. All GTPases require a Mg^{2+} cofactor to function, and a highly conserved Ser is critical for Mg^{2+} coordination and holding it in the nucleotide binding site [136]. In the GTPγS conformation, Mg^{2+} has an octahedral geometry and in addition to a Ser residue, is coordinated to a Thr residue, the β and γ phosphates of the nucleotide, and two water molecules. Uncoupling the conformational change from GTPase

activity is critical for investigating the time the protein remains in the active state because it bypasses the much slower rate of nucleotide exchange [169].

The single turnover rate of GTP hydrolysis was measured using two indirect, pre-steady-state techniques. The fluorescence approach that was first used monitored the change in the hydrophobicity of key tryptophan residues that track conformational changes. As Mg^{2+} was added to apo G_{α}•GTP, the fluorescence intensity increased as a result of burial of Trp residues in the active state, but it quickly returned to zero as the bound GTP was hydrolyzed to GDP and inorganic phosphate (P_i) (Figure 23A, inset) [103]. The half-life ($t_{1/2}$) of the decay process was found to be 13.9 s for WT $G_{\alpha i1}$ and 11.9 s for WT $G_{\alpha s}$ (Figure 23B). From $t_{1/2}$, k_{cat} values were calculated from the equation: $k_{cat} = \ln(2)*t_{1/2}^{-1}$, resulting in a k_{cat} of 2.9 ± 0.2 min^{-1} for WT $G_{\alpha i1}$ and 3.4 ± 0.5 min^{-1} for WT $G_{\alpha s}$ (Table 9). Previous research showed the rate of hydrolysis for WT $G_{\alpha i1}$ to be 0.42 min^{-1} [102, 169], but upon the addition of RGS4, a GTPase activating protein (GAP), it was found to increase from 2.0 to 4.0 min^{-1} *via* stabilization of the transition state [102, 175, 178, 179]. WT $G_{\alpha s}$ shows a turnover rate comparable to $G_{\alpha i1}$ at 3.4 ± 0.5 min^{-1} (Table 9), and with the value that was with the value that was previously reported, 3.5 min^{-1} [180]. A malachite green assay was also used to confirm the fluorescence measurements. With this technique, the k_{cat} value for P_i formation resulting from GTP hydrolysis was found to be 3.0 ± 0.1 min^{-1} for WT $G_{\alpha i1}$ while for WT $G_{\alpha s}$ it was 3.6 ± 0.2 min^{-1} (Table 9). The R208Q $G_{\alpha i1}$ showed lower k_{cat} values by both methods: 1.5 ± 0.3 min^{-1} using fluorescence spectroscopy and 1.9 ± 0.3 min^{-1} with malachite green, indicating that the mutant has diminished hydrolytic activity. Conversely, the R231H mutant showed higher rates of GTP hydrolysis compared to WT $G_{\alpha s}$ with k_{cat} values of 4.8 ± 0.2

min^{-1} and 4.4 ± 0.9 min^{-1} for the fluorescence and malachite green assays, respectively (Table 9).

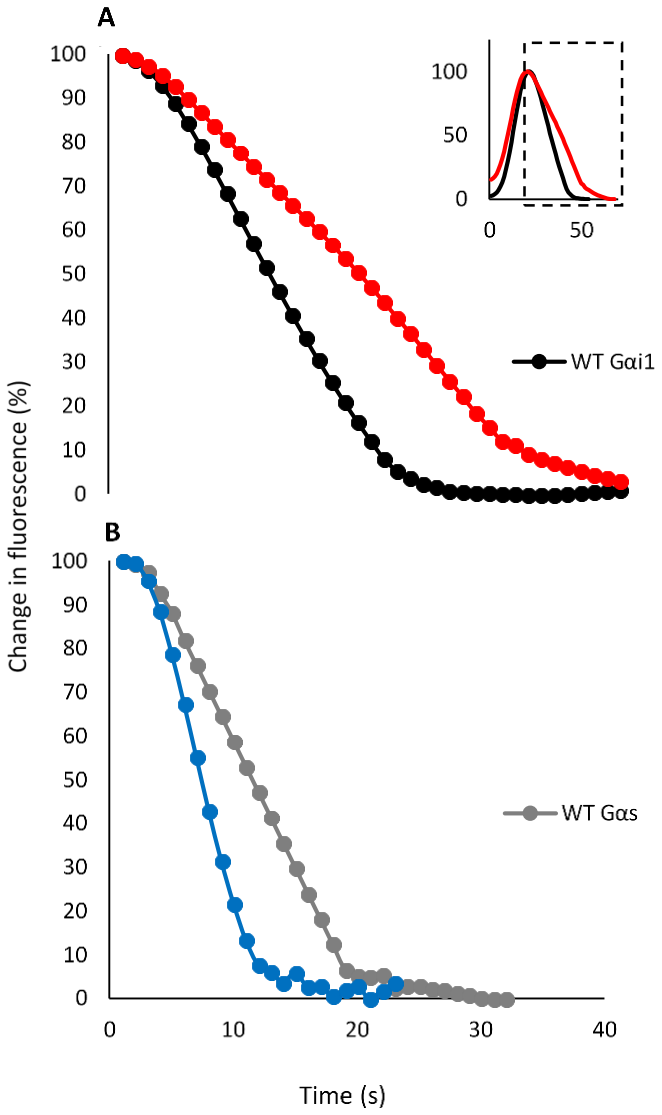

Figure 23. GTP hydrolysis monitored by time-based fluorescence emission. Due to differences in Trp environments, the maximal fluorescence intensities of WT and mutant proteins were different. The decays were therefore normalized to a range of 0 to 100. The assay was initiated by addition of Mg^{2+} at time zero (inset). (A) WT $G_{\alpha i1}$ (black) vs R208Q $G_{\alpha i1}$ (red). (B) WT $G_{\alpha s}$ (gray) vs R231H $G_{\alpha s}$ (blue).

Structure of the R208Q $G_{\alpha i1}$ Mutant

The R208Q $G_{\alpha i1}$ structure was solved at a resolution 2.05 Å (deposited in the PDB under: 1GIA (Figure 23)). The data was processed in the space group P 32 2 1, refined to a final R_{work}/R_{free} (%) 16.8/19.7 and, to a resolution of 2.07Å. The X-ray crystal structure of the R208Q $G_{\alpha i1}$ mutant closely resembles the previously solved WT $G_{\alpha i1}$ structure (PDB entry 1GIA [117]). The most pronounced changes occur within the switch II region where the mutation is located. Compared to the WT $G_{\alpha i1}$ protein, the R208Q mutation causes the Cα of the Q208 residue to move slightly toward the α3 helix by approximately 0.7 Å thereby resulting in an increase in its radius.

Superimposition of the WT$G_{\alpha i1}$•GTPγS and the R208Q$G_{\alpha i1}$•GTPγS structures revealed a root mean square deviation (RMSD) of 0.653 Å at the site of the mutation, but only 0.255 Å between 345 aligned alpha carbons (C_α) in the overall proteins. However, the functionally important motifs saw relatively more deviation from the WT. The RMSD of the switch I region (residues 177-183) almost doubles (0.502 Å). Focusing only on the switch II motif (residues 202-215), the RMSD also increases to 0.453 Å. The switch III region (residues 232-240) experiences an approximate 50% change with an RMSD of 0.355 Å. The α4-β6 loop, which is important for effector binding and is located near the posterior surface relative to the nucleotide binding site, has an RMSD value of 0.244 Å. These calculations suggest that the microenvironments in the immediate vicinity of the mutation are altered while the distal motifs are left unperturbed. Given that the mutation is located on the flexible switch II region and is positioned near the similarly flexible switch I region, these results are not surprising. B-factors for the switch II

region of both the WT and the mutant are relatively high. Because we were unable to obtain crystals for R231H $G_{\alpha s}$, a similar analysis was not possible.

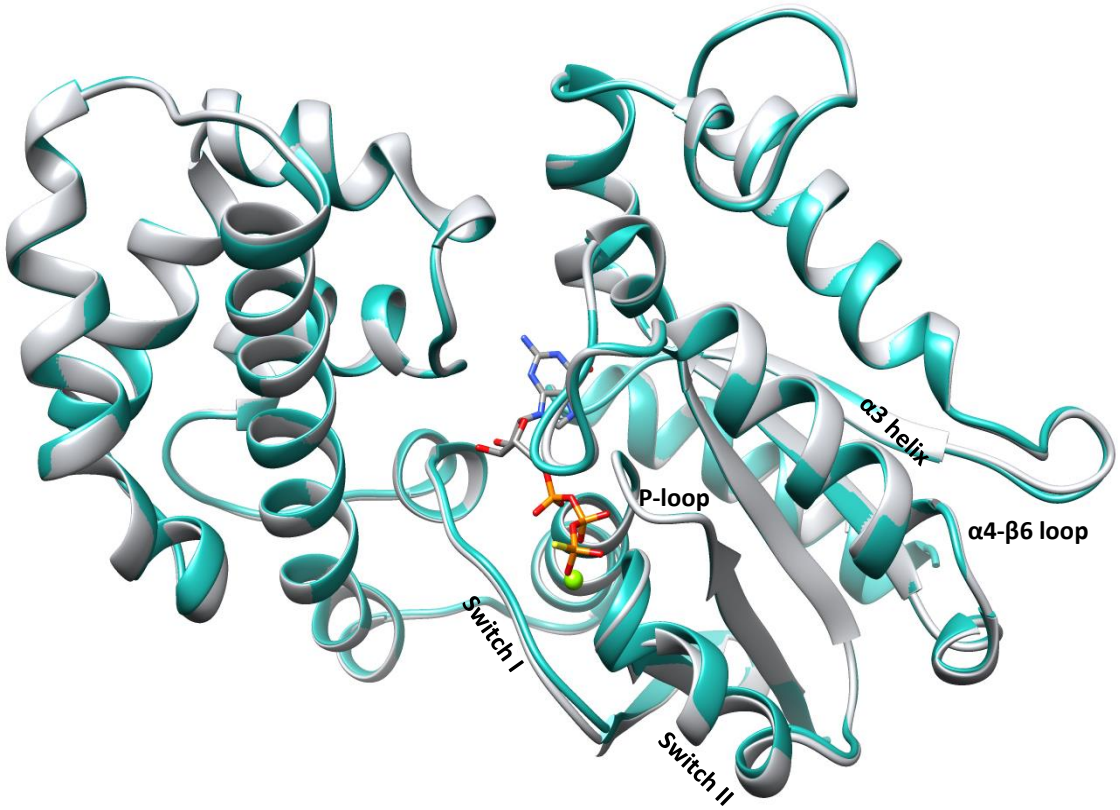

Figure 24. Structure of R208Q $G_{\alpha i1}$•GTPγS (teal) superimposed on the structure of WT $G_{\alpha i1}$•GTPγS (PDB ID 1GIA, gray). Mg^{2+} (green) and GTPγS bind at the active site, which is surrounded by the three switch regions.

Computer Modeling of Intermolecular Interactions

G-proteins are highly conserved proteins both at the primary and the secondary structure levels. Key residues for GTP hydrolysis by $G_{\alpha i1}$ have been identified: R242 [181], E43 [181], and S47 [182] (Figure 25). These residues are known to make up an intricate network involving hydrogen bonds, electrostatic interactions, and hydrophobic forces. R178 has been shown to be

directly involved in hydrolysis by stabilizing the negative charge on the γ-PO_4^{2-} [117]. Solving the crystal structure for the R208Q $G_{\alpha i1}$ mutant provided the opportunity for using computer modeling to probe intermolecular interactions in a dynamic state. It has been reported that the R208A $G_{\alpha i1}$ mutant has an insignificant effect on GTP hydrolysis [169]. This mutant proved to be useful in understanding the interactions present in GTP hydrolysis. We were able to model the R208A $G_{\alpha i1}$ mutant after the previously solved WT $G_{\alpha i1}$ structure [117]. Although we were unable to obtain crystals for the R231H $G_{\alpha s}$ protein, the mutation was also simulated from the previously solved WT structure [22].

As WT $G_{\alpha i1}$•GTPγS shifts into the active conformation, a π-cation interaction is formed between R208 and W211, which contributes to the stability of the switch II region [107, 108]. A similar interaction in WT $G_{\alpha s}$ occurs between the corresponding R231 and W234 residues. Following our MD simulation, the RMSD between the Cα of the 208 residue in $G_{\alpha i1}$ became 3.82 Å and 1.3 Å for the corresponding 231 position in $G_{\alpha s}$, which suggests that the region around the mutation has become unstable in the $G_{\alpha i1}$ but much less so in $G_{\alpha s}$.

We calculated interaction energies to determine if the destabilization of the switch II region propagated to the switch I and the α3 helix regions and, if present, how it affected the specific interactions involved in GTP hydrolysis (Table 10). R242 in WT $G_{\alpha i1}$ is located at the other end of the α3 helix relative to the affected W258. Its interaction with E43 has been shown to promote the transition to active state and allow for nucleotide exchange [181]. The WT $G_{\alpha i1}$•GTPγS had a total interaction energy (sum of electrostatic and van der Waals) of -60.1 kcal*mol^{-1} at a distance of 3.0 Å between R242 and E43, while, for the R208A $G_{\alpha i1}$ mutant, the

value was -62.3 kcal*mol^{-1} at a similar distance. The R208Q $G_{\alpha i1}$ mutant exhibited an interaction with a magnitude of approximately half (-30.8 kcal*mol^{-1}) of the WT protein at an increased distance of 5.2 Å (Table 10). The $G_{\alpha s}$ counterparts are R265 and E50. Table 2 shows that the corresponding interactions in $G_{\alpha s}$ remained unchanged and so did the interresidue distances.

Table 10. Interaction energies and distances between networking residues that are involved in GTP hydrolysis. Interaction energies calculated are a combination of electrostatic and van der Waals interactions

$G_{\alpha i1}$	Interaction Energy			Distance (Å)			$G_{\alpha s}$	Interaction Energy		Distance (Å)	
Interaction	WT	R208Q	R208A	WT	R208Q	R208A	Interaction	WT	R231H	WT	R231H
R242 - E43	-60.1	-30.8	-62.3	3	5.2	2	R265 - E50	-87.2	-84.6	2.1	2
E43 - R178	-33	-92	-32	4.6	1.8	5.1	E50 - R201	-34.6	-32	4	4.8
R178 – γPO_4^{2-}	-100	-27	-72.7	2.8	5.6	2.8	R201 – γPO_4^{-}	-40.8	-103.5	6.9	3.4

Interaction Energy reported in kcal*mol^{-1}

The P-loop is located near the β and γ phosphates of GTP and is a critical motif for the transition to the active state. In the inactive GDP-bound conformation, it forms an electrostatic interaction with the catalytic R178 $G_{\alpha i1}$ (R201 $G_{\alpha s}$) that is known to stabilize the leaving P_i in the switch I region [117, 177]. A key difference between heterotrimeric G_α proteins and their Ras counterpart is the noticeable lack of an equivalent Arg in the latter. Ras proteins have significantly lower rates of basal GTP hydrolysis, however, the rate is dramatically increased by GTPase Activating Proteins (GAP), which contains a functionally equivalent switch I Arg [183]. For WT $G_{\alpha i1}$ and R208A $G_{\alpha i1}$ proteins, E43 was at a distance of 4.6 Å or 5.1 Å from R178 and with similar interaction energies. In the R208Q $G_{\alpha i1}$ mutant, E43 was positioned between the nucleotide and R178 at a much shorter distance (1.8 Å), resulting in a strong electrostatic interaction of -92.0 kcal*mol^{-1} (Table 10 and Figure 25B). For WT $G_{\alpha s}$ and R231H $G_{\alpha s}$, both E50

and R201 remained at comparable distances (Table 10 and Figure 25A) to that between E43 and R178 in WT $G_{\alpha i1}$, 4.0 and 4.8 Å, respectively, vs. 4.6 Å.

Simulating the interaction between the R178 and γ-PO_4^{2-} resulted in an E_i of -100.0 kcal*mol^{-1} for WT $G_{\alpha i1}$ and -72.7 kcal*mol^{-1} for R208A mutant at a distance of 2.8 Å for both. The R208Q interaction was drastically decreased to -27.0 kcal*mol^{-1} at a distance of 5.6 Å (Table 10). Therefore, the increased interaction with E43 hinders R178 from binding to γ-PO_4^{2-} (Figure 25A). $G_{\alpha s}$ experienced the opposite trend where WT interacted with γ-PO_4^{2-} with an E_i of -40.8 kcal*mol^{-1} at a distance of 6.9 Å while the R231H mutant exhibited an attraction of -103.5 kcal*mol^{-1} at a distance of 3.4 Å. In neither case, however, was there any structural hindrance of the Arg residue with γ-PO_4^{2-}, as seen in $G_{\alpha i1}$.

Also in the P-loop are highly conserved Ser residues necessary for Mg^{2+} binding: S47 in $G_{\alpha i1}$ and S54 in $G_{\alpha s}$. Across all three $G_{\alpha i1}$ simulations, this interaction was minimally altered: -38.9 kcal*mol^{-1} for WT $G_{\alpha i1}$, -30.2 kcal*mol^{-1} for R208Q $G_{\alpha i1}$, and -30.3 kcal*mol^{-1} for R208A $G_{\alpha i1}$, and the difference in the movement was 0.1 Å (Table 10 and Figure 25A) $G_{\alpha s}$ underwent a more drastic change in which the R231H mutant showed an increased affinity for the Mg^{2+} ion with an E_i of -46.9 kcal*mol^{-1} vs -29.7 kcal*mol^{-1} seen in the WT protein. GTPase activity has been shown to be regulated by Mg^{2+} concentration [184], therefore the increased affinity for Mg^{2+} could be contributing to the higher rate of GTP hydrolysis seen in the R231H mutant. The R208Q mutation affected $G_{\alpha i1}$ through perturbations in the α3 helix, and propagated to the P-loop and the switch I region, which ultimately prevented R178 from interacting with γ-PO_4^{2-}.

Conversely, the α3 helix was not affected significantly in the R231H $G_{\alpha s}$ mutant, however, D223 in the switch II region moved further from the γ-PO_4^{2-} and Mg^{2+}, respectively.

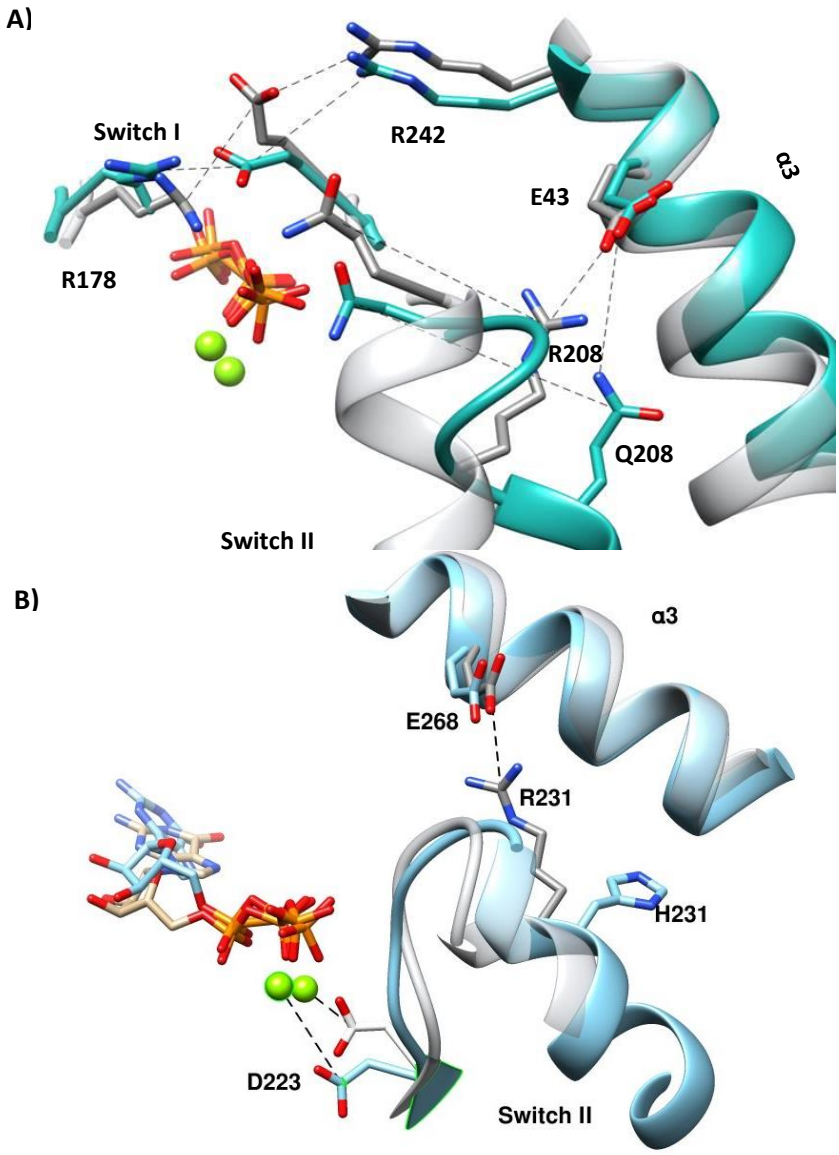

Figure 25. Superposition of the WT and mutant nucleotide binding sites after simulation. (A) R208Q $G_{\alpha i1}$ mutant (teal) and WT $G_{\alpha i1}$ (gray). (B) R231H $G_{\alpha s}$ mutant (blue) and WT $G_{\alpha s}$ (gray). Mg^{2+} is shown in green and the phosphates of the nucleotide are depicted in orange.

Within the switch II region, an interaction between F215 and W258 in the WT $G_{\alpha i1}$ seems to be missing in the R208Q mutant, which causes the α3 helix to shift away compared to WT. This interaction is not found in WT $G_{\alpha s}$ and therefore the α3 helix is left largely unperturbed.

In both proteins, Q204 in $G_{\alpha i1}$ (Q227 in $G_{\alpha s}$) is believed to be crucial for hydrolysis to occur *via* interactions with a nucleophilic water [44]. Our simulations are inconclusive as to whether the catalytic R178 is affected by the R208Q mutation because this residue may orient the nucleophilic water but cannot be observed in a water box and remain in the nucleotide binding site. We attempted to use the nucleotide as a reference point but the modeled R208A $G_{\alpha i1}$ interaction energies were not significantly different from those for the R208Q $G_{\alpha i1}$ mutant, which is not consistent with the known similarity of the rates of GTP hydrolysis of WT and R208A proteins.

There are currently no crystal structures of $G_{\alpha i1}$ in complex with AC but the contact residues have been identified as E207, R208, K209, and I212 from the switch II region, and K312, R313, K314, K315, T316, and E318 of the α4-β6 loop [22]. To determine if the oncogenic phenotype is a result of an inability to properly bind AC, the surface accessible surface area (SASA) values for the $G_{\alpha s}$-AC complex interface were compared to those for WT $G_{\alpha i1}$ and its R208Q $G_{\alpha i1}$ mutant alone (Figure 26A). Of these, only the R313 and K314 residues have significantly different SASA values. WT R313 has a SASA value of 156.9 ± 13.4 $Å^2$ and is less exposed to solvent than R313 in the R208Q mutant, which has a SASA of 178.5 ± 12.6 $Å^2$. The SASA value of K314 in WT $G_{\alpha i1}$ was 56.5 ± 8.2 $Å^2$ vs 102.3 ± 12.6 $Å^2$ in the R208Q mutant. The

difference in SASA between the WT and R208Q proteins is -34.9 $Å^2$, suggesting that the interface between the R208Q $G_{\alpha i1}$ – AC would be largely left unaltered, and the interaction with AC would be similarly efficient. Using the overall SASA values for gleaning information on the WT$G_{\alpha i1}$ – AC and R208Q $G_{\alpha i1}$ – AC interfaces are limited by the fact that they are calculations based on simulations rather than on actual structures of $G_{\alpha i1}$ complexes. This assessment also fails to take into account the post-translational myristoylation at glycine 2 that has been shown to be necessary for $G_{\alpha i1}$ to bind AC (22).

Although $G_{\alpha s}$ undergoes a post-translational lipidation in which a palmitoyl group is added to the N-terminus, that allows it to bind the membrane, however, it is not necessary to bind AC [185]. A crystal structure of $G_{\alpha s}$ in complex with AC has been solved (PDB ID 1AZS) and the interface is known. R231, R232, W234, Q236, N239, L272, N279, R280, W281, L282, R283, and T284 have been shown to interact with the C2 domain of AC [51]. *In vivo* studies have previously shown that the R231H $G_{\alpha s}$ mutation decreases cAMP accumulation [79, 186]. Furthermore, it has been shown that the R231H mutation does not inhibit binding of $G_{\alpha s}$ to AC [79]. Using the structure of WT $G_{\alpha s}$ complexed with AC [51], we were able to confirm these results by modeling the interface residues. The sum of the interactions between interface residues is -192.9 $kcal*mol^{-1}$ for WT $G_{\alpha s}$ and -191.5 $kcal*mol^{-1}$ for the R231H mutant (Figure 27).

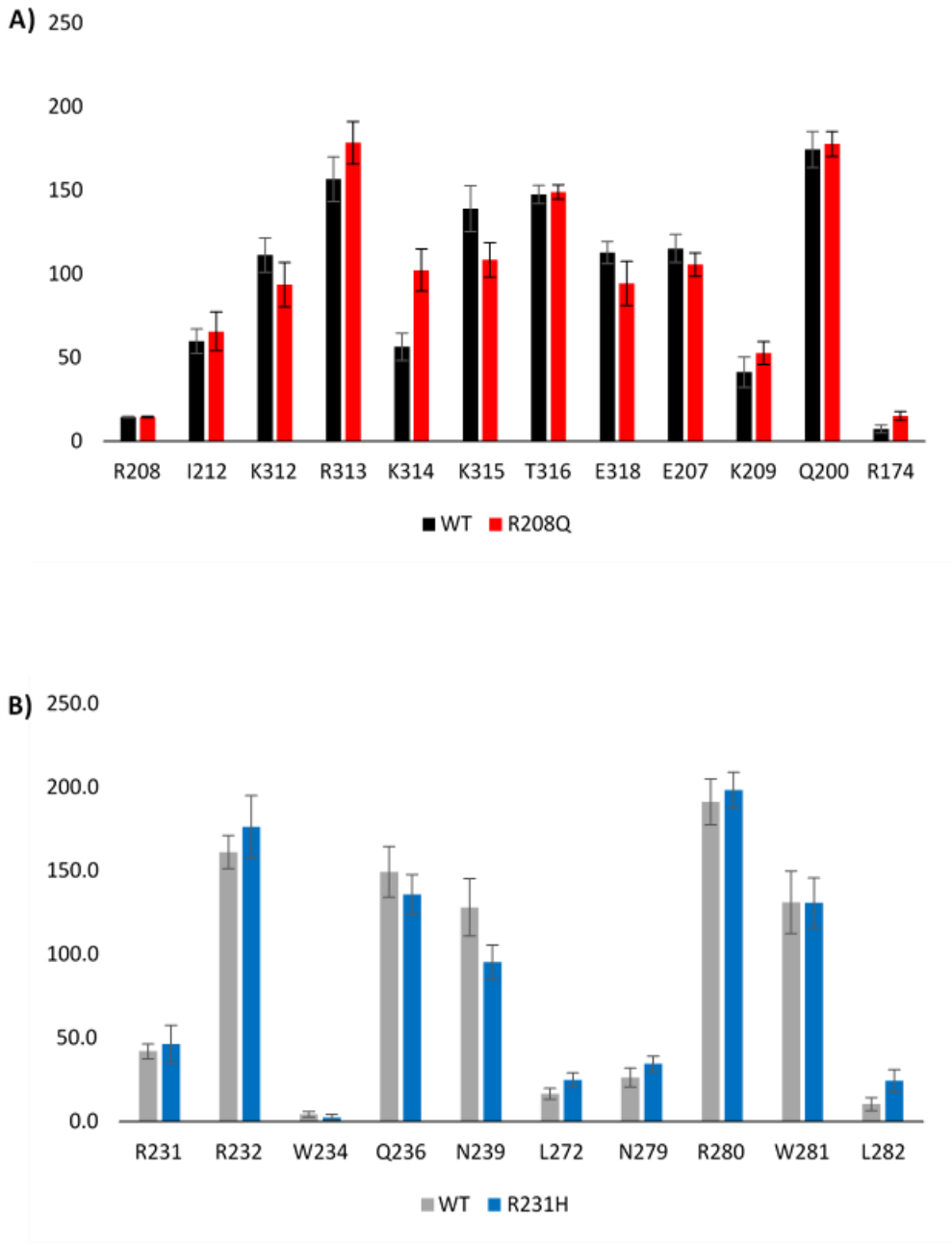

Figure 26. SASA of the residues that interact with the C1 domain of AC. A) WT Gαi1 (black) vs R208Q Gαi1 (red) B) WT Gαs (gray) vs R231H Gαs (blue). Values given in Å2, and errors reported as standard deviation

Furthermore, the SASA of $G_{\alpha s}$ alone was comparable to the results seen in $G_{\alpha i1}$, the surface area of all the residues that contact AC was not changed significantly (Figure 28). These calculations agree with those findings by showing that since the R231H $G_{\alpha s}$ mutant shows an

increased rate of GTP hydrolysis, the overall duration of the stimulating $G_{\alpha s}$ – AC interaction would be shorter, therefore, resulting in decreased cAMP production by AC. Conversely, the lower GTPase activity of $G_{\alpha i1}$ results in a longer inhibiting $G_{\alpha i1}$ – AC interaction that would also lead to lower cAMP concentrations.

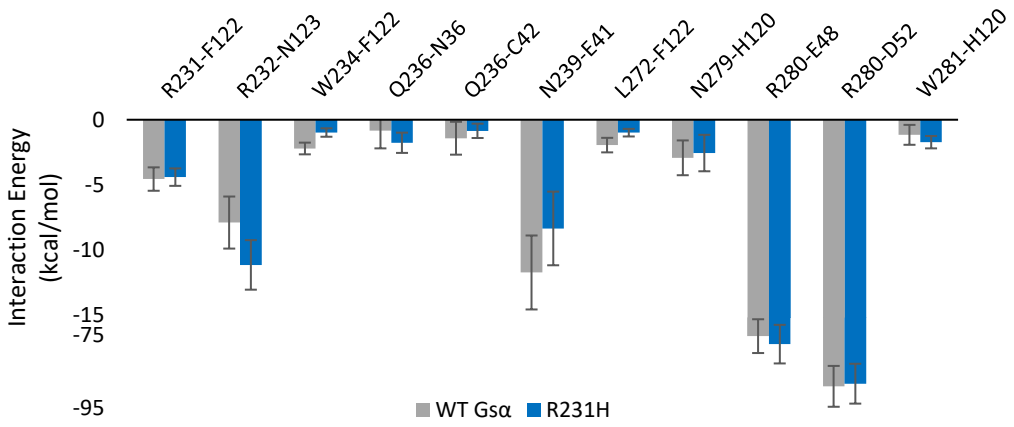

Figure 27. Interaction energies between $G_{\alpha s}$ and AC modeled from 1AZS structure. WT $G_{\alpha s}$ (gray) vs simulated R231H $G_{\alpha s}$ (blue). Units of kcal*mol^{-1}, errors reported as standard deviations.

Conclusion

The crystal structure of the R208Q $G_{\alpha i1}$ mutant is similar to the WT but important differences in the switch regions likely affect the function of the protein. Using two indirect experimental approaches, we showed that the GTPase activity decreased in the $G_{\alpha i1}$ mutant but increased in the $G_{\alpha s}$ mutant. MD simulations suggest that the microenvironments in the vicinity of the mutations are altered thereby affecting the interaction of key residues in the nucleotide binding site. In R208Q $G_{\alpha i1}$, the energy of the interaction between E43 and R178 increased hindering catalysis by preventing the guanidinium group of the R178 from stabilizing the negative charge on the leaving P_i. R231H $G_{\alpha s}$ is affected in the opposite manner with an

increase in E_i between the comparable R201 and γ-PO_4^{2-} compared to the WT protein, which is amplified by the increased E_i seen between S50 and the Mg^{2+} cofactor. Modeling the binding site of G_α proteins and AC showed that the interface is minimally affected suggesting that the differences in cAMP accumulation reported by *in vivo* studies are primarily a result of changes in the rates of GTP hydrolysis.

REFERENCES

1. Tompa, P. (2016) The principle of conformational signaling. *Chem. Soc. Rev. 45*, 4252-4284.

2. Gilman, A. G. (1995) Nobel lecture. G proteins and regulation of adenylyl cyclase. *Biosci. Rep. 15*, 65-97.

3. Rodbell, M. (1995) Nobel lecture. signal transduction: Evolution of an idea. *Biosci. Rep. 15*, 117-133.

4. Ringertz, N. (1997) *Nobel lectures in physiology or medicine 1991-1995.* World Scientific Publishing Company, Singapore.

5. Syrovatkina, V., Alegre, K. O., Dey, R., and Huang, X. Y. (2016) Regulation, signaling, and physiological functions of G-proteins. *J. Mol. Biol. 428*, 3850-3868.

6. Higashijima, T., Ferguson, K. M., Sternweis, P. C., Smigel, M. D., and Gilman, A. G. (1987) Effects of Mg^{2+} and the βγ-subunit complex on the interactions of guanine nucleotides with G proteins. *J. Biol. Chem. 262*, 762-766.

7. Van Eps, N., Preininger, A. M., Alexander, N., Kaya, A. I., Meier, S., Meiler, J., Hamm, H. E., and Hubbell, W. L. (2011) Interaction of a G protein with an activated receptor opens the interdomain interface in the α subunit. *Proc. Natl. Acad. Sci. U. S. A. 108*, 9420-9424.

8. McCudden, C. R., Hains, M. D., Kimple, R. J., Siderovski, D. P., and Willard, F. S. (2005) G-protein signaling: Back to the future. *Cell Mol. Life Sci. 62*, 551-577.

9. Chen, C. A., and Manning, D. R. (2001) Regulation of G proteins by covalent modification. *Oncogene. 20*, 1643-1652.

10. Oldham, W. M., and Hamm, H. E. (2008) Heterotrimeric G protein activation by G-protein-coupled receptors. *Nat. Rev. Mol. Cell Biol. 9*, 60-71.

11. Sunahara, R. K., Dessauer, C. W., Whisnant, R. E., Kleuss, C., and Gilman, A. G. (1997) Interaction of $G_{s\alpha}$ with the cytosolic domains of mammalian adenylyl cyclase. *J. Biol. Chem. 272*, 22265-22271.

12. Lefkowitz, R. J. (2007) Seven transmembrane receptors: Something old, something new. *Acta Physiol. (Oxf). 190*, 9-19.

13. Rasmussen, S. G., DeVree, B. T., Zou, Y., Kruse, A. C., Chung, K. Y., Kobilka, T. S., Thian, F. S., Chae, P. S., Pardon, E., Calinski, D., Mathiesen, J. M., Shah, S. T., Lyons, J. A., Caffrey, M., Gellman, S. H., Steyaert, J., Skiniotis, G., Weis, W. I., Sunahara, R. K., and Kobilka, B. K. (2011) Crystal structure of the β2 adrenergic receptor-G_s protein complex. *Nature. 477*, 549-555.

14. Taylor, J. M., Jacob-Mosier, G. G., Lawton, R. G., VanDort, M., and Neubig, R. R. (1996) Receptor and membrane interaction sites on G_β. A receptor-derived peptide binds to the carboxyl terminus. *J. Biol. Chem. 271*, 3336-3339.

15. Eason, M. G., and Liggett, S. B. (1995) Identification of a G_s coupling domain in the amino terminus of the third intracellular loop of the α2-adrenergic receptor. evidence for distinct structural determinants that confer G_s versus G_i coupling. *J. Biol. Chem. 270*, 24753-24760.

16. Taylor, J. M., Jacob-Mosier, G. G., Lawton, R. G., Remmers, A. E., and Neubig, R. R. (1994) Binding of an α2 adrenergic receptor third intracellular loop peptide to G_β and the amino terminus of G_α. *J. Biol. Chem. 269*, 27618-27624.

17. Ceruso, M. A., Periole, X., and Weinstein, H. (2004) Molecular dynamics simulations of transducin: Interdomain and front to back communication in activation and nucleotide exchange. *J. Mol. Biol. 338*, 469-481.

18. Marin, E. P., Krishna, A. G., and Sakmar, T. P. (2002) Disruption of the α5 helix of transducin impairs rhodopsin-catalyzed nucleotide exchange. *Biochemistry. 41*, 6988-6994.

19. Marin, E. P., Krishna, A. G., and Sakmar, T. P. (2001) Rapid activation of transducin by mutations distant from the nucleotide-binding site: Evidence for a mechanistic model of receptor-catalyzed nucleotide exchange by G proteins. *J. Biol. Chem. 276*, 27400-27405.

20. Wennerberg, K., Rossman, K. L., and Der, C. J. (2005) The ras superfamily at a glance. *J. Cell. Sci. 118*, 843-846.

21. Liu, W., and Northup, J. K. (1998) The helical domain of a G protein α subunit is a regulator of its effector. *Proc. Natl. Acad. Sci. U. S. A. 95*, 12878-12883.

22. Sunahara, R. K., Tesmer, J. J., Gilman, A. G., and Sprang, S. R. (1997) Crystal structure of the adenylyl cyclase activator G_s. *Science. 278*, 1943-1947.

23. Lambright, D. G., Sondek, J., Bohm, A., Skiba, N. P., Hamm, H. E., and Sigler, P. B. (1996) The 2.0 Å crystal structure of a heterotrimeric G protein. *Nature. 379*, 311-319.

24. Li, Q., and Cerione, R. A. (1997) Communication between switch II and switch III of the transducin α subunit is essential for target activation. *J. Biol. Chem. 272*, 21673-21676.

25. Spoerner, M., Herrmann, C., Vetter, I. R., Kalbitzer, H. R., and Wittinghofer, A. (2001) Dynamic properties of the ras switch I region and its importance for binding to effectors. *Proc. Natl. Acad. Sci. U. S. A. 98*, 4944-4949.

26. Neer, E. J. (1995) Heterotrimeric G proteins: Organizers of transmembrane signals. *Cell. 80*, 249-257.

27. Logothetis, D. E., Kurachi, Y., Galper, J., Neer, E. J., and Clapham, D. E. (1987) The βγ subunits of GTP-binding proteins activate the muscarinic K^+ channel in heart. *Nature. 325*, 321-326.

28. Pitcher, J. A., Inglese, J., Higgins, J. B., Arriza, J. L., Casey, P. J., Kim, C., Benovic, J. L., Kwatra, M. M., Caron, M. G., and Lefkowitz, R. J. (1992) Role of βγ subunits of G proteins in targeting the β-adrenergic receptor kinase to membrane-bound receptors. *Science. 257*, 1264-1267.

29. Stephens, L., Smrcka, A., Cooke, F. T., Jackson, T. R., Sternweis, P. C., and Hawkins, P. T. (1994) A novel phosphoinositide 3 kinase activity in myeloid-derived cells is activated by G protein βγ subunits. *Cell. 77*, 83-93.

30. Thomason, P. A., James, S. R., Casey, P. J., and Downes, C. P. (1994) A G-protein βγ-subunit-responsive phosphoinositide 3-kinase activity in human platelet cytosol. *J. Biol. Chem. 269*, 16525-16528.

31. Smrcka, A. V. (2008) G protein βγ subunits: Central mediators of G protein-coupled receptor signaling. *Cell Mol. Life Sci. 65*, 2191-2214.

32. Clapham, D. E., and Neer, E. J. (1993) New roles for G-protein βγ dimers in transmembrane signalling. *Nature. 365*, 403-406.

33. Pronin, A. N., and Gautam, N. (1992) Interaction between G-protein βγ subunit types is selective. *Proc. Natl. Acad. Sci. U. S. A. 89*, 6220-6224.

34. Spring, D. J., and Neer, E. J. (1994) A 14-amino acid region of the G protein γ subunit is sufficient to confer selectivity of γ binding to the β subunit. *J. Biol. Chem. 269*, 22882-22886.

35. Cabrera-Vera, T. M., Vanhauwe, J., Thomas, T. O., Medkova, M., Preininger, A., Mazzoni, M. R., and Hamm, H. E. (2003) Insights into G protein structure, function, and regulation. *Endocr. Rev. 24*, 765-781.

36. Iniguez-Lluhi, J. A., Simon, M. I., Robishaw, J. D., and Gilman, A. G. (1992) G protein βγ subunits synthesized in Sf9 cells. functional characterization and the significance of prenylation of γ. *J. Biol. Chem. 267*, 23409-23417.

37. Ueda, N., Iniguez-Lluhi, J. A., Lee, E., Smrcka, A. V., Robishaw, J. D., and Gilman, A. G. (1994) G protein βγ subunits. simplified purification and properties of novel isoforms. *J. Biol. Chem. 269*, 4388-4395.

38. Zhang, S., Coso, O. A., Lee, C., Gutkind, J. S., and Simonds, W. F. (1996) Selective activation of effector pathways by brain-specific G protein beta5. *J. Biol. Chem. 271*, 33575-33579.

39. Burack, W. R., and Shaw, A. S. (2000) Signal transduction: Hanging on a scaffold. *Curr. Opin. Cell Biol. 12*, 211-216.

40. Vetter, I. R., and Wittinghofer, A. (2001) The guanine nucleotide-binding switch in three dimensions. *Science. 294*, 1299-1304.

41. Tesmer, J. J., Sunahara, R. K., Fancy, D. A., Gilman, A. G., and Sprang, S. R. (2002) Crystallization of Complex between Soluble Domains of Adenylyl Cyclase and Activated $G_{s\alpha}$, in *Methods in Enzymology: G Protein Pathways Part C: Effector Mechanisms* (R. Iyengar, and J. D. Hildebrandt, Eds.) pp 198-206, Academic Press, Pasadena, California.

42. Coleman, D. E., and Sprang, S. R. (1998) Crystal structures of the G protein $G_{i\alpha 1}$ complexed with GDP and Mg^{2+}: A crystallographic titration experiment. *Biochemistry. 37*, 14376-14385.

43. Warner, D. R., Weng, G., Yu, S., Matalon, R., and Weinstein, L. S. (1998) A novel mutation in the switch 3 region of $G_{s\alpha}$ in a patient with albright hereditary osteodystrophy impairs GDP binding and receptor activation. *J. Biol. Chem. 273*, 23976-23983.

44. Sprang, S. R. (2016) Invited review: Activation of G proteins by GTP and the mechanism of G_{α} -catalyzed GTP hydrolysis. *Biopolymers. 105*, 449-462.

45. Maracci, C., and Rodnina, M. V. (2016) Review: Translational GTPases. *Biopolymers. 105*, 463-475.

46. Birnbaumer, L., and Zurita, A. R. (2010) On the roles of Mg^{2+} in the activation of G proteins. *J. Recept. Signal Transduct. Res. 30*, 372-375.

47. Carvalho, A. T., Szeler, K., Vavitsas, K., Aqvist, J., and Kamerlin, S. C. (2015) Modeling the mechanisms of biological GTP hydrolysis. *Arch. Biochem. Biophys. 582*, 80-90.

48. Halls, M. L., and Cooper, D. M. (2017) Adenylyl cyclase signalling complexes - pharmacological challenges and opportunities. *Pharmacol. Ther. 172*, 171-180.

49. Sadana, R., and Dessauer, C. W. (2009) Physiological roles for G protein-regulated adenylyl cyclase isoforms: Insights from knockout and overexpression studies. *Neurosignals. 17*, 5-22.

50. Dessauer, C. W., Watts, V. J., Ostrom, R. S., Conti, M., Dove, S., and Seifert, R. (2017) International union of basic and clinical pharmacology. CI. structures and small molecule modulators of mammalian adenylyl cyclases. *Pharmacol. Rev. 69*, 93-139.

51. Tesmer, J. J., Sunahara, R. K., Gilman, A. G., and Sprang, S. R. (1997) Crystal structure of the catalytic domains of adenylyl cyclase in a complex with $G_{s\alpha}$ •GTPγS. *Science. 278*, 1907-1916.

52. Grishina, G., and Berlot, C. H. (1997) Identification of common and distinct residues involved in the interaction of $G_{i\alpha 2}$ and $G_{s\alpha}$ with adenylyl cyclase. *J. Biol. Chem. 272*, 20619-20626.

53. Taussig, R., Tang, W. J., Hepler, J. R., and Gilman, A. G. (1994) Distinct patterns of bidirectional regulation of mammalian adenylyl cyclases. *J. Biol. Chem. 269*, 6093-6100.

54. Tengholm, A., and Gylfe, E. (2017) cAMP signalling in insulin and glucagon secretion. *Diabetes Obes. Metab. 19 Suppl 1*, 42-53.

55. Yan, K., Gao, L. N., Cui, Y. L., Zhang, Y., and Zhou, X. (2016) The cyclic AMP signaling pathway: Exploring targets for successful drug discovery (review). *Mol. Med. Rep. 13*, 3715-3723.

56. Bastepe, M. (2007) The GNAS locus: Quintessential complex gene encoding $G_{s\alpha}$, XL $G_{s\alpha}$, and other imprinted transcripts. *Curr. Genomics. 8*, 398-414.

57. Kozasa, T., Itoh, H., Tsukamoto, T., and Kaziro, Y. (1988) Isolation and characterization of the human $G_{s\alpha}$ gene. *Proc. Natl. Acad. Sci. U. S. A. 85*, 2081-2085.

58. Herberg, F. W., Doyle, M. L., Cox, S., and Taylor, S. S. (1999) Dissection of the nucleotide and metal-phosphate binding sites in cAMP-dependent protein kinase. *Biochemistry. 38*, 6352-6360.

59. Dowlatshahi, D., MacQueen, G. M., Wang, J. F., Reiach, J. S., and Young, L. T. (1999) G protein-coupled cyclic AMP signaling in postmortem brain of subjects with mood disorders: Effects of diagnosis, suicide, and treatment at the time of death. *J. Neurochem. 73*, 1121-1126.

60. O'Hayre, M., Vazquez-Prado, J., Kufareva, I., Stawiski, E. W., Handel, T. M., Seshagiri, S., and Gutkind, J. S. (2013) The emerging mutational landscape of G proteins and G-protein-coupled receptors in cancer. *Nat. Rev. Cancer. 13*, 412-424.

61. Weinstein, L. S., Chen, M., and Liu, J. (2002) $G_{s\alpha}$ mutations and imprinting defects in human disease. *Ann. N. Y. Acad. Sci. 968*, 173-197.

62. Kottler, M. L. (2015) Paternal *GNAS* mutations: Which phenotypes? What genetic counseling? *Ann. Endocrinol. (Paris). 76*, 105-109.

63. Ngai, Y. F., Chijiwa, C., Mercimek-Mahmutoglu, S., Stewart, L., Yong, S. L., Robinson, W. P., and Gibson, W. T. (2010) Pseudohypoparathyroidism type 1a and the *GNAS* p.R231H mutation: Somatic mosaicism in a mother with two affected sons. *Am. J. Med. Genet. A. 152A*, 2784-2790.

64. Lietman, S. A., Goldfarb, J., Desai, N., and Levine, M. A. (2008) Preimplantation genetic diagnosis for severe albright hereditary osteodystrophy. *J. Clin. Endocrinol. Metab. 93*, 901-904.

65. Abdulaev, N. G., Mao, X., Ramon, E., Ngo, T., Mysliwy, J., Marino, J. P., and Ridge, K. D. (2009) Designing point mutants to detect structural coupling in a heterotrimeric G protein α-subunit by NMR spectroscopy. *Photochem. Photobiol. 85*, 431-436.

66. Mantovani, G., Spada, A., and Elli, F. M. (2016) Pseudohypoparathyroidism and gsalpha-cAMP-linked disorders: Current view and open issues. *Nat. Rev. Endocrinol. 12*, 347-356.

67. Turan, S. (2017) Current nomenclature of pseudohypoparathyroidism: Inactivating parathyroid hormone/parathyroid hormone-related protein signaling disorder. *J. Clin. Res. Pediatr. Endocrinol. 9*, 58-68.

68. Mantovani, G. (2011) Clinical review: Pseudohypoparathyroidism: Diagnosis and treatment. *J. Clin. Endocrinol. Metab. 96*, 3020-3030.

69. Lania, A., Mantovani, G., and Spada, A. (2001) G protein mutations in endocrine diseases. *Eur. J. Endocrinol. 145*, 543-559.

70. Weinstein, L. S., Liu, J., Sakamoto, A., Xie, T., and Chen, M. (2004) Minireview: *GNAS*: Normal and abnormal functions. *Endocrinology. 145*, 5459-5464.

71. Pugh, T. J., Weeraratne, S. D., Archer, T. C., Pomeranz Krummel, D. A., Auclair, D., Bochicchio, J., Carneiro, M. O., Carter, S. L., Cibulskis, K., Erlich, R. L., Greulich, H., Lawrence, M. S., Lennon, N. J., McKenna, A., Meldrim, J., Ramos, A. H., Ross, M. G., Russ, C., Shefler, E., Sivachenko, A., Sogoloff, B., Stojanov, P., Tamayo, P., Mesirov, J. P.,

Amani, V., Teider, N., Sengupta, S., Francois, J. P., Northcott, P. A., Taylor, M. D., Yu, F., Crabtree, G. R., Kautzman, A. G., Gabriel, S. B., Getz, G., Jager, N., Jones, D. T., Lichter, P., Pfister, S. M., Roberts, T. M., Meyerson, M., Pomeroy, S. L., and Cho, Y. J. (2012) Medulloblastoma exome sequencing uncovers subtype-specific somatic mutations. *Nature. 488*, 106-110.

72. Wu, J., Matthaei, H., Maitra, A., Dal Molin, M., Wood, L. D., Eshleman, J. R., Goggins, M., Canto, M. I., Schulick, R. D., Edil, B. H., Wolfgang, C. L., Klein, A. P., Diaz, L. A.,Jr, Allen, P. J., Schmidt, C. M., Kinzler, K. W., Papadopoulos, N., Hruban, R. H., and Vogelstein, B. (2011) Recurrent *GNAS* mutations define an unexpected pathway for pancreatic cyst development. *Sci. Transl. Med. 3*, 92ra66.

73. Hsu, M., Sasaki, M., Igarashi, S., Sato, Y., and Nakanuma, Y. (2013) *KRAS* and *GNAS* mutations and p53 overexpression in biliary intraepithelial neoplasia and intrahepatic cholangiocarcinomas. *Cancer. 119*, 1669-1674.

74. Vetter, I. R., and Wittinghofer, A. (2001) The guanine nucleotide-binding switch in three dimensions. *Science. 294*, 1299-1304.

75. Malumbres, M., and Barbacid, M. (2003) RAS oncogenes: The first 30 years. *Nat. Rev. Cancer. 3*, 459-465.

76. Turan, S., and Bastepe, M. (2013) The *GNAS* complex locus and human diseases associated with loss-of-function mutations or epimutations within this imprinted gene. *Horm. Res. Paediatr. 80*, 229-241.

77. Saggio, I., Remoli, C., Spica, E., Cersosimo, S., Sacchetti, B., Robey, P. G., Holmbeck, K., Cumano, A., Boyde, A., Bianco, P., and Riminucci, M. (2014) Constitutive expression of $G_{s\alpha}$ (R201C) in mice produces a heritable, direct replica of human fibrous dysplasia bone pathology and demonstrates its natural history. *J. Bone Miner. Res. 29*, 2357-2368.

78. Wilson, C. H., McIntyre, R. E., Arends, M. J., and Adams, D. J. (2010) The activating mutation R201C in *GNAS* promotes intestinal tumourigenesis in apc(min/+) mice through activation of wnt and ERK1/2 MAPK pathways. *Oncogene. 29*, 4567-4575.

79. Iiri, T., Farfel, Z., and Bourne, H. R. (1997) Conditional activation defect of a human $G_{s\alpha}$ mutant. *Proc. Natl. Acad. Sci. U. S. A. 94*, 5656-5661.

80. Selkoe, D. J. (2003) Folding proteins in fatal ways. *Nature. 426*, 900-904.

81. Ashraf, G. M., Greig, N. H., Khan, T. A., Hassan, I., Tabrez, S., Shakil, S., Sheikh, I. A., Zaidi, S. K., Akram, M., Jabir, N. R., Firoz, C. K., Naeem, A., Alhazza, I. M., Damanhouri, G. A., and

Kamal, M. A. (2014) Protein misfolding and aggregation in Alzheimer's disease and type 2 diabetes mellitus. *CNS Neurol. Disord. Drug Targets. 13*, 1280-1293.

82. Li, H. T., Du, H. N., Tang, L., Hu, J., and Hu, H. Y. (2002) Structural transformation and aggregation of human alpha-synuclein in trifluoroethanol: Non-amyloid component sequence is essential and β-sheet formation is prerequisite to aggregation. *Biopolymers. 64*, 221-226.

83. Chou, H., Maji, S. K., Riek-Loher, D., Verel, R., Manning, G., Stahlberg, H., and Riek, R. (2008) The fold of α-synuclein fibrils. *Proc. Natl. Acad. Sci. USA. 105*, 8637.

84. Campbell, I. D. (2012) *Biophysical Techniques.* Oxford University Press, Oxford.

85. Dill, K. A., and MacCallum, J. L. (2012) The protein-folding problem, 50 years on. *Science. 338*, 1042-1046.

86. Shea, J. E., and Brooks, C. L.,3rd. (2001) From folding theories to folding proteins: A review and assessment of simulation studies of protein folding and unfolding. *Annu. Rev. Phys. Chem. 52*, 499-535.

87. Chandel, T. I., Zaman, M., Khan, M. V., Ali, M., Rabbani, G., Ishtikhar, M., and Khan, R. H. (2018) A mechanistic insight into protein-ligand interaction, folding, misfolding, aggregation and inhibition of protein aggregates: An overview. *Int. J. Biol. Macromol. 106*, 1115-1129.

88. Monge, A., Lathrop, E. J., Gunn, J. R., Shenkin, P. S., and Friesner, R. A. (1995) Computer modeling of protein folding: Conformational and energetic analysis of reduced and detailed protein models. *J. Mol. Biol. 247*, 995-1012.

89. Gopi, S., Paul, S., Ranu, S., and Naganathan, A. N. (2018) Extracting the hidden distributions underlying the mean transition state structures in protein folding. *J. Phys. Chem. Lett. 9*, 1771-1777.

90. Freilich, R., Arhar, T., Abrams, J. L., and Gestwicki, J. E. (2018) Protein-protein interactions in the molecular chaperone network. *Acc. Chem. Res. 51,* 940-949.

91. Klamt, A. (1996) Calculation of UV/vis spectra in solution. *J. Phys. Chem. 100*, 3349-3353.

92. Sheehan, D. (2009) *Physical Biochemistry : Principles and Applications.* 2nd ed., Wiley-Blackwell, Chichester.

93. Sauer, M. (2011) *Handbook of Fluorescence Spectroscopy and Imaging : From Single Molecules to Ensembles.* Wiley-VCH, Weinheim.

94. Weiss, S. (1999) Fluorescence spectroscopy of single biomolecules. *Science. 283*, 1676-1683.

95. Marcu, L., French, P., and Elson, D. (2015) *Fluorescence Lifetime Spectroscopy and Imaging : Principles and Applications in Biomedical Diagnostics.* CRC Press, Florida; Boca Raton.

96. Weber, G., and Laurence, D. J. (1954) Fluorescent indicators of adsorption in aqueous solution and on the solid phase. *Biochem. J. 56*, 151-156.

97. Berlman, I. B. (1971) *Handbook of Fluorescence Spectra of Aromatic Molecules.* 2nd ed., Academic Press, New York ; London.

98. Vivian, J. T., and Callis, P. R. (2001) Mechanisms of tryptophan fluorescence shifts in proteins. *Biophys. J. 80*, 2093-2109.

99. Doring, K., Konermann, L., Surrey, T., and Jahnig, F. (1995) A long lifetime component in the tryptophan fluorescence of some proteins. *Eur. Biophys. J. 23*, 423-432.

100. Ferguson, K. M., Higashijima, T., Smigel, M. D., and Gilman, A. G. (1986) The influence of bound GDP on the kinetics of guanine nucleotide binding to G proteins. *J. Biol. Chem. 261*, 7393-7399.

101. Burley, S. K., and Petsko, G. A. (1986) Amino-aromatic interactions in proteins. *FEBS Lett. 203*, 139-143.

102. Lambert, N. A., Johnston, C. A., Cappell, S. D., Kuravi, S., Kimple, A. J., Willard, F. S., and Siderovski, D. P. (2010) Regulators of G-protein signaling accelerate GPCR signaling kinetics and govern sensitivity solely by accelerating GTPase activity. *Proc. Natl. Acad. Sci. U. S. A. 107*, 7066-7071.

103. Higashijima, T., Ferguson, K. M., Smigel, M. D., and Gilman, A. G. (1987) The effect of GTP and Mg^{2+} on the GTPase activity and the fluorescent properties of G_o. *J. Biol. Chem. 262*, 757-761.

104. Higashijima, T., Ferguson, K. M., Sternweis, P. C., Ross, E. M., Smigel, M. D., and Gilman, A. G. (1987) The effect of activating ligands on the intrinsic fluorescence of guanine nucleotide-binding regulatory proteins. *J. Biol. Chem. 262*, 752-756.

105. Faurobert, E., Otto-Bruc, A., Chardin, P., and Chabre, M. (1993) Tryptophan W207 in transducin $G_{\alpha t}$ is the fluorescence sensor of the G protein activation switch and is involved in the effector binding. *EMBO J. 12*, 4191-4198.

106. Noel, J. P., Hamm, H. E., and Sigler, P. B. (1993) The 2.2 Å crystal structure of transducin-α complexed with GTPγS. *Nature. 366*, 654-663.

107. Najor, M. S., Olsen, K. W., Graham, D. J., and Mota de Freitas, D. (2014) Contribution of each trp residue toward the intrinsic fluorescence of the $G_{i\alpha1}$ protein. *Protein Sci. 23*, 1392-1402.

108. Hamm, H. E., Meier, S. M., Liao, G., and Preininger, A. M. (2009) Trp fluorescence reveals an activation-dependent cation-pi interaction in the switch II region of $G_{i\alpha1}$ proteins. *Protein Sci. 18*, 2326-2335.

109. Riley, K. E., and Tran, K. A. (2017) Strength and character of R-X...pi interactions involving aromatic amino acid sidechains in protein-ligand complexes derived from crystal structures in the protein data bank. *Crystals. 7*, 273.

110. Tayubi, I. A., and Sethumadhavan, R. (2010) Nature of cation-pi interactions and their role in structural stability of immunoglobulin proteins. *Biochemistry (Mosc). 75*, 912-918.

111. *Circular Dichroism and the Conformational Analysis of Biomolecules.* (1996) Plenum Press, New York ; London.

112. *Circular Dichroism : Principles and Applications.* (2000) 2nd ed., Wiley-VCH, New York ; Chichester.

113. Miles, A. J., and Wallace, B. A. (2016) Circular dichroism spectroscopy of membrane proteins. *Chem. Soc. Rev. 45*, 4859-4872.

114. *Modern Techniques for Circular Dichroism and Synchrotron Radiation Circular Dichroism Spectroscopy.* (2009) IOS Press; Gazelle Books distributor, Amsterdam; Lancaster.

115. Oldham, W. M., and Hamm, H. E. (2006) Structural basis of function in heterotrimeric G proteins. *Q. Rev. Biophys. 39*, 117-166.

116. Mixon, M. B., Lee, E., Coleman, D. E., Berghuis, A. M., Gilman, A. G., and Sprang, S. R. (1995) Tertiary and quaternary structural changes in $G_{i\alpha1}$ induced by GTP hydrolysis. *Science. 270*, 954-960.

117. Coleman, D. E., Berghuis, A. M., Lee, E., Linder, M. E., Gilman, A. G., and Sprang, S. R. (1994) Structures of active conformations of $G_{i\alpha1}$ and the mechanism of GTP hydrolysis. *Science. 265*, 1405-1412.

118. Bae, H., Anderson, K., Flood, L. A., Skiba, N. P., Hamm, H. E., and Graber, S. G. (1997) Molecular determinants of selectivity in 5-hydroxytryptamine1B receptor-G protein interactions. *J. Biol. Chem. 272*, 32071-32077.

119. Pace, N. C., Scholtz, J. M., and Grimsley, G. R. (2014) Forces stabilizing proteins. *FEBS Lett. 588*, 2177-2184.

120. Englander, S. W., and Mayne, L. (2014) The nature of protein folding pathways. *Proc. Natl. Acad. Sci. U. S. A. 111*, 15873-15880.

121. Schiffrin, B., Brockwell, D. J., and Radford, S. E. (2017) Outer membrane protein folding from an energy landscape perspective. *BMC Biol. 15*, 123-017-0464-5.

122. Baldwin, R. L., and Rose, G. D. (2013) Molten globules, entropy-driven conformational change and protein folding. *Curr. Opin. Struct. Biol. 23*, 4-10.

123. Shortle, D. (1996) The denatured state (the other half of the folding equation) and its role in protein stability. *FASEB J. 10*, 27-34.

124. Bhattacharyya, S., and Varadarajan, R. (2013) Packing in molten globules and native states. *Curr. Opin. Struct. Biol. 23*, 11-21.

125. Weinstein, L. S., Shenker, A., Gejman, P. V., Merino, M. J., Friedman, E., and Spiegel, A. M. (1991) Activating mutations of the stimulatory G protein in the McCune-Albright syndrome. *N. Engl. J. Med. 325*, 1688-1695.

126. Berrettini, W. H., Vuoristo, J., Ferraro, T. N., Buono, R. J., Wildenauer, D., and Ala-Kokko, L. (1998) Human G(olf) gene polymorphisms and vulnerability to bipolar disorder. *Psychiatr. Genet. 8*, 235-238.

127. Dorsam, R. T., and Gutkind, J. S. (2007) G-protein-coupled receptors and cancer. *Nature reviews cancer. 7*, 79-94.

128. Lee, E., Linder, M. E., and Gilman, A. G. (1994) Expression of G-protein α subunits in *Escherichia coli*. *Methods Enzymol. 237*, 146-164.

129. Brandts, J. F. (1964) The thermodynamics of protein denaturation. I. the denaturation of chymotrypsinogen. *J. Am. Chem. Soc. 86*, 4291-4301.

130. Olsen, K. W. (1994) Thermal denaturation procedures for hemoglobin. *Methods Enzymol. 231*, 514-524.

131. Provencher, S. W., and Glockner, J. (1981) Estimation of globular protein secondary structure from circular dichroism. *Biochemistry. 20*, 33-37.

132. Whitmore, L., and Wallace, B. A. (2008) Protein secondary structure analyses from circular dichroism spectroscopy: Methods and reference databases. *Biopolymers. 89*, 392-400.

133. Sreerama, N., Venyaminov, S. Y., and Woody, R. W. (2000) Estimation of protein secondary structure from circular dichroism spectra: Inclusion of denatured proteins with native proteins in the analysis. *Anal. Biochem. 287*, 243-251.

134. Berman, H. M., Westbrook, J., Feng, Z., Gilliland, G., Bhat, T. N., Weissig, H., Shindyalov, I. N., and Bourne, P. E. (2000) The protein data bank. *Nucleic Acids Res. 28*, 235-242.

135. Arnold, K., Bordoli, L., Kopp, J., and Schwede, T. (2006) The SWISS-MODEL workspace: A web-based environment for protein structure homology modelling. *Bioinformatics. 22*, 195-201.

136. Lambright, D. G., Noel, J. P., Hamm, H. E., and Sigler, P. B. (1994) Structural determinants for activation of the α-subunit of a heterotrimeric G protein. *Nature. 369*, 621-628.

137. Sondek, J., Lambright, D. G., Noel, J. P., Hamm, H. E., and Sigler, P. B. (1994) GTPase mechanism of G-proteins from the 1.7-Å crystal structure of transducin α-GDP•AlF^{-4}. *Nature. 372*, 276-279.

138. Humphrey, W., Dalke, A., and Schulten, K. (1996) VMD: Visual molecular dynamics. *J. Mol. Graph. 14*, 33-8, 27-8.

139. Phillips, J. C., Braun, R., Wang, W., Gumbart, J., Tajkhorshid, E., Villa, E., Chipot, C., Skeel, R. D., Kale, L., and Schulten, K. (2005) Scalable molecular dynamics with NAMD. *J. Comput. Chem. 26*, 1781-1802.

140. Tanaka, T., Kohno, T., Kinoshita, S., Mukai, H., Itoh, H., Ohya, M., Miyazawa, T., Higashijima, T., and Wakamatsu, K. (1998) α helix content of G protein α subunit is decreased upon activation by receptor mimetics. *J. Biol. Chem. 273*, 3247-3252.

141. Streiff, J., Warner, D. O., Klimtchuk, E., Perkins, W. J., Jones, K., and Jones, K. A. (2004) The effects of hexanol on $G_{i\alpha 1}$ subunits of heterotrimeric G proteins. *Anesth. Analg. 98*, 660-7, table of contents.

142. Northup, J. K., Smigel, M. D., Sternweis, P. C., and Gilman, A. G. (1983) The subunits of the stimulatory regulatory component of adenylate cyclase. resolution of the activated 45,000-dalton (alpha) subunit. *J. Biol. Chem. 258*, 11369-11376.

143. Stryer, L. (1968) Fluorescence spectroscopy of proteins. *Science. 162*, 526-533.

144. Chiti, F., and Dobson, C. M. (2017) Protein misfolding, amyloid formation, and human disease: A summary of progress over the last decade. *Annu. Rev. Biochem. 86*, 27-68.

145. Morris, A. M., Watzky, M. A., and Finke, R. G. (2009) Protein aggregation kinetics, mechanism, and curve-fitting: A review of the literature. *Biochim. Biophys. Acta. 1794*, 375-397.

146. Dao, K. K., Pey, A. L., Gjerde, A. U., Teigen, K., Byeon, I. J., Doskeland, S. O., Gronenborn, A. M., and Martinez, A. (2011) The regulatory subunit of PKA-I remains partially structured and undergoes beta-aggregation upon thermal denaturation. *PLoS One. 6*, e17602.

147. Fandrich, M., Forge, V., Buder, K., Kittler, M., Dobson, C. M., and Diekmann, S. (2003) Myoglobin forms amyloid fibrils by association of unfolded polypeptide segments. *Proc. Natl. Acad. Sci. U. S. A. 100*, 15463-15468.

148. Plaza del Pino, I. M., Ibarra-Molero, B., and Sanchez-Ruiz, J. M. (2000) Lower kinetic limit to protein thermal stability: A proposal regarding protein stability in vivo and its relation with misfolding diseases. *Proteins. 40*, 58-70.

149. Gallivan, J. P., and Dougherty, D. A. (1999) Cation-pi interactions in structural biology. *Proc. Natl. Acad. Sci. U. S. A. 96*, 9459-9464.

150. Dougherty, D. A. (2013) The cation-pi interaction. *Acc. Chem. Res. 46*, 885-893.

151. Prajapati, R. S., Sirajuddin, M., Durani, V., Sreeramulu, S., and Varadarajan, R. (2006) Contribution of cation-pi interactions to protein stability. *Biochemistry. 45*, 15000-15010.

152. Senisterra, G., Chau, I., and Vedadi, M. (2012) Thermal denaturation assays in chemical biology. *Assay Drug Dev. Technol. 10*, 128-136.

153. Fink, A. L., Oberg, K. A., and Seshadri, S. (1998) Discrete intermediates versus molten globule models for protein folding: Characterization of partially folded intermediates of apomyoglobin. *Fold. Des. 3*, 19-25.

154. Wettschureck, N., and Offermanns, S. (2005) Mammalian G proteins and their cell type specific functions. *Physiol. Rev. 85*, 1159-1204.

155. Sprang, S. R. (1997) G protein mechanisms: Insights from structural analysis. *Annu. Rev. Biochem. 66*, 639-678.

156. Phillips, W. J., and Cerione, R. A. (1988) The intrinsic fluorescence of the α subunit of transducin. measurement of receptor-dependent guanine nucleotide exchange. *J. Biol. Chem. 263*, 15498-15505.

157. Piovesan, D., Minervini, G., and Tosatto, S. C. (2016) The RING 2.0 web server for high quality residue interaction networks. *Nucleic Acids Res. 44*, W367-74.

158. Warner, D. R., Romanowski, R., Yu, S., and Weinstein, L. S. (1999) Mutagenesis of the conserved residue Glu259 of $G_{s\alpha}$ a demonstrates the importance of interactions between switches 2 and 3 for activation. *J. Biol. Chem. 274*, 4977-4984.

159. Pinheiro, S., Soteras, I., Gelpi, J. L., Dehez, F., Chipot, C., Luque, F. J., and Curutchet, C. (2017) Structural and energetic study of cation-pi-cation interactions in proteins. *Phys. Chem. Chem. Phys. 19*, 9849-9861.

160. Dougherty, D. A. (1996) Cation-pi interactions in chemistry and biology: A new view of benzene, phe, tyr, and trp. *Science. 271*, 163-168.

161. Cockroft, S. L., and Hunter, C. A. (2007) Chemical double-mutant cycles: Dissecting non-covalent interactions. *Chem. Soc. Rev. 36*, 172-188.

162. Carter, P. J., Winter, G., Wilkinson, A. J., and Fersht, A. R. (1984) The use of double mutants to detect structural changes in the active site of the tyrosyl-tRNA synthetase (bacillus stearothermophilus). *Cell. 38*, 835-840.

163. Hauryliuk, V., Hansson, S., and Ehrenberg, M. (2008) Cofactor dependent conformational switching of GTPases. *Biophys. J. 95*, 1704-1715.

164. Davidi, D., Noor, E., Liebermeister, W., Bar-Even, A., Flamholz, A., Tummler, K., Barenholz, U., Goldenfeld, M., Shlomi, T., and Milo, R. (2016) Global characterization of in vivo enzyme catalytic rates and their correspondence to in vitro kcat measurements. *Proc. Natl. Acad. Sci. U. S. A. 113*, 3401-3406.

165. Zhang, B., Sun, N., Mu, X., Zhi, L., Zhai, L., Jiang, Y., Fu, Z., and Yao, Z. (2017) $G_{s\alpha}$ subunit promotes cell proliferation of renal cell carcinoma with involvement of protein kinase A signaling. *DNA Cell Biol. 36*, 237-242.

166. Hanahan, D., and Weinberg, R. A. (2011) Hallmarks of cancer: The next generation. *Cell. 144*, 646-674.

167. Fajardo, A. M., Piazza, G. A., and Tinsley, H. N. (2014) The role of cyclic nucleotide signaling pathways in cancer: Targets for prevention and treatment. *Cancers (Basel). 6*, 436-458.

168. Alakus, H., Babicky, M. L., Ghosh, P., Yost, S., Jepsen, K., Dai, Y., Arias, A., Samuels, M. L., Mose, E. S., Schwab, R. B., Peterson, M. R., Lowy, A. M., Frazer, K. A., and Harismendy, O. (2014) Genome-wide mutational landscape of mucinous carcinomatosis peritonei of appendiceal origin. *Genome Med. 6*, 43.

169. Thomas, C. J., Du, X., Li, P., Wang, Y., Ross, E. M., and Sprang, S. R. (2004) Uncoupling conformational change from GTP hydrolysis in a heterotrimeric G protein alpha-subunit. *Proc. Natl. Acad. Sci. U. S. A. 101*, 7560-7565.

170. Carter, S. G., and Karl, D. W. (1982) Inorganic phosphate assay with malachite green: An improvement and evaluation. *J. Biochem. Biophys. Methods. 7*, 7-13.

171. Wu, Z. L. (2011) Phosphatase-coupled universal kinase assay and kinetics for first-order-rate coupling reaction. *PLoS One. 6*, e23172.

172. Morikawa, T., Muroya, A., Nakajima, Y., Tanaka, T., Hirai, K., Sugio, S., Wakamatsu, K., and Kohno, T. (2007) Crystallization and preliminary X-ray crystallographic analysis of the receptor-uncoupled mutant of $G_{i\alpha1}$. *Acta Crystallogr. Sect. F. Struct. Biol. Cryst. Commun. 63*, 139-141.

173. Adams, P. D., Grosse-Kunstleve, R. W., Hung, L. W., Ioerger, T. R., McCoy, A. J., Moriarty, N. W., Read, R. J., Sacchettini, J. C., Sauter, N. K., and Terwilliger, T. C. (2002) PHENIX: Building new software for automated crystallographic structure determination. *Acta Crystallogr. D Biol. Crystallogr. 58*, 1948-1954.

174. Pettersen, E. F., Goddard, T. D., Huang, C. C., Couch, G. S., Greenblatt, D. M., Meng, E. C., and Ferrin, T. E. (2004) UCSF chimera--a visualization system for exploratory research and analysis. *J. Comput. Chem. 25*, 1605-1612.

175. Kleuss, C., Raw, A. S., Lee, E., Sprang, S. R., and Gilman, A. G. (1994) Mechanism of GTP hydrolysis by G-protein α subunits. *Proc. Natl. Acad. Sci. U. S. A. 91*, 9828-9831.

176. Antonny, B., and Chabre, M. (1992) Characterization of the aluminum and beryllium fluoride species which activate transducin. analysis of the binding and dissociation kinetics. *J. Biol. Chem. 267*, 6710-6718.

177. Thaker, T. M., Sarwar, M., Preininger, A. M., Hamm, H. E., and Iverson, T. M. (2014) A transient interaction between the phosphate binding loop and switch I contributes to the allosteric network between receptor and nucleotide in $G_{i\alpha1}$. *J. Biol. Chem. 289*, 11331-11341.

178. Tesmer, J. J., Berman, D. M., Gilman, A. G., and Sprang, S. R. (1997) Structure of RGS4 bound to AlF^{4-} activated $G_{i\alpha1}$: Stabilization of the transition state for GTP hydrolysis. *Cell. 89*, 251-261.

179. Berman, D. M., Kozasa, T., and Gilman, A. G. (1996) The GTPase-activating protein RGS4 stabilizes the transition state for nucleotide hydrolysis. *J. Biol. Chem. 271*, 27209-27212.

180. Graziano, M. P., and Gilman, A. G. (1989) Synthesis in *Escherichia coli* of GTPase-deficient mutants of $G_{s\alpha}$. *J. Biol. Chem. 264*, 15475-15482.

181. Johnston, C. A., Willard, F. S., Jezyk, M. R., Fredericks, Z., Bodor, E. T., Jones, M. B., Blaesius, R., Watts, V. J., Harden, T. K., Sondek, J., Ramer, J. K., and Siderovski, D. P. (2005) Structure of $G_{i\alpha1}$ bound to a GDP-selective peptide provides insight into guanine nucleotide exchange. *Structure. 13*, 1069-1080.

182. Slepak, V. Z., Katz, A., and Simon, M. I. (1995) Functional analysis of a dominant negative mutant of $G_{i\alpha2}$. *J. Biol. Chem. 270*, 4037-4041.

183. Ahmadian, M. R., Stege, P., Scheffzek, K., and Wittinghofer, A. (1997) Confirmation of the arginine-finger hypothesis for the GAP-stimulated GTP-hydrolysis reaction of ras. *Nat. Struct. Biol. 4*, 686-689.

184. Zhang, B., Zhang, Y., Wang, Z., and Zheng, Y. (2000) The role of Mg^{2+} cofactor in the guanine nucleotide exchange and GTP hydrolysis reactions of rho family GTP-binding proteins. *J. Biol. Chem. 275*, 25299-25307.

185. Wedegaertner, P. B., Chu, D. H., Wilson, P. T., Levis, M. J., and Bourne, H. R. (1993) Palmitoylation is required for signaling functions and membrane attachment of $G_{\alpha q}$ and $G_{s\alpha}$. *J. Biol. Chem. 268*, 25001-25008.

186. Farfel, Z., Iiri, T., Shapira, H., Roitman, A., Mouallem, M., and Bourne, H. R. (1996) Pseudohypoparathyroidism, a novel mutation in the betagamma-contact region of gsalpha impairs receptor stimulation. *J. Biol. Chem. 271*, 19653-19655.

VITA

The author, Brian Leverson, was born January 13, 1986 in Chicago, IL. In August 2005, he started his undergraduate studies at Chicago State University. In May 2009, he received a Bachelor of Science degree in chemistry.

In August of 2012, he was admitted to the Ph.D. program in chemistry at Loyola